*Institute of Space and Aeronautical Science, University of Tokyo*
*Report No. 473, December 1971*

# Monte Carlo Calculation of Hypersonic Rarefied Gas Flows past Two-Dimensional and Axisymmetric Bodies*

*By*

Michitoshi TAKAGI**

*Summary*: A direct simulation Monte Carlo method is developed to solve the flow field around a two-dimensional or axisymmetric body immersed in a hypersonic rarefied gas flow. A steady solution is obtained as the non-steady solution at the time of infinity by the present method.

The method is applied to the flow field on a highly cooled flat plate placed parallel to the direction of a uniform flow. Another case with a higher Mach number than in the preceding case and the same body temperature is also calculated. The results in the above-mentioned two cases show how the uniform flow Mach number affects the flow field. In addition, physical properties concerning the body surface, that is, the pressure, skin friction, heat transfer and slip velocity distributions are also calculated. All the present results are compared with other theoretical and experimental results and show good agreements with them.

Flow fields around circular cylinders and spheres with highly cooled and near adiabatic conditions are investigated in order to study the effect of the body temperature on the flow field. The solutions for the bodies with different radii are also obtained so as to study the effect of the Knudsen number. Physical properties concerning the body, that is, the pressure and heat transfer distributions and the drag are calculated also in these cases. The experiments of the surface pressure distributions of the circular cylinder and the sphere, and the drag of the sphere are performed in order to examine the Monte Carlo results. The Monte Carlo results agree well with the present and other experimental results and other theoretical results.

## NOMENCLATURE

$a$ constant in a cell, lower boundary of $\xi$
$A$ nondimensional parameter defining flow field
$b$ upper boundary of $\xi$
$B$ representative value of $Y_c$
$c_m$ most probable speed
$c_p$ specific heat at constant pressure
$c_x$ thermal velocity component
$c_y$ thermal velocity component
$c_z$ thermal velocity component

* Central Engineering Laboratories, Nissan Motor Company Limited.
** This work was accomplished as the Doctor Thesis while the author was a postgraduate student in the Institute of Space and Aeronautical Science, University of Tokyo.

$\bar{c}$ mean thermal speed
$\bar{c}^2$ mean square speed
$C$ nondimensional thermal speed, Chapman-Rubesin coefficient
$C_D$ drag coefficient
$C_f$ skin friction coefficient
$C_h$ local heat transfer coefficient defined by (2–33)
$C'_h$ local heat transfer coefficient defined by (2–35)
$C_{p1}$ pressure coefficient defined by (2–27)
$C_{p2}$ pressure coefficient defined by (2–28)
$C_X$ nondimensional thermal velocity component
$C_Y$ nondimensional thermal velocity component
$C_Z$ nondimensional thermal velocity component
$d$ skin friction, drag
$erf$ error function
$f$ function expressing body surface, sample size in a class, probability density function
$F$ rectangular random number, probability density function
$G$ function of M defined by (4–15)
$H$ function of M defined by (4–15)
$I_i$ $i$th-order Bessel function of first kind with imaginary argument
$k$ number of classes, index
$K$ constant
$Kn$ Knudsen number
$l$ characteristic dimension, number of classes
$L$ length of interval of aperiodicity
$m$ sample size, mass of a molecule
$m_s$ number of steps of sampling
$\hat{m}$ sample size calculated by probability density function
$M$ Mach number of uniform flow, modulus
$n$ number density
$n_1$ constant
$n_2$ constant
$N$ number of molecules
$N_i$ number of molecules to maintain uniform flow
$N_0$ number of molecules initially generated
$N_\infty$ number of molecules involved by a volume of unity in uniform flow
$p$ pressure
$\hat{p}$ integral of probability density function
$P_c$ probability of a collision
$P_m$ probability of a collision of any two molecules
$Pr$ Prandtl number
$P_M$ Maxwell-Boltzmann distribution function
$\dot{q}$ heat flux to body
$r$ radius

$R$ nondimensional radius, gas constant, rectangular random number in (0, 1)
$\mathrm{Re}_1$ Reynolds number defined by (4–2) and (4–11)
$\mathrm{Re}_2$ Reynolds number defined by (4–12)
$\mathrm{Re}_3$ Reynolds number defined by (4–14)
$s_b$ characteristic area of body
$S$ speed ratio of uniform flow, random number with specified distribution function
$t$ time, number of times of test
$t_c$ characteristic time
$t_s$ time when sampling starts
$T$ temperature
$u$ uniform flow velocity
$v_x$ velocity component of molecule
$v_y$ velocity component of molecule
$v_z$ velocity component of molecule
$V$ volume, voltage
$V_0$ standard voltage
$V_R$ nondimensional relative speed used to select collision pair
$V_S$ nondimensional slip velocity
$V_X$ nondimensional velocity component of molecule
$V_Y$ nondimensional velocity component of molecule
$V_Z$ nondimensional velocity component of molecule
$\overline{V}_X$ nondimensional macroscopic velocity component
$\overline{V}_Y$ nondimensional macroscopic velocity component
$\overline{V}_Z$ nondimensional macroscopic velocity component
$\overline{V}_{\infty,x}$ rarefaction parameter
$x$ coordinate, variable
$x'$ x-axis with origin at leading edge of flat plate
$X$ nondimensional x
$X'$ nondimensional x′
$y$ coordinate, variable
$Y$ nondimensional y
$z$ coordinate
$Z$ nondimensional z
$\alpha$ apex angle of sector, level of significance
$\gamma$ specific heat ratio
$\delta$ angle between tangent to body surface and center line
$\Delta s$ surface element
$\Delta t$ time interval of a collision cycle
$\Delta t_s$ sampling time interval
$\varepsilon$ density ratio across Rankine-Hugoniot shock
$\xi$ direction cosine, random variable
$\eta$ direction cosine, random variable

$\zeta$ direction cosine
$\theta$ angle defining a position on body surface
$\lambda$ mean free path
$\mu$ viscosity coefficient
$\nu$ collision frequency
$\rho$ density
$\sigma$ molecular diameter
$\tau_c$ mean time necessary for a collision
$\tau_f$ characteristic time
$\varphi$ angle, function of $\eta$
$\bar{\chi}$ hypersonic interaction parameter
$\chi^2$ variable defined by (2–40) and (2–42)
${}_1\chi^2$ variable defined by (2–43)
${}_2\chi^2$ variable defined by (2–44)
$\chi_i^2$ Chi-square distribution with $i$ degrees of freedom
$\Omega$ nondimensional relative speed

SUBSCRIPT

$b$ body
$c$ cell
fm free molecule value
$i$ i-th step, i-th class, inviscid
$j$ j-th step, j-th class
max maximum value
$ab$ in cell adjacent to body
$o$ stagnation
$s$ behind Rankine-Hugoniot shock
1 first step, first class
2 second step, second class
$\infty$ uniform flow

SUPERSCRIPT

$\sim$ nondimensionalized by quality in uniform flow
$'$ after collision

## I. INTRODUCTION

The flow field around a body immersed in a hypersonic rarefied gas flow is different from that at ordinary densities, because the rarefaction of the flow causes several characteristic phenomena, such as the thickening of the shock wave, which can be neglected under normal circumstances.

It is difficult to solve the entire flow field with a single strategy, and then several methods of analysis to deal with some specific regime of the flow have been proposed. Investigations of the hypersonic flow past a flat plate and a blunt body are

summarized respectively in § 1 and § 2 (an excellent review of these problems is given in Ref. 1), and Monte Carlo studies are surveyed and the outline of the present study is described in § 3 of this chapter.

### *§ 1. Hypersonic Rarefied Flow past Sharp-Leading-Edge Flat Plate*

The hypersonic rarefied flow past a semi-infinite sharp-leading-edge flat plate is outlined below. There is a hypersonic interaction region on the upstream side of the classical boundary layer region, where the thin shock wave and the thick boundary layer interact through a narrow inviscid flow region, which is divided into two subregions, that is, the weak and strong interaction regions, according to the degree of the interaction. The weak and strong interaction theories are applied to these subregions, respectively [*2, 3*]. The solution of the weak interaction theory coincides, of course, with that of the classical boundary layer theory in its downstream limit.

There is a merged layer, where the shock wave and the boundary layer are merged and the inviscid flow vanishes, on the upstream side of the strong interaction region. Oguchi [*4*] proposed a viscous layer theory on the assumption that the shock wave is still thin, and obtained a wedge-like solution as the upstream limit, a strong interaction-type solution as the downstream limit and a locally similar solution between the upstream and downstream limits. He also obtained a solution taking account of the effect of the velocity slip at the body surface [*5*]. The thin shock wave assumption was removed [*6–9*] subsequently, because it was experimentally found that the incident gas is not compressed up to the density given by the Rankine-Hugoniot relation and that the shock layer is no longer thin enough to be treated as a discontinuity [*18, 20*]. Recently Shorenstein et al. [*9*] refined Oguchi's analysis, that is, they included the effects of the shock curvature, the velocity slip at the wall and the finite Mach number. Their results agree quantitatively well with the experimental results obtained in the same flow conditions.

The continuum flow theory can not be applied to the region upstream of the merged layer regime, since the physical properties there are not so different from those in the undisturbed rarefied flow. Therefore, the analyses of this regime are performed by the kinetic theory of gases [*10, 11*].

The free molecule flow theory [*12, 13*] may be invalid even at the leading edge, since the effect of the body penetrates into the region somewhat upstream of the body. However, the solution by the free molecule theory is often used to examine the validity of the theoretical and experimental results.

Recently Huang et al. [*14*] obtained a solution covering almost all the flow regions cited above, integrating the B-G-K model equation by a discrete ordinate method in the case of a supersonic flow. Afterwards the solution in the case of a hypersonic flow was also obtained [*15*].

Numerous experimental studies with respect to the surface pressure, skin friction, heat transfer and shock shape are reported [*16–29*]. The technique of the electron beam densitometry is considered to be desirable, because it enables us to obtain informations of the wide flow field without disturbing it by a probe [*24–29*].

## § 2. *Hypersonic Rarefied Flow past Blunt Body*

The hypersonic flow past a blunt body is difficult to solve even if the flow can be regarded as inviscid, mainly because of the existence of the detached bow shock and the subsonic flow region. The additional "rarefied" condition makes the problem more complex [*30*], unless the free molecule flow condition is satisfied. (In the free molecule flow the problem is very simple and its solution can be easily obtained [*64, 65*].) Consequently the subjects referred to subsequently have been investigated.

*Physical Properties along Stagnation Streamline*

Ho et al. solved the Navier-Stokes equations introducing a local similarity scheme on the assumption of a thin shock layer, and found the changes in the physical properties along the stagnation streamline between the shock wave and the body wall [*31, 111*]. Cheng [*32*] removed the thin shock wave assumption and found the solution in the shock layer. Oguchi et al. [*33*] refined the Cheng's method so that the discontinuity between the solutions of the shock and boundary layers was removed. Levinsky et al. [*34*] and Kao [*35*] solved the problem independently by the integration of the Navier-Stokes equations from the forward stagnation point of the body to the upstream of the shock layer. All works cited above are on the basis of the continuum theory. On the other hand, Ho [*36*] attacked this problem from the kinetic theory side, that is, he used the B-G-K model equation with Kao's solution as the zeroth approximation. Recently Sugimura et al. [*37*] obtained the density profile along the stagnation streamline with the kinetic theory by the moment method.

Experimental studies were performed by the electron beam densitometry [*26,38, 39, 112–114*]. Some of above references also dealt with the stagnation region off the stagnation streamline.

*Pressure at Forward Stagnation Point of Body*

In a low density wind tunnel study it is very important to obtain the relation between the pressure at the forward stagnation point of the body and the Pitot pressure given by the Rankine-Hugoniot relation, since the flow properties are determined by the latter (often referred to as the ideal impact pressure) and the pressure measured by the Pitot tube is the former (often referred to as the measured impact pressure), and they are in general not same.

The theoretical treatment is very laborious as pointed out in the preceding paragraph and a near free molecule approach is reported [*40*] in addition to the references cited above, and this problem mainly is experimentally investigated [*41–44*].

*Stagnation Point Heat Transfer*

It is important to evaluate the heat transfer from the surrounding gas to the forward stagnation point of the blunt body, since, for example, it is an information necessary in designing a re-entry body.

Reshotko et al. [*45*] solved this problem by the potential flow and boundary layer theories on the assumption of the existence of a thin shock wave, an inviscid flow region and a boundary layer. Lees [*46*] obtained the solution of the equation

based on the modified Newtonian theory and the boundary layer theory with the local similarity. Ferri et al. [*47, 48*] took account of the vorticity which is one of the second-order effects. Van Dyke [*49, 50*] used the second-order boundary layer equation taking account of the seven second-order effects. Cheng et al. made use of a shock-boundary-layer matching scheme, that is, on the basis of the assumption that the two layers are thick [*32, 51*].

Experimental results are reported by several authors [*17, 47, 48, 52, 115*].

*Surface Pressure Distribution*

The pressure distribution on the body surface predicted by the modified Newtonian theory (inviscid), though simple, is an excellent approximation in the front part of the body even in the rarefied flow. The calculation by Gorislawsky et al. [*111*] and several experiments [*53–55, 116*] confirm this fact. There is no theory available to predict the pressure distribution in the rear part of the body except for the free molecule flow theory, and the study in this part is made by the experiments.

*Heat Transfer Distribution*

The heat transfer from the gas to the body surface decreases monotonically from the forward stagnation point to the separation point. Davis et al. [*56*] used the first- and second-order boundary layer equations with thin shock layer assumption and evaluated the second-order effects. Lees's result cited above [*46*] is often used to examine the validity of the experimental results because of the simplicity of his formula. Experimental results are obtained by several authors [*17, 54, 57, 58, 115*].

*Wake*

Theoretical treatments [*59*] include many rough assumptions or empirical relations, since the flow field in the front part of the body is not perfectly solved as shown above. Therefore the studies in this regime are mainly based on the experiments [*60–64*] except those by the free molecule flow theory [*63–65*].

*Drag*

Drag force exerted by the flow on the body is calculated from the distributions of surface pressure and skin friction. Therefore it is very difficult to evaluate it theoretically, since there is no available theory about the surface pressure and skin friction distributions, especially in the rear part of the body, as mentioned above. Davis et al. [*56*] calculated the drag of a sphere by the first- and second-order boundary layer theory, and a few investigations by the near free molecule flow theory are reported [*37, 66–68*]. Recently Whitfield [*69*] obtained, by the kinetic theory, an expression which is valid in a relatively wide regime between the continuum and free molecule limits. Many authors reported experimental results covering wide Mach number, Knudsen number and temperature ratio ranges [*70–77*].

## *§ 3. Monte Carlo Studies*

Many studies by the Monte Carlo method about the rarefied gas dynamics have been made since it enables us to treat problems which can not be otherwise solved theoretically, and which are practically impossible to investigate experimentally.

Relaxation phenomena [*78–80*], the relaxation of binary and ternary gas mixtures [*81*], shock wave structures [*79, 82–84*], shock waves in binary gas mixtures [*85, 86*], the formation and reflection of shock waves [*87*], Couette flows [*80, 88, 89, 117*], the heat transfer between parallel plates [*80, 90, 91, 118*] and the rarefied flow through ducts or tubes [*92, 93*] are reported. Two dimensional and axisymmetric problems, that is, flows past a flat plate, a wedge, a circular cylinder, a cone and a sphere are mainly investigated by the technique developed by Bird [*94–97*]. Recently Yoshizawa [*98*] obtained the results of the region very close to the leading edge of a flat plate on the assumption that the distribution function defined in each physical cell is a product of function of $V_X$ component only and that of $V_Y$ component only. His method explicitly involves the concept of the evolution of the probability distribution, and so is distinguished from that of Bird.

The Monte Carlo method is hard to be applied to subsonic problems, since the effect of the body extends far and wide, and then a very wide flow field is to be considered. Therefore, the subsonic problems treated by this method are restricted to those with two symmetrical planes or the outer boundaries. Yasinsky [*119*] investigated the flow fields about the staggered cylinder and wing in subsonic flows, and showed the appearance of a supersonic region in the latter case. Applications of the Monte Carlo method to the reacting gas and the rarefied plasma were also made [*99, 100*].

In the present paper the flow fields over a flat plate, and around a circular cylinder and a sphere immersed in hypersonic rarefied flows are calculated by a Monte Carlo method which does not include the sampling in the velocity space and then is similar to that of Bird, and the quantities are obtained which are important from the practical viewpoint, that is, the pressure, the skin friction, the drag force and the heat transfer. Experiments are also carried out in order to obtain the surface pressure distributions of a circular cylinder and a sphere, and the drag of a sphere in order to examine the Monte Carlo results.

The Monte Carlo method used in this study is discussed in chapter II, the experimental apparatus is described in chapter III, the Monte Carlo and experimental results are compared with those obtained by other authors and discussed in chapter IV, and the conclusion of this study is described in chapter V, respectively.

## II. Description of Method

One of the features of the Monte Carlo method is to directly simulate some statistical process by generating the random numbers in obedience to the probability density function governing the process. Therefore, if the probability density function is known, even if it is empirical and can not be written analytically, the solution can be obtained. It is advantageous that it is unnecessary to write down the equation system exactly describing the process.

In the rarefied gas dynamics frequently the gas is not regarded as a continuum but is considered to be a set of gas particles in a so-called thermal motion obeying some probability density function, in particular the Maxwell-Boltzmann distribu-

tion function in the equilibrium, and is studied by the kinetic theory of the gas particles. The application of the Monte Carlo method to the problem in the rarefied gas dynamics requires no effort to obtain the solution of the Boltzmann equation which is a nonlinear integro-differential equation and can not be solved easily. Several works have been made by the aid of large electronic computers, and show that the Monte Carlo method is of use in this field as described in the preceding chapter. Of course the problem in the conventional gas dynamics can be treated by this method in principle, which, however, demands a monstrous electronic computer, and then is not practical.

The flow fields above a flat plate and around a circular cylinder and a sphere in steady rarefied supersonic flows are treated in this study, making use of a direct simulation technique similar to that developed by Bird, which is more suitable for the two-dimensional and axisymmetric cases than others'. The method is proven to be equivalent to the procedure to introduce the Boltzmann equation in Ref. 120. The steady solution is obtained as the non-steady solution at the time of infinity by this method. Two variations of the method are used in the case of the two-dimensional flow. One of them takes account of the effect of the velocity component along the third coordinate axis (Method A), but another does not (Method B), the latter of which is applied to the cases where the Knudsen numbers are small. (Suffix a is attached to the number of the formula for the Method A and b for the Method B in the following sections.) The minimum Knudsen numbers, which are restricted by the total computer storage, are 0.025, 0.05 and 0.1 in the cases of the flat plate, the circular cylinder and the sphere, respectively, making use of a HITAC 5020F computer with core memories of 65K words.

Before the calculation the following assumptions are made.

(1) Only binary collisions occur.

(2) Gas molecules are hard sphere molecules
($\gamma=5/3, \lambda\propto n^{-1}, \mu\propto\sqrt{T}, Pr=2/3$).

(3) Molecules reflect fully diffusely from the body surface (fully accommodated).

The procedure of the Monte Carlo calculation is explained in the following sections.

## *§ 1. Introduction of Dimensionless Quantities*

The $x$-axis is taken parallel to the direction of the uniform flow, and the $y$-axis perpendicular to it, and to the body axis in the two-dimensional case (Fig. 1). Linear dimensions are nondimensionalized by the mean free path in the uniform flow $\lambda_\infty=(\sqrt{2}\pi\sigma^2 n_\infty)^{-1}$, where $\sigma$ and $n_\infty$ are the diameter of the molecule and the number density in the uniform flow, respectively, that is, the nondimensional coordinates are defined as follows.

$$X=\frac{x}{\lambda_\infty},\quad Y=\frac{y}{\lambda_\infty},\quad Z=\frac{z}{\lambda_\infty}.$$

Velocity components and speeds are nondimensionalized by the most probable

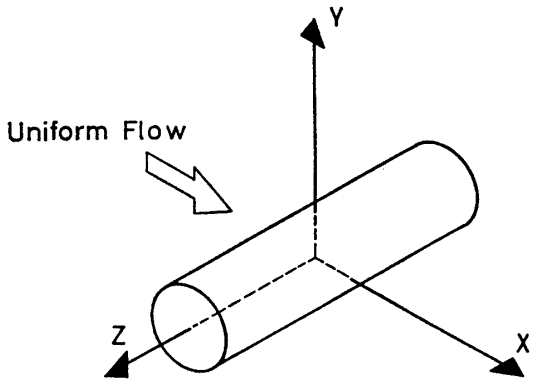


Two-Dimensional Flow

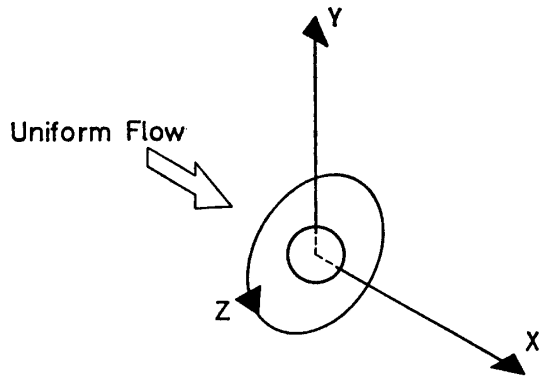


Axisymmetric Flow

FIG. 1. Coordinate System

speed in the uniform flow $c_{m_\infty}=\sqrt{2RT_\infty}$, where $R$ and $T_\infty$ are respectively the gas constant for the gas considered and the temperature in the uniform flow, for example, velocity components and thermal velocity components of a molecule and the uniform flow velocity are expressed as follows.

$$V_X=\frac{v_x}{c_{m_\infty}},\quad V_Y=\frac{v_y}{c_{m_\infty}},\quad V_Z=\frac{v_z}{c_{m_\infty}},$$

$$C_X=\frac{c_x}{c_{m_\infty}},\quad C_Y=\frac{c_y}{c_{m_\infty}},\quad C_Z=\frac{c_z}{c_{m_\infty}},\quad S=\frac{u_\infty}{c_{m_\infty}}$$

where S is the so-called speed ratio of the uniform flow, and is written in terms of the uniform flow Mach number $M$ as $S=\sqrt{\gamma/2}\,M$.

Similarly, the number density, the temperature and the time are nondimensionalized by the quantities in the uniform flow:

$$\tilde{n}=\frac{n}{n_\infty},\quad \tilde{T}=\frac{T}{T_\infty},\quad \tilde{t}=\frac{t}{t_{c\infty}},$$

where $t_{c_\infty}=\lambda_\infty/c_{m_\infty}$. It is possible that the time is nondimensionalized by the mean collision time in the uniform flow, which, however, can not satisfy the relation that the linear dimension is equal to the product of the speed and the time after the nondimensionalization.

## § 2. *Uniform Flow*

It is desirable but impossible in practice that the probability density function with the six arguments $C_X, C_Y, C_Z, X, Y,$ and $Z$ whose domains are respectively from minus infinity to plus infinity be used in the calculation. Therefore, a truncated probability density function is used. The truncation is performed by the restrictions of the ranges of possible values of the arguments as shown below. It is soon noticed that the third coordinate $Z$ need not be taken into account, because of the symmetricity of the flow with respect to a $Z$=const. plane in a two-dimensional or axisymmetric flow. The domain with negative $Y$ can be also excluded from the consideration in the present cases.

What characterize a molecule in the two-dimensional and axisymmetric flows are its coordinates $X$ and $Y$, and its velocity components $V_X, V_Y$ and $V_Z$ (the last is not used in the Method B). In the uniform flow, $X$ and $Y$ are uniformly distributed in the space, and $V_Y$ and $V_Z$ obey the Maxwell-Boltzmann distribution, on the other hand $V_X$ is the sum of the thermal velocity component with the Mexwell-Boltzmann distribution and the uniform flow velocity.

*Two-Dimensional Case*

The ranges of possible values of $X$ and $Y$ are respectively restricted from-$A$ to $A$ and from 0 to $A$. Three boundaries $X=-A$, $X=A$, and $Y=A$ determined by the value of the parameter $A$ are to be located so far from the body that the disturbance from the body can not arrive at them. This condition is often not satisfied except at the upstream boundary $X=-A$, because the limitation of the computer storage does not permit a very large value of $A$. However, the boundaries are considered to affect only some region which is very narrow, and then the region near the body, which is most important, is scarcely affected by the boundaries. The range of possible values of $Z$ can be taken arbitrarily, because it is unimportant as discussed above. It is selected from $-1/2$ to $1/2$ so that the volume of the unit cell is equal to unity.

The division of the flow field ($-A\leqq X<A, 0\leqq Y<A, -1/2<Z<1/2$) by the cells, each of which is a cube with the volume of unity makes $2A^2$ cells (see Fig. 2a). Let $N_0$ be the total number of the molecules initially generated, and then the number density in the uniform flow or the number of the molecules initially assigned to each cell is

$$n_\infty=\frac{N_0}{2A^2}. \tag{2-1}$$

The coordinates of a molecule in the $(X_c, Y_c)$ cell (a cell is distinguished by the coordinates of its left lower corner) are given as follows.

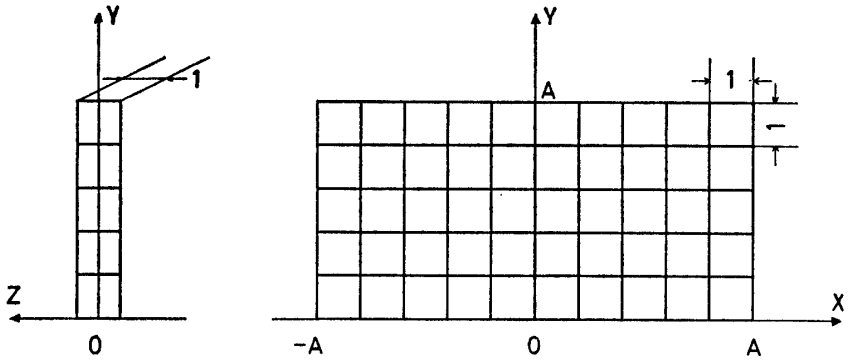


(a)

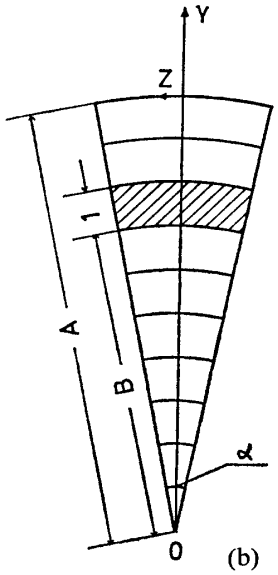


(b)

FIG. 2. (a) Two-Dimentional Flow Field
(b) Axisymmetric Flow Field

$$X=X_c+R_i \tag{2-2}$$

$$Y=Y_c+R_j, \tag{2-3}$$

where $R_i$ and $R_j$ are random numbers uniformly distributed in the range 0 to 1.

*Axisymmetric Case*

The flow field is cut by the sector with the apex angle $\alpha$ in the $Y$-$Z$ plane (see Fig. 2b), and its cross sectional area is $A^2\alpha/2$, and the area of the hatched part is $(2B+1)\alpha/2$. If the same division in the $X$-$Y$ plane as in the two-dimensional case is made, the number of the molecules contained in a sectorial slice is $N_0/2A$. Therefore, $(2B+1)\ N_0/2A^3$ molecules are assigned to the hatched $(X_c, B)$ cell, and the number density in the uniform flow is

$$n_\infty=\frac{N_0}{A^3\alpha}. \tag{2-1'}$$

The value of $\alpha$ can be taken arbitrarily, and is equal to two in this study so that the volume of the cell just adjacent to the center line is unity.

It may arise that $(2B+1)N_0/2A^3$ is not an integer, because the upper limit of $N_0$ is decided by th computer storage. In that case it is determined by the second scheme in § 8 how many molecules are to be generated in obedience to the probability $(2B+1)N_0/2A^3$.

If one molecule is determined to belong some $(X_c, B)$ cell, its $X$-coordinate is decided by (2–2), but $Y$-coordinate is not given by (2–3), since the width of the flow field increases proportionally to $Y$ and therefore the number of the molecules is also a linear function of $Y$. Let $aY$ be the probability density function of $Y$-coordinate of one molecule contained in the $(X_c, B)$ cell, and then $\int_B^{B+1} aYdY=1$ from the definition. Therefore, the value of the constant $a$ is $2/(2B+1)$. By the first scheme in § 8,

$$\frac{2}{2B+1}\int_B^{S_i} YdY=R_i, \quad \text{and then} \quad S_i=\sqrt{B^2+(2B+1)R_i}$$

After all it is seen that in the axisymmetric case (2–3′) is used instead of (2–3) in order to obtain $Y$-coordinate of a molecule in the $(X_c, Y_c)$ cell.

$$Y=\sqrt{Y_c^2+(2Y_c+1)R_j} \tag{2–3′}$$

*Velocity Components*

The thermal speed $C$ obeys the Maxwell-Boltzmann distribution function (2–4).

$$P_M=KC^2\exp(-C^2) \tag{2–4}$$

$P_M$ has the maximum value at $C=1$, then,

$$\frac{P_M}{P_{M\max}}=C^2\exp(1-C^2). \tag{2–5}$$

How to generate the random number which obeys (2–5) is discussed in § 8 (second scheme). The range of possible values of $C$ is restricted from zero to three in this study. Once the value of $C$ is found, three thermal velocity components are calculated as follows, because the distribution of the direction of the thermal velocity is uniform in the space.

$$\begin{aligned} C_X&=C\sin\pi R_i\cos 2\pi R_j \\ C_Y&=C\sin\pi R_i\sin 2\pi R_j \\ C_Z&=C\cos\pi R_i \end{aligned} \tag{2–6a}$$

where $R_i$ and $R_j$ are rectangular random numbers in the range 0 to 1. Three velocity components of a molecule in the uniform flow are, then,

$$\begin{aligned} V_X&=S+C_X \\ V_Y&=C_Y \\ V_Z&=C_Z \end{aligned} \tag{2–7a}$$

In the Method B the terms with the argument $R_i$ in (2–6a) are respectively replaced by their mean values in the range of $R_i$ from 0 to 1, that is, (2–6b) and (2–7b) are used to obtain the velocity components of the molecule in the uniform flow.

$$C_X=\frac{2}{\pi}C\cos 2\pi R_i \qquad C_Y=\frac{2}{\pi}C\sin 2\pi R_i \tag{2–6b}$$

$$V_X=S+C_X \qquad V_Y=C_Y \tag{2–7b}$$

Thus, the effect of the velocity component along the third coordinate axis is neglected, and then it is implicitly assumed that it scarcely changes from that given by the third equation of (2–6a) for the Method $B$ to be valid.

## § 3. *Insertion of Body*

When $N_0$ molecules are distributed into the flow field, the flat plate with the leading edge at $(X=A-1/Kn,\ Y=0)$ and the trailing edge at $(X=A,\ Y=0)$ or the circular cylinder or the sphere with the center $(0,\ 0)$ and the radius $1/2Kn$ is inserted into the flow field. The length of the flat plate parallel to the uniform flow or the diameter of the circular cylinder or the sphere is taken as the characteristic dimension in defining the Knudsen number.

The molecules found inside the body are omitted from the calculation, and the cells perfectly wrapped in the body are considered to be lost. The volumes of the cells which are partly cut off by the body are recalculated.

## § 4. *Calculation of Collision*

There appears the region where $n$ is large and $\lambda$ is small in the neighborhood of the body, because of the collisions between the molecules and the body. The cells there may be divided into smaller cells, since the collisions are considered to occur between the molecules apart by the order of magnitude of $\lambda$ from each other (see the introduction of (2–11)), and in order to obtain more precise information about the flow.

In this study a cell is divided into two or four smaller cells, when it is necessary, as shown below.

| | | |
|---|---|---|
| | $\tilde{n}\leq n_1$ | kept intact |
| | $n_1<\tilde{n}\leq n_2$ | divided into two |
| | $n_2<\tilde{n}$ | divided into four |
| where | $n_1=1.2,\ n_2=2.4$ | for the flat plate |
| | $n_1=1.5,\ n_2=3.0$ | for the circular cylinder and the sphere |

The division of the cell adjacent to the body surface is very laborious in the case of the circular cylinder or the sphere, because the function $f(X)$ representing the body surface is curved. In practice no division into four cells may occur in the case of the flat plate. In the Method B the divisions of the cell are not programmed, so as to spare the computer storage. Therefore, the Method B is less strict in case that the density becomes very high.

The molecular collisions are considered to occur simultaneously in all cells and successively in a cell. The calculation of the collisions is made as follows. Firstly, it is decided whether or not collisions can occur in the cell considered in an appropriate time interval $\Delta t$, making use of random numbers. Secondly, if the molecules to collide are found, their velocity components after the collision are evaluated by using random numbers, and then the molecules are moved by the distance of the product of the velocity after the collision and the time interval $\Delta t$. The molecule which undergoes no collision is moved by the product of its intact velocity and $\Delta t$. Finally, it is investigated what cell contains each molecule, and all molecules are re-arranged for the next calculation, some cells are divided as mentioned above if necessary, and the next collision calculation is made. The repetition of this process, which is sometimes called the collision cycle, produces a macroscopically steady condition. Once the steady condition is established, the sampling of the data is begun (see § 6 and 7).

The time interval $\Delta t$ should be smaller than the characteristic time $\tau_f = l/u_\infty$ where $l$ is the characteristic dimension of a cell, since the presence of the collisions and the velocities after the collisions are calculated on the basis of the condition at some instant. The following relation is obtained in a nondimensional form.

$$\Delta \tilde{t} < \tilde{\tau}_f = O\left(\frac{1}{S}\right) \tag{2-8}$$

*§ 4–1. Choice of Pair of Molecules to Collide I*

The number of the times of the collision taking place per unit time in the cell with the volume $V$ and the number of the molecules $N$ is [*101*]

$$\frac{n}{2}\nu V = \frac{N}{2}\nu = \frac{N}{2}\frac{\bar{c}}{\lambda},$$

where $\nu$ and $\bar{c}$ are the collision frequency and the mean thermal speed, respectively. The mean time $\tau_c$ necessary for one collision is, therefore,

$$\tau_c = \frac{2}{N}\frac{\lambda}{\bar{c}}. \tag{2-9}$$

The probability $P_c$ in which one collision takes place in the time interval $\Delta t$ in that cell is considered to be given as (2–10).

$$P_c = \frac{\Delta t}{\tau_c} = \frac{\Delta \tilde{t}}{\tilde{\tau}_c} = \frac{N \tilde{c} \Delta \tilde{t} \tilde{n}}{2} \tag{2-10}$$

The presence of a collision can be examined by comparing $P_c$ with a rectangular random number $R_i$ in the range 0 to 1, that is, a collision occurs in that cell if $P_c$ is equal to or greater than $R_i$ (second scheme in § 8). If it is true that a collision occurs in the cell, a collision pair (two molecules to collide with each other) can be chosen as shown below. The probability $P_m$ in which any two molecules collide with each other is proportional to the relative speed $V_R$ of them from the analogy of (2–9) and (2–10) neglecting the difference between their coordinates. (Recall that the dimension of a cell, and then the distance between two molecules arbitrarily chosen in that cell are always smaller than the mean free path there at least in the Method A.) It is easily seen that the collision pair can be chosen by the probability (2–11),

$$\frac{P_m}{P_{m\max}}=\frac{V_R}{V_{R\max}}, \tag{2–11}$$

where $V_{R\max}$ is the maximum value of $V_R$-s for all the combinations of the molecules in the cell.

*§ 4–2. Choice of Pair of Molecules to Collide II*

The way mentioned in § 4–1 is strictly theoretical, but it increases the complexity of the calculation and demands the superfluous computer storage to calculate and store $\bar{c}$ at each cell beforehand. The next way proposed by Bird is simpler.

The time required by the collision of two molecules which are chosen arbitrarily in the cell and whose relative speed is $V_R$ is analogous to (2–9), that is,

$$\tilde{\tau}_c=\frac{2\tilde{\lambda}}{NV_R} \tag{2–12}$$

The probability in which they collide in the interval $\Delta t$ is

$$P_c=\frac{\Delta\tilde{t}}{\tilde{\tau}_c}=\frac{NV_R\Delta\tilde{t}\tilde{n}}{2} \tag{2–13}$$

A collision pair can be chosen by a single step according to this criterion. This criterion is always used in the Method B.

*§ 4–3. Selection of Time Interval $\Delta t$*

The probability $P_c$ in (2–10) or (2–13) can not exceed unity in principle. Rewriting (2–10),

$$P_c=\frac{N\bar{c}n}{2c_{m\infty}n_\infty}\Delta\tilde{t}\leq 1.$$

Then,

$$\Delta\tilde{t}\leq\frac{\sqrt{\pi}}{N\tilde{n}\sqrt{\tilde{T}}}$$

Finally (2–14) is obtained for the above inequality to be valid for all the cells.

$$\Delta\tilde{t} \leq \frac{\sqrt{\pi}}{(N\tilde{n}\sqrt{\tilde{T}})_{\max}}, \tag{2–14}$$

where $(N\tilde{n}\sqrt{\tilde{T}})_{\max}$ is the maximum value of $(N\tilde{n}\sqrt{\tilde{T}})$-s at all the cells in the flow field, and can be inferred beforehand for the given problem. The value of $\Delta\tilde{t}$ may be so selected as to satisfy (2–8) and (2–14).

The value of $\Delta\tilde{t}$ can also be so decided that each molecule in the cell whose number of the times of the collision may be maximal undergoes at most one collision. If $P_c$, which is the collision frequency rather than the probability in this case, is greater than unity, the next collision can occur in obedience to the following expression.

$$P_c = \frac{\Delta\tilde{t} - \tilde{\tau}_{c_1}}{\tilde{\tau}_{c_2}}$$

Thus, the possibility of the collision remains in the cell, until $P_c$ becomes negative. The inequality for $\Delta\tilde{t}$ is

$$\Delta\tilde{t} \leq \frac{\sqrt{\pi}}{2} \frac{1}{(\tilde{n}\sqrt{\tilde{T}})_{\max}}. \tag{2–15}$$

The value of $\Delta\tilde{t}$ is so selected as to satisfy at least (2–8) and (2–15) throughout this study.

### *§ 4–4. Velocity Components after Collision*

The velocity components after a collision are given by the following formulae, since the momentum and the energy are conserved throughout the collision [*102*].

$$\begin{aligned}
V'_{X_1} &= V_{X_1} + \xi\Omega \\
V'_{Y_1} &= V_{Y_1} + \eta\Omega \\
V'_{Z_1} &= V_{Z_1} + \zeta\Omega \\
V'_{X_2} &= V_{X_2} - \xi\Omega \\
V'_{Y_2} &= V_{Y_2} - \eta\Omega \\
V'_{Z_2} &= V_{Z_2} - \zeta\Omega \\
\Omega &= \xi(V_{X_2} - V_{X_1}) + \eta(V_{Y_2} - V_{Y_1}) + \zeta(V_{Z_2} - V_{Z_1}),
\end{aligned} \tag{2–16a}$$

where $\xi, \eta, \zeta$ are the direction consines of the impact line of the molecules and written as follows.

$$\begin{aligned}
\xi &= \sin \pi R_i \cos 2\pi R_j \\
\eta &= \sin \pi R_i \sin 2\pi R_j \\
\zeta &= \cos \pi R_i
\end{aligned} \tag{2–17a}$$

Here again $R_i$ and $R_j$ are rectangular random numbers in the range 0 to 1. Similarly, in the Method *B*,

$$\begin{aligned} V'_{X_1} &= V_{X_1} + \xi\Omega \\ V'_{Y_1} &= V_{Y_1} + \eta\Omega \\ V'_{X_2} &= V_{X_2} - \xi\Omega \\ V'_{Y_2} &= V_{Y_2} - \eta\Omega \end{aligned} \tag{2–16b}$$

$$\begin{aligned} \Omega &= \xi(V_{X_2} - V_{X_1}) + \eta(V_{Y_2} - V_{Y_1}) \\ \xi &= \cos 2\pi R_i \\ \eta &= \sin 2\pi R_i \end{aligned} \tag{2–17b}$$

are obtained.

Equation (2–17) means that the distribution of the direction of the impact line is uniform in the space, which is valid in case of the collision of the hard sphere molecules.

## § 4–5. *New Position and Velocity of Molecule*

*Two-Dimensional Case*

A molecule with the velocity components $V_X$, $V_Y$ and $V_Z$ at the coordinates $X_1$ and $Y_1$ at some instant has the same velocity components at the coordinates $X_2$ and $Y_2$, given by (2–18), after the interval $\Delta\tilde{t}$.

$$\begin{aligned} X_2 &= X_1 + V_X \Delta\tilde{t} \\ Y_2 &= Y_1 + V_Y \Delta\tilde{t} \end{aligned} \tag{2–18}$$

*Axisymmetric Case*

The directions of the $Y$-axes before and after the motion of the molecule are different, therefore the velocity components are also different. The following relations about the new coordinates and velocity components of a molecule are obtained from Fig. 3 which shows the motion of a molecule in the $Y$-$Z$ plane.

$$\begin{aligned} X_2 &= X_1 + \Delta\tilde{t} V_X \\ Y_2 &= \sqrt{(V_{Y_1}\Delta\tilde{t} + Y_1)^2 + (V_{Z_1}\Delta\tilde{t})^2} \\ \varphi &= \tan^{-1} \frac{Y_1 + V_{Y_1}\Delta\tilde{t}}{V_{Z_1}\Delta\tilde{t}} \\ V_{Y_2} &= V_{Z_1}\cos\varphi + V_{Y_1}\sin\varphi \\ V_{Z_2} &= V_{Z_1}\sin\varphi - V_{Y_1}\cos\varphi \end{aligned} \tag{2–18′}$$

It is the reason why the Method B can not be applied to the axisymmetric case that $V_{Y_2}$ is calculated not only by $V_{Y_1}$ but also by $V_{Z_1}$.

## § 5. *Boundary Conditions*

Three planes $X=\pm A$, $Y=A$ are sinks of the molecules. In other words, when a molecule passes through one of them, the molecule is omitted from the calculation. $Y=0$ plane is the one of the specular reflection in the case of the two-dimensional flow (In the case of the axisymmetric flow $Y$-coordinate of a molecule

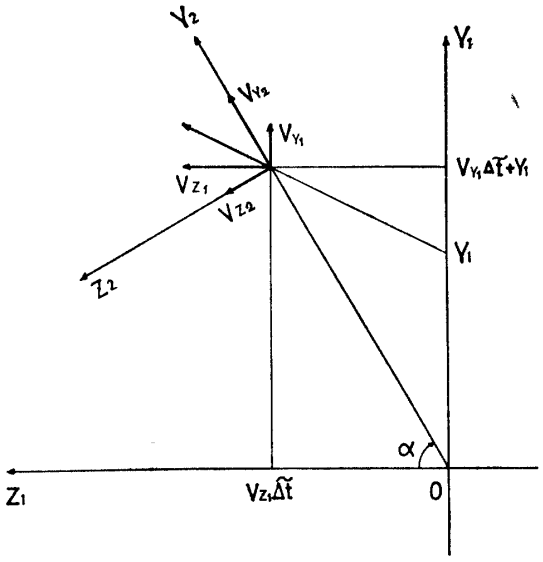


FIG. 3. Molecular Motion in Y-Z Plane in Axisymmetric Flow

is always non-negative by the second formula of (2–18′)).

The molecules in the uniform flow move along the $X$-axis in the interval $\Delta\tilde{t}$ by the distances, the mean value of which is equal to the product $S\Delta\tilde{t}$. In order to maintain the inflow of the uniform flow, the molecules with uniform flow velocity components, given by (2–5) to (2–7), are generated at every collision cycle as shown below.

*Two-Dimensional Case*

$$\begin{aligned} N_i &= \frac{N_0}{2A^2} S\Delta\tilde{t} \\ X &= -A + S\Delta\tilde{t}R_i \\ Y &= Y_c + R_j \end{aligned} \tag{2–19}$$

*Axisymmetric Case*

$$\begin{aligned} N_i &= \frac{2Y_c+1}{2A^3} N_0 S\Delta\tilde{t} \\ X &= -A + S\Delta\tilde{t}R_i \\ Y &= \sqrt{Y_c^2+(2Y_c+1)R_j} \end{aligned} \tag{2–19′}$$

In the above formulae $N_i$ is the number of the molecules to be generated in the region $Y_c \leq Y < Y_c+1$ $(Y_c=0, 1, \cdots, A-1)$, and $X$ and $Y$ are coordinates of a molecule determined to be generated.

If the molecules reflect fully diffusely from the body surface, the reflected molecules have the speeds obeying the Maxwell-Boltzmann distribution (2–20) at the body temperature $T_b$

$$\frac{P_M}{P_{M_{\max}}}=\frac{C^2}{\tilde{T}_b}\exp\left(1-\frac{C^2}{\tilde{T}_b}\right) \tag{2-20}$$

The range of possible values of $C$ is taken from zero to three times square root of the body temperature ($0\leq C\leq 3\sqrt{\tilde{T}_b}$). A molecule reflected from the body surface has the velocity components given below.
In the Method A,

$$\begin{aligned} V_X&=C\sin\pi R_i\cos(\pi R_j+\delta)\\ V_Y&=C\sin\pi R_i\sin(\pi R_j+\delta)\\ V_Z&=C\cos\pi R_i. \end{aligned} \tag{2-21a}$$

In the Method B,

$$\begin{aligned} V_X&=\frac{2}{\pi}C\cos(\pi R_i+\delta)\\ V_Y&=\frac{2}{\pi}C\sin(\pi R_i+\delta). \end{aligned} \tag{2-21b}$$

$$\delta=\tan^{-1}\left(\frac{df(X)}{dX}\right), \tag{2-22}$$

where $f(X)$ is the function representing the body surface (see Fig. 4).

It is to be noted that the body temperature $T_b$ must be not so different from the temperature $T_\infty$ in the uniform flow in the Method B, since the distribution of $V_Z$ is assumed to undergo a little change throughout the flow field.

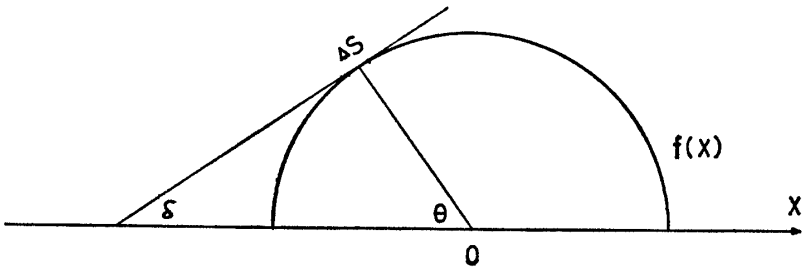


Fig. 4. Some Relationships at Body

## § 6. *Number Density, Macroscopic Velocity and Temperature*

Once the steady condition is established, the sampling of the macroscopic quantities are started. The sampling is made at intervals of 10 to 20 times $\Delta\tilde{t}$ so as not to be affected by its foregoing step, until the desired accuracy is obtained. Here, it is implicitly assumed that the macroscopic properties are not so altered after the establishment of the steady state and the process to obtain some quantity as a mean value wih respect to many molecules in a cell at a time can be replaced by the similar one with respect to the sum of the molecules at different times whose

number is not so many at a time. The former process is the definition of a macroscopic quantity and the latter is used in the Monte Carlo method, since the total number of the molecules is limited by the computer storage.

The number density is calculated from the number of the molecules in that cell,

$$\tilde{n}=\frac{m}{n_\infty V_c m_s}, \qquad m=\sum_{j=1}^{m_s} N_j, \tag{2-23}$$

where $N_j$ is the number of the molecules in that cell at $j$-th step of the sampling and $m_s$ is the number of the steps of the sampling, and $m$ is the total number of the molecules in that cell at all the steps and is sometimes called the sample size.

The macroscopic velocity components are

$$\begin{aligned}\bar{V}_X&=\frac{1}{m}\sum_{i=1}^{m} V_{X_i}\\ \bar{V}_Y&=\frac{1}{m}\sum_{i=1}^{m} V_{Y_i}\\ \bar{V}_Z&=\frac{1}{m}\sum_{i=1}^{m} V_{Z_i}\end{aligned} \tag{2-24}$$

The temperature is obtained from the formula $3RT=\bar{c}^2$;

$$\tilde{T}=\frac{2}{3}\left\{\frac{1}{m}\sum_{i=1}^{m}(V_X^2+V_Y^2+V_Z^2)-\bar{V}_X^2-\bar{V}_Y^2-\bar{V}_Z^2\right\}. \tag{2-25a}$$

In the Method B, $2RT=\bar{c}^2$, since the degrees of freedom of the molecules are diminished to two;

$$\tilde{T}=\frac{1}{m}\sum_{i=1}^{m}(V_X^2+V_Y^2)-\bar{V}_X^2-\bar{V}_Y^2. \tag{2-25b}$$

### *§ 7. Physical Properties on or near Body*

Physical properties on or near the body are calculated as follows after the establishment of the steady state.

#### *§ 7–1. Slip Velocity*

The slip velocity at the surface of the flat plate is given by the macroscopic $X$ velocity component in the cell just adjacent to the body.

$$V_s=(\bar{V}_X)_{ab} \tag{2-26}$$

The slip velocity evaluated by (2–26) may be overestimated, since molecules apart from the body by the order of magnitude of the mean free path in the uniform flow are included in the summation to obtain $(\bar{V}_X)_{ab}$.

#### *§ 7–2. Surface Pressure*

The surface pressure on the body is calculated from the changes in the momentum of the molecules which collide with the body, that is,

$$p=\frac{m}{\Delta t_s \Delta s}\sum_{\Delta s}\{(v_x-v_x')\cos\theta-(v_y-v_y')\sin\theta\},$$

where $\theta$ is the angle which decides the position on the surface and $\Delta s$ is the surface elements at $\theta$ (see Fig. 4), and m and $\Delta t_s$ are the mass of a molecule and the time interval in which the sampling is made, respectively. The above summation is taken over the molecules colliding to $\Delta s$. A pressure coefficient $C_{p1}$ is defined by (2–27).

$$\begin{aligned} C_{p1}&=\frac{p}{(1/2)\rho_\infty u_\infty^2}=\frac{1}{S^2}\frac{p}{p_\infty} \\ &=\frac{2}{N_\infty S^2 \Delta\tilde{t}_s \Delta\tilde{s}}\sum_{\Delta\tilde{s}}\{(V_X-V_X')\cos\theta-(V_Y-V_Y')\sin\theta\}, \end{aligned} \tag{2–27}$$

where $N_\infty$ is the number of the molecules involved by a volume of unity in the uniform flow. Another pressure coefficient $C_{p2}$ defined by (2–28) is also calculated, which is the ordinary definition of the pressure coefficient.

$$C_{p2}=\frac{p-p_\infty}{(1/2)\rho_\infty u_\infty^2}=C_{p1}-\frac{1}{S^2}. \tag{2–28}$$

Other values of $C_{p1}$ and $C_{p2}$ are calculated by the density and the temperature in the cell just adjacent to the body.

$$C_{p1}=\frac{1}{S^2}(\tilde{n}\tilde{T})_{ab} \tag{2–29}$$

$$C_{p2}=\frac{1}{S^2}(\tilde{n}\tilde{T}-1)_{ab} \tag{2–30}$$

Two values of $C_{p1}$ or $C_{p2}$ are in general not same, since there may exist the density and temperature gradients near the body surface. In the following sections the values of $C_{p1}$ and $C_{p2}$ are given by (2–27) and (2–28), unless otherwise noted.

*§ 7–3. Skin Friction and Drag*

The skin friction exerted on the flat plate or the drag force on the circular cylinder and the sphere is given by the changes in the $X$ component of the momentum of the molecules which collide with the body;

$$d=\frac{m}{\Delta t_s}\sum(v_x-v_x').$$

The above summation is taken over the molecules colliding with $\Delta s$ with respect to the skin friction, and total body surface to the drag force, respectively. The skin friction coefficient $C_f$ and the drag coefficient $C_D$ are defined by (2–31) and (2–32), respectively.

$$C_f=\frac{d}{(1/2)\rho_\infty u_\infty^2 \Delta s}=\frac{2}{N_\infty S^2 \Delta\tilde{t}_s \Delta\tilde{s}}\sum_{\Delta\tilde{s}}(V_X-V_X'). \tag{2–31}$$

$$C_D=\frac{d}{(1/2)\rho_\infty u_\infty^2 s_b}=\frac{2}{N_\infty S^2 \Delta\tilde{t}_s \tilde{s}_b}\sum_{\text{body}}(V_X-V'_X), \tag{2-32}$$

where $s_b$ is the characteristic area of the body and is the cross sectional area perpendicular to the uniform flow of the circular cylinder or the sphere.

### *§ 7–4. Heat Transfer*

The heat transfer per unit area and unit time to the body is obtained from the changes in the kinetic energy of the molecules colliding with the body.

$$\dot{q}=\frac{m}{2\Delta s\Delta t_s}\sum_{\Delta s}(v_x^2+v_y^2+v_z^2-v_x'^2-v_y'^2-v_z'^2).$$

A heat transfer coefficient $C_h$ is defined by (2–33).

$$\begin{aligned} C_h&=\frac{\dot{q}}{\rho_\infty u_\infty c_p(T_0-T_b)}\\ &=\frac{\gamma-1}{\gamma N_\infty S(\tilde{T}_0-\tilde{T}_b)\Delta\tilde{s}\Delta\tilde{t}_s}\sum_{\Delta\tilde{s}}(V_X^2+V_Y^2+V_Z^2-V_X'^2-V_Y'^2-V_Z'^2), \end{aligned} \tag{2-33}$$

where $c_p$ and $\gamma$ are the specific heat at constant pressure and the specific heat ratio, respectively. $T_0$ is the stagnation temperature of the uniform flow and is given by (2–34).

$$\tilde{T}_0=1+\frac{\gamma-1}{2}M^2=1+\frac{\gamma-1}{\gamma}S^2 \tag{2-34}$$

If $T_b$ is equal to $T_0$, $C'_h$ defined by (2–35) is used

$$C'_h=\frac{\gamma-1}{\gamma N_\infty S\tilde{T}_0\Delta\tilde{s}\Delta\tilde{t}_s}\sum_{\Delta\tilde{s}}(V_X^2+V_Y^2+V_Z^2-V_X'^2-V_Y'^2-V_Z'^2). \tag{2-35}$$

### *§ 8. Generation of Random Number*

Many kinds of the random number are used in the Monte Carlo method. It is important what type of the rectangular random number is generated, since any sort of the random number is produced from the rectangular random number as shown below [*103, 104*].

### *§ 8–1. Rectangular Random Number*

Several rectangular random number tables are already published [*105, 106*]. However, its application is not practical, since it requires superfluous computer storage and its number of the terms is small. Therefore, the random number usually is generated by the use of appropriate arithmetic expressions. In that sense it is distinguished from the real random number, and is called the pseudo-random number.

The congruential method employed in the present study consists of the following formulae.

$$R_{n+2}=\frac{1}{M}F_{n+2},\quad F_{n+2}=[F_n+F_{n+1}]\ (\mathrm{mod}\ M),\quad M=2^{44},\qquad (2\text{–}36)$$

where $M$ is the modulus and $F_0$ and $F_1$ are given initially. A sequence of rectangular random numbers in the range 0 to 1 is obtained by (2–36).

A number $R_{i+1}$ has a strong correlation with $R_i$ in this method. So $R_{i+10}$ is used in the next place of $R_i$ in this study.

### *§ 8–2. Random Number with Specified Distribution Function*

The random number $S_i$ obeying some probability density function can be made of the one $R_i$ uniformly distributed in the range 0 to 1, in the two ways below.
a) There is a theorem that if the random variable $\xi$ has a probability density function $f(\xi)$, the distribution of the random variable

$$\eta=\int_{-\infty}^{\xi}f(x)dx \qquad (2\text{–}37)$$

is uniform in the range 0 to 1. If the above integration is executed and $\xi$ can be described as a function of $\eta$, that is $\xi=\varphi(\eta)$, $S_i=\varphi(R_i)$ is the desired random number which obeys the probability density function $f(\xi)$.

b) When $\xi$ is not written as an explicit function of $\eta$, the routine described below is available. If the range of possible values of $\xi$ is unbounded on one or both sides, it is necessary to transform $f$ to a corresponding truncated distribution. It is assumed that the range of possible values for the truncated distribution is the interva $a$ to $b$. The transformation of variables

$$\eta=\frac{\xi-a}{b-a}$$

produces a random variable $\eta$ with the probability density function

$$F(y)=(b-a)f[a+(b-a)y]$$

Let $F_{\max}$ be the maximum value of $F(\eta)$, and then the probability density function

$$\frac{b-a}{F_{\max}}f[a+(b-a)y]$$

is contained within a unit square.

If two values of the rectangular random number $R_{2i-1}$ and $R_{2i}$ are chosen, and

$$R_{2i}\leq\frac{b-a}{F_{\max}}f[a+(b-a)R_{2i-1}] \qquad (2\text{–}38)$$

is valid,

$$S_i=a+(b-a)R_{2i-1} \qquad (2\text{–}39)$$

is the desired random number.

It is to be noted that the scheme above is equivalent to the calculation of the integral (2–37) by the Monte Carlo method.

### *§ 8–3. Chi-Square Goodness-of-Fit Tests*

It is necessary to test whether the pseudo-random numbers generated in § 8–1 and 8–2 imitate the real random numbers. The chi-square goodness-of-fit tests [*107, 108*] shown below are made in this study.

The range of possible values taken by the pseudo-random numbers is divided to $k$ classes, and let $f_i$ be the number of pseudo-random numbers belonging to the $i$-th class. If the real random numbers are considered, their number in the $i$-th class is known by $\hat{p}_i$ which is the value of the integral of the probability density function from the lower to upper limits of the $i$-th class. Let $m$ be the sample size, and the value of $\chi^2$ is calculated by (2–40).

$$\chi^2=\sum_{i=1}^{k}\frac{(f_i-\hat{m}_i)^2}{\hat{m}_i},\qquad \hat{m}_i=m\hat{p}_i \tag{2–40}$$

It can be tested whether the pseudo-random numbers imitate the real random numbers by comparing the value of $\chi^2$ with the values of the chi-square distribution with $k$-1 degrees of freedom for the level of significance $\alpha$ and the confidence level 1-$\alpha$. If

$$\chi^2_{k-1}(1-\alpha)<\chi^2<\chi^2_{k-1}(\alpha) \tag{2–41}$$

is valid, the pseudo-random numbers are acceptable. The value of $\alpha$ is selected to be 0.05 in this study.

It is to be noted that the value of $\hat{m}_i$ is selected to be greater than five and that the classes where $\hat{m}_i>5$ is invalid may be got together to one new class.

*Test of Periodicity of Rectangular Random Numbers*

When the $(L+1)$-st pseudo-random number coincides with the $i$-th $(1\leq i\leq L)$, $L$ and $(L-i+1)$ are called the length of the interval of aperiodicity and the length of period respectively. Let $L_j$ be the former with the initial condition $(F_0, F_1)_j$, and

$$\eta=\frac{1}{M}\sum_{j=1}^{t}L_j^2$$

may have the chi-square distribution with $2t$ degrees of freedom [*103*], where $t$ is the number of the times of the test.

The random numbers generated by (2–36) are reported to have a period approximately equal to $2.5\times10^{13}$. It is ascertained that at least the period is greater than $10^8$ in this study.

*Test of Uniformity of Rectangular Random Numbers*

In the case of the rectangular random numbers, (2–40) is rewritten into (2–42).

$$\chi^2=\frac{1}{\hat{m}}\sum_{i=1}^{k}(f_i-\hat{m})^2 \tag{2–42}$$

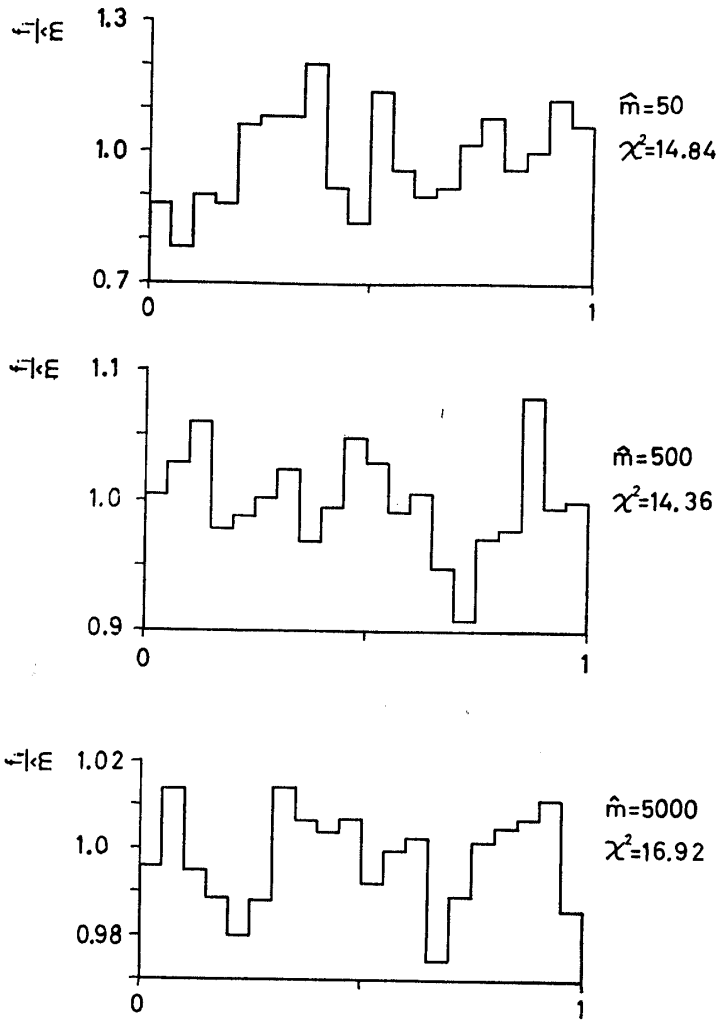


FIG. 5. Uniformity of Rectangular Random Numbers (1-Dimensional)

The range 0 to 1 is divided into 20 classes and the values of $\hat{m}$ are selected to be 50, 500, and 5000 (Fig. 5). The values of $\chi^2$ are between $\chi^2_{19}(.95)=10.12$ and $\chi^2_{19}(.05)=30.14$ in all the cases.

Two-dimensional test of rectangular random numbers is also employed [*109*]. The unit square is divided to $kl$ classes and pairs of random numbers are generated. Then,

$$ {}_1\chi^2=\frac{1}{\hat{m}}\sum_{i=1}^{k}\sum_{j=1}^{l}(f_{ij}-\hat{m})^2-\frac{1}{l\hat{m}}\sum_{i=1}^{k}\left(\sum_{j=1}^{l}f_{ij}-l\hat{m}\right)^2 \qquad (2\text{–}43) $$

and

$$ {}_2\chi^2=\frac{1}{\hat{m}}\sum_{i=1}^{k}\sum_{j=1}^{l}(f_{ij}-\hat{m})^2-\frac{2}{l\hat{m}}\sum_{i=1}^{k}\left(\sum_{j=1}^{l}f_{ij}-l\hat{m}\right)^2 \qquad (2\text{–}44) $$

should have the chi-square distributions with $k(l\text{-}1)$ and $(k\text{-}1)$ $(l\text{-}1)$ degrees of freedom, respectively.

TABLE 1. Two-dimensional Test of Uniformity of Rectangular Random Numbers

| $f_{ij}$ | $j=1$ | 2 | 3 | 4 | 5 | $\sum_{j=1}^{5}$ |
|---|---|---|---|---|---|---|
| $i=1$ | 64 | 81 | 70 | 79 | 92 | 386 |
| 2 | 73 | 81 | 69 | 82 | 86 | 391 |
| 3 | 74 | 81 | 87 | 84 | 81 | 407 |
| 4 | 67 | 92 | 82 | 80 | 82 | 403 |
| 5 | 93 | 75 | 72 | 80 | 93 | 413 |

A result under the condition of $k=5$ and $l=5$ is shown in Table 1, where $\hat{m}$ is 80. The calculated values of ${}_1\chi^2$ and ${}_2\chi^2$ are 18.29 and 17.03 respectively, and they are between $\chi^2_{20}(.95)=10.85$, $\chi^2_{20}(.05)=31.41$ and $\chi^2_{16}(.95)=7.96$, $\chi^2_{16}(.05)=26.30$, respectively.

Thus, there is no reason to state that the pseudo-random numbers generated by (2–36) do not imitate the real rectangular random numbers.

*Test of Pseudo-Random Numbers Obeying (2–5)*

The range taken by the values of the thermal speed $C$ is restricted from 0 to 3, and is divided into 21 classes; 0–0.2, 0.2–0.3,. . . . . , 2.0–2.1, 2.1–3.0. A result with the sample size of 500 is shown in Fig. 6, and the value of $\chi^2$ is 25.5, on the other hand $\chi^2_{20}(.95)=10.85$ and $\chi^2_{20}(.05)=31.41$. Therefore, the pseudo-random numbers generated by (2–5) can be considered to imitate well the real random numbers in obedience to the Maxwell-Boltzmann distribution.

## § 9. *Values of Necessary Parameters for Calculation*

Several parameters, mentioned in the preceding sections, are to be determined

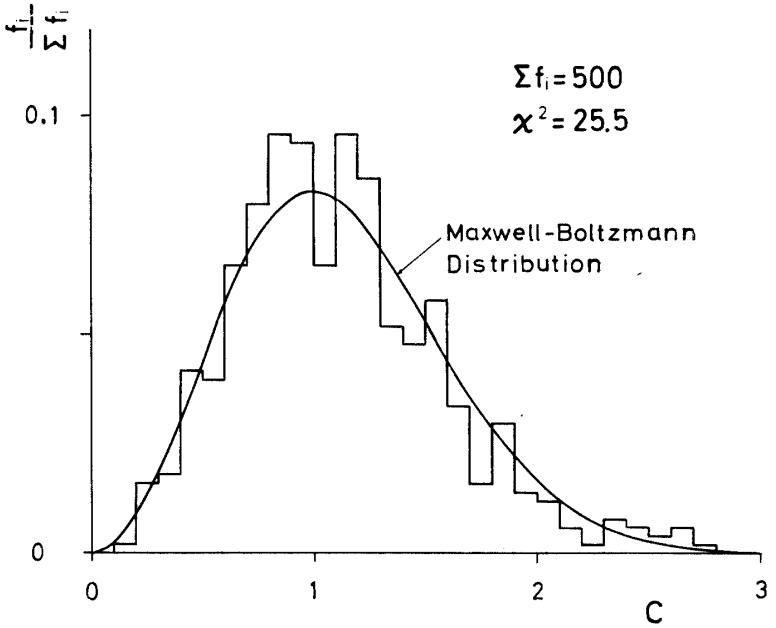


FIG. 6. Random Numbers with Maxwell-Boltzmann Distribution

before the practice of the calculation. They are the total number of the cells $2A^2$, the total number of the molecules initially generated $N_0$, the time interval of a collision cycle $\Delta\tilde{t}$, the time when the sampling starts $t_s$, and the number of the steps of the sampling $m_s$. The ranges of their values made use of in this study are summarized as follows.

$$2A^2=200-1250$$
$$N_0=5000-7500$$
$$\Delta\tilde{t}=0.05-0.1$$
$$\tilde{t}_s=40\Delta\tilde{t}-100\Delta\tilde{t}$$
$$m_s=20-40$$

## III. Experimental Apparatus

A low density wind tunnel at the Institute of Space and Aeronautical Science, University of Tokyo, is used to investigate the surface pressure distributions of a circular cylinder and a sphere, and the drag of a sphere in rarefied supersonic flows.

### *§ 1. Surface Pressure Distribution*

The surface pressures of a circular cylinder in rarefied supersonic flows are measured, making use of a model made of brass. The experimental technique in the present study is similar to that in Ref. 55. The diameter of the model is 3 mm and that of the pressure hole is 0.15 mm. A Pirani pressure gauge head for the Autovac 3294B vacuum gauge is directly attached to the model to avoid the error in the pressure reading induced by the tubing. The model is attached to a rotation mechanism and the value of $\theta$ is varied from 0 to 180 degrees (see Fig. 7a). Measurements are made at intervals of 5°. Two nozzles are put to use at the stagnation pressures of 0.6 and 6 Torr, respectively, the former of which turns out a flow with $M=3.0$ and $Re_1=9$, and the latter $M=4.1$ and $Re_1=53$.

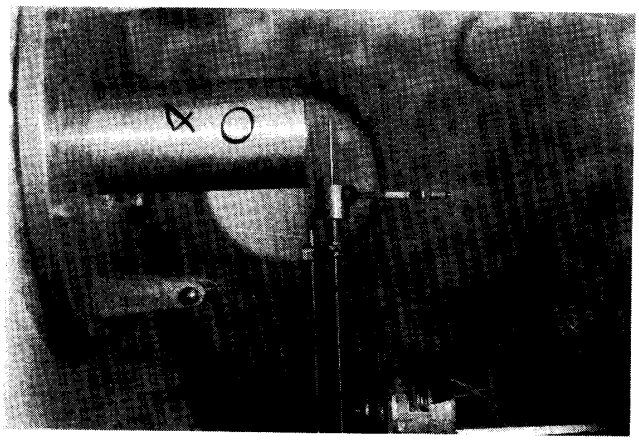

Fig. 7. Experimental Apparatus (a) Pressure Distribution Model (Circular Cylinder)

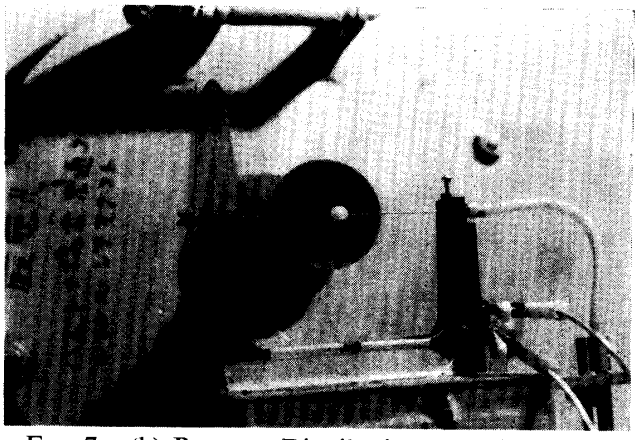

FIG. 7. (b) Pressure Distribution Model (Sphere)

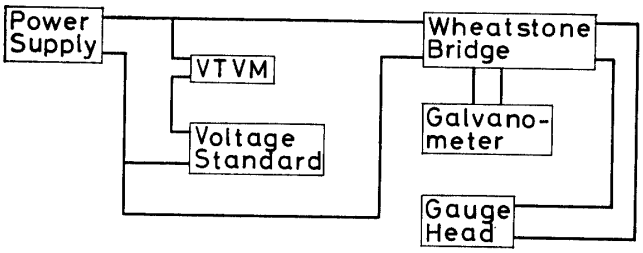


| | |
|---|---|
| Power Supply | Metronix 521A |
| VTVM | Hewlett Packard 410C |
| Voltage Standard | Yokogawa Elec. GOS-31 |
| Galvanometer | Yokogawa Elec. D 2 |

FIG. 7. (c) Schematic Diagram of Pirani Gauge

The effect of the thermal transpiration to the pressure reading is not taken into account, since the stagnation temperature is equal to the body temperature, approximately.

The surface pressure of a sphere is also measured by the method similar to that in Ref. 55. A Pirani gauge head (a fine tungsten wire) is installed in the model made of plastics with the diameter of 10 mm (Fig. 7b). The electrical circuit controlling the gauge head is diagramed in Fig. 7c. A constant-temperature operation of the Pirani gauge is employed here, that is, the pressure is related to the voltage $V$ applied by a variable power supply to the Wheatstone bridge and that $V_0$ at a very low pressure ($V_0=1.2$ volt in the present case). The values of $V$ and $V_0$ are read to 0.1 $mV$ by a VTVM and a variable voltage standard. The calibration curve of the Pirani gauge is shown in Fig. 7d. A simple conical nozzle is used at $p_0=0.6$ Torr, and the flow condition is $M=2.9$ and $Re_1=32$.

## *§ 2. Sphere Drag*

The sphere drag is measured by the method similar to that by Ashkenas [*70, 72*]. This investigation is made mainly by Dr. Hinada and Mr. Terada [*77*]. A sphere

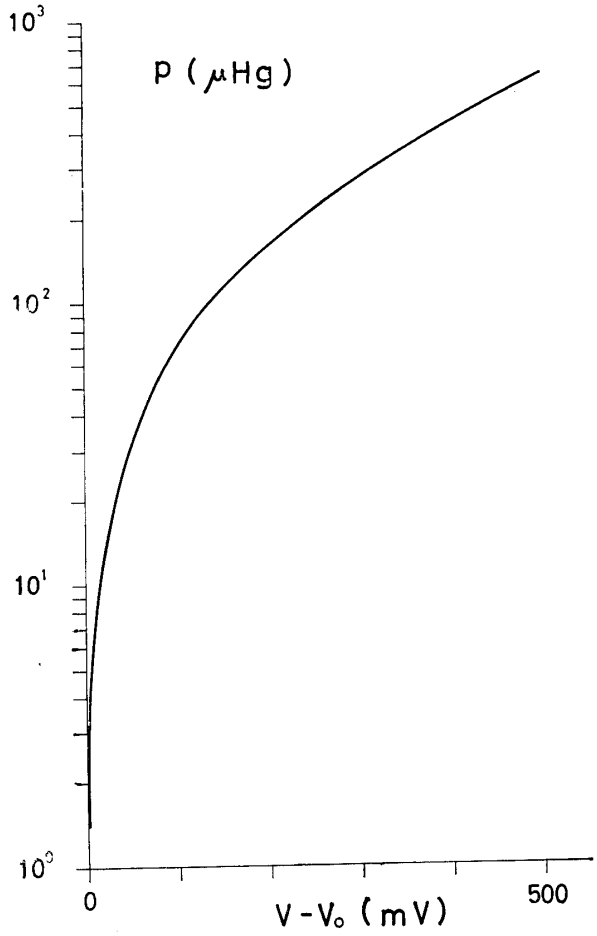


FIG. 7. (d) Calibration Curve of Pirani Gauge

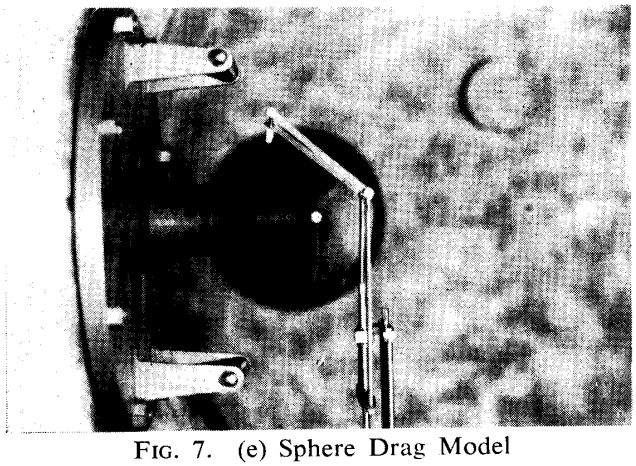

FIG. 7. (e) Sphere Drag Model

model is supported by a fine wire made of nylon 0.147 mm in diameter. The models are made of plastics, and their diameters are selected to be 5.5, 10, 13 and 20 mm, in order to study the effect of the Reynolds number. When the model is immersed in a rarefied supersonic flow, it is moved toward downstream by the drag force and the supporting wire is deflected (see Fig. 7e). The magnitude of the

drag force is calculated from the deflection angle of the supporting wire and the mass of the model. An additional mass is attached to the model by the aid of a fine wire in order to set the deflection angle in a favorable range, since the plastics used here are too light. Of course the additional mass is located out of the uniform flow. The Mach numbers of the uniform flow are selected to be about 2 to 3.5. The drag force exerted on the supporting wire itself is measured and subtracted from the value obtained above, since it can not be neglected in the cases of small models.

## IV. Results and Discussion

Results obtained by the Monte Carlo method and by the experiments concerning the velocity, density, temperature, pressure and heat transfer profiles and so forth are shown in the succeeding figures, and they are compared with other results and discussed in the following sections.

### *§ 1. Flat Plate*

The flow field on a flat plate placed parallel to the direction of a uniform flow when $S=5$ and $\tilde{T}_b=1$ is investigated by the Method A of the Monte Carlo method with the criterion to select the collision pair discussed in section 4–1 in chapter II, and afterwards it is again investigated by that with the criterion in secton 4–2. The Method B with the latter criterion is applied to the case where $M=10$ and $\tilde{T}_b=1$.

*Comparison of Two Criteria*

Figs. 8 and 9 show the results calculated making use of the criteria in sectoins 4–1 and 4–2, respectively, about the flow field when $S=5$ and $\tilde{T}_b=1$. The values of the mean thermal speed in all the cells are renewed at intervals equal to those in case of the sampling steps, when the former criterion is applied.

It is easily seen that there are no appreciable differences in the equi-speed lines, equi-density lines and equi-temperature lines, respectively, in the two figures. It may indicate that the mean value of the relative speeds scarcely differs from the mean thermal speed in a cell. Therefore, the simpler criterion in section 4–2 is employed below.

*Flow Field over a Flat Plate, $S=5$ and $\tilde{T}_b=1$*

The equi-speed lines (Fig. 9a) show that the flow in the neighborhood of the body is decelerated toward the body and the downstream, since the speed of the molecule which has collided with the body is diminished from about five (uniform flow velocity) to the order of one (square root of the body temperature), and the number of such slow-speed molecules increases toward the body and the downstream. Therefore these lines may be located closer to the body because the molecules that have collided with the body possess larger speeds in the case where the body temperature is higher than in the present case.

The density profile consists of a peak at $X\fallingdotseq 5$ and $Y\fallingdotseq 0$, a ridge running from

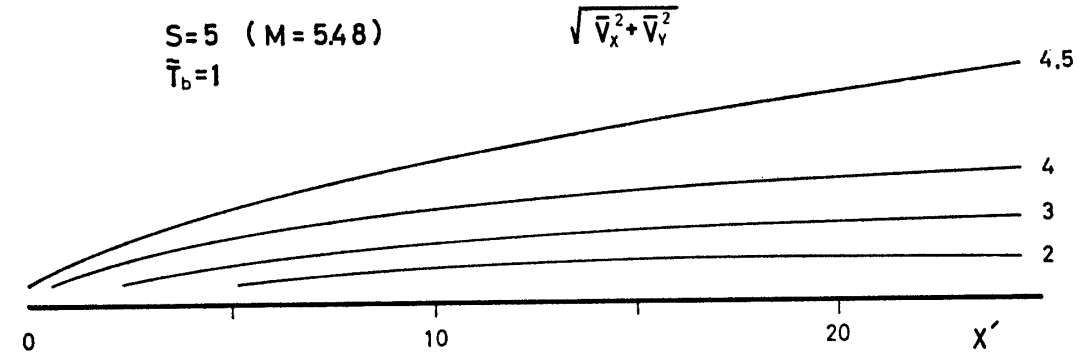


FIG. 8. Flow Fied over a Flat Plate Obtained by Method in Section 4–1
(a) Equi-Speed Lines

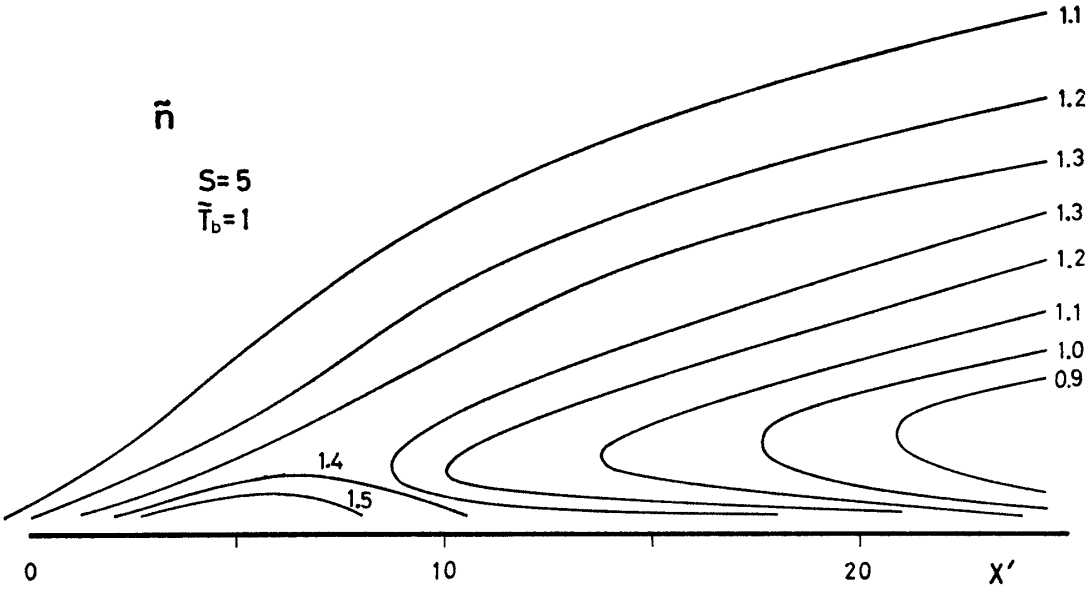


FIG. 8. (b) Equi-Density Lines

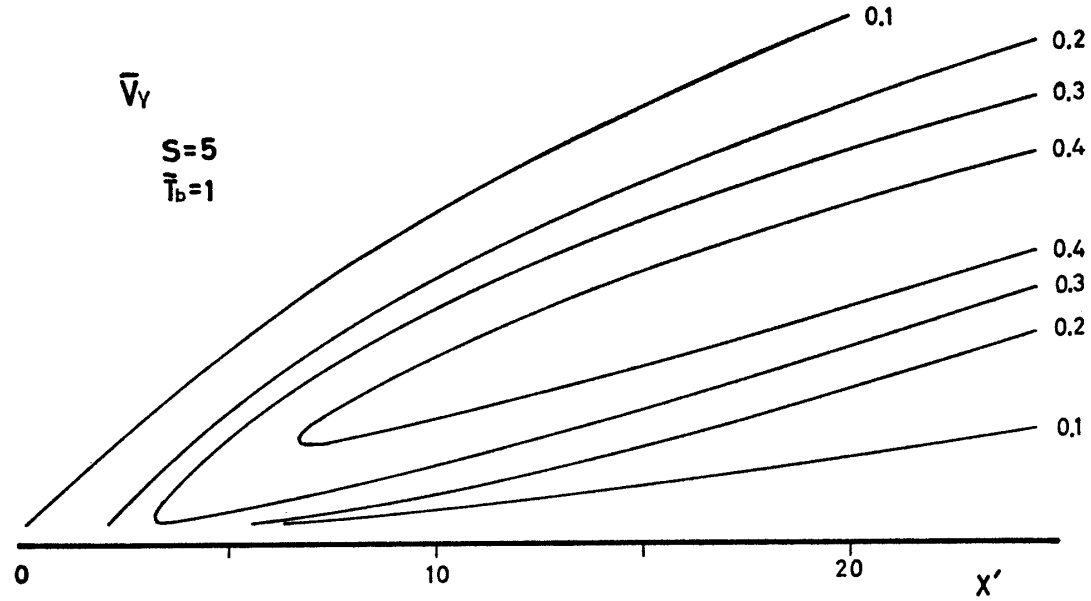


FIG. 8. (c) Equi-Normal-Velocity-Component Lines

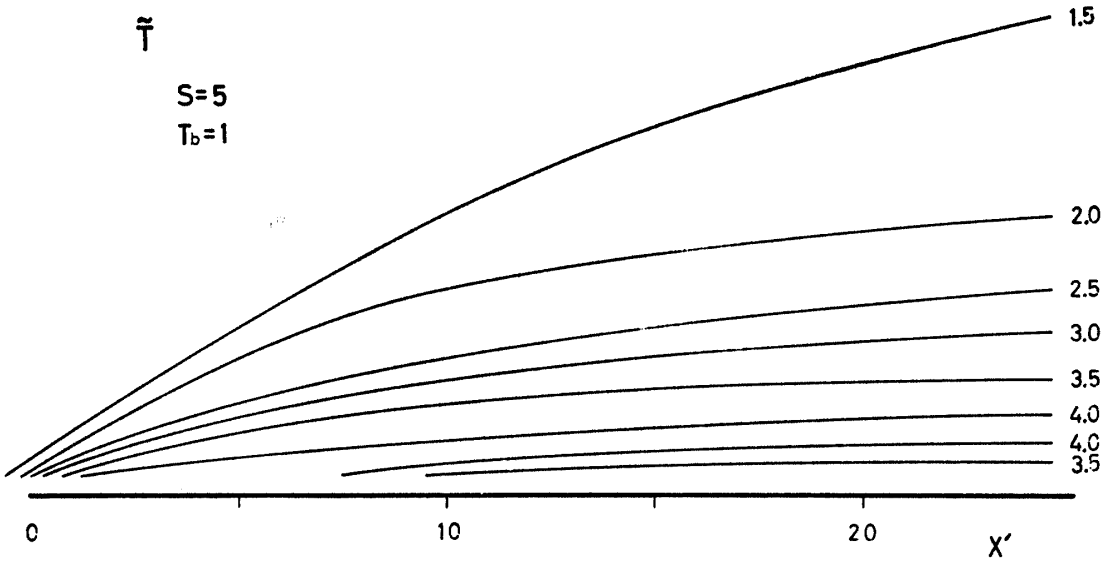


FIG. 8. (d) Equi-Temperature Lines

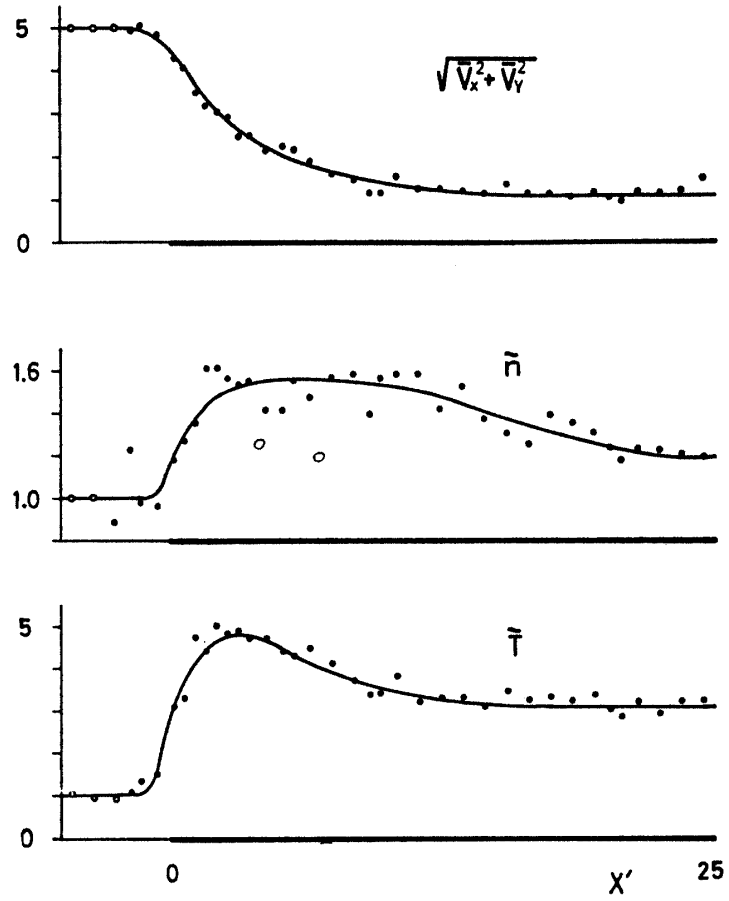


FIG. 8. (e) Physical properties along $X$-Axis

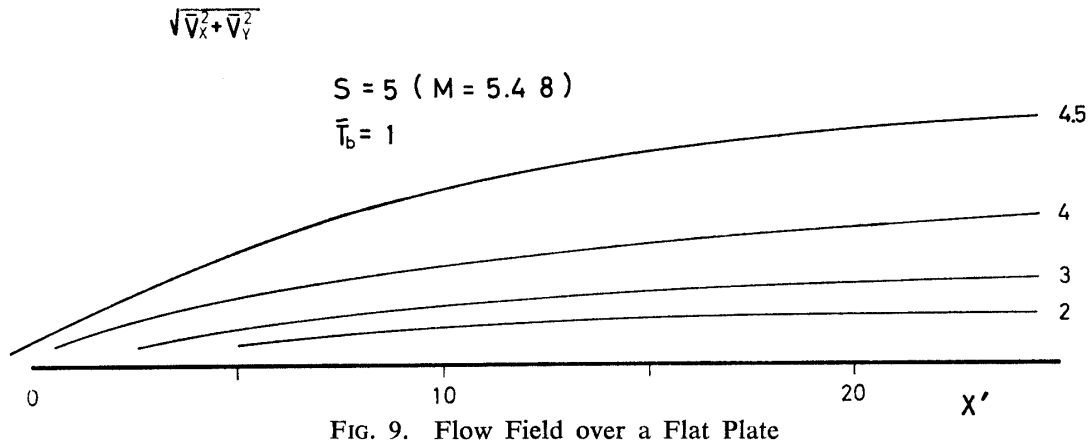


FIG. 9. Flow Field over a Flat Plate
(a) Equi-Speed Lines

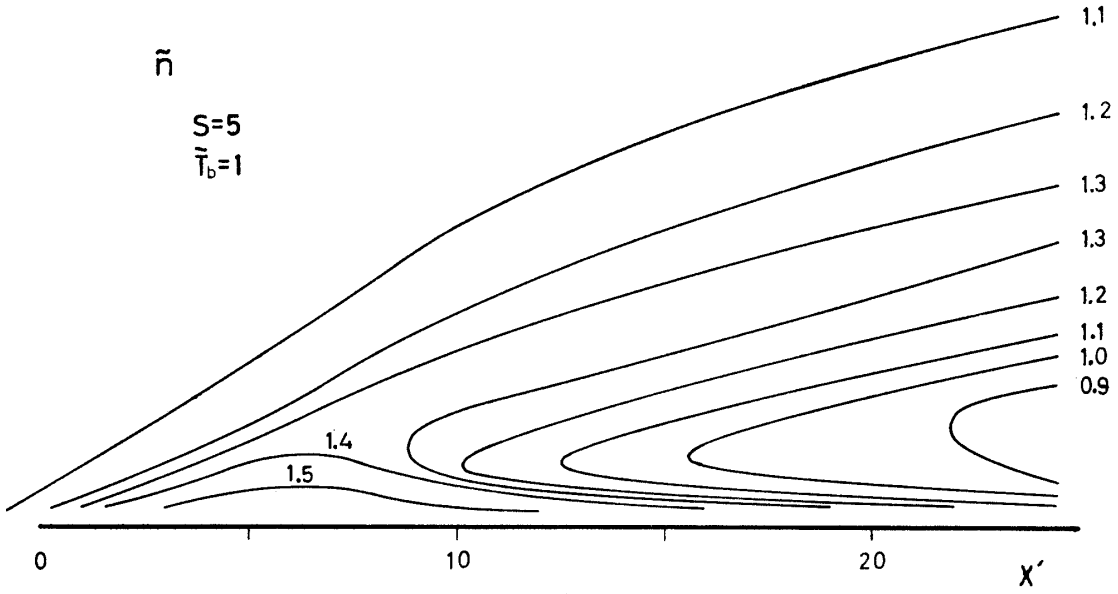


FIG. 9. (b) Equi-Density Lines

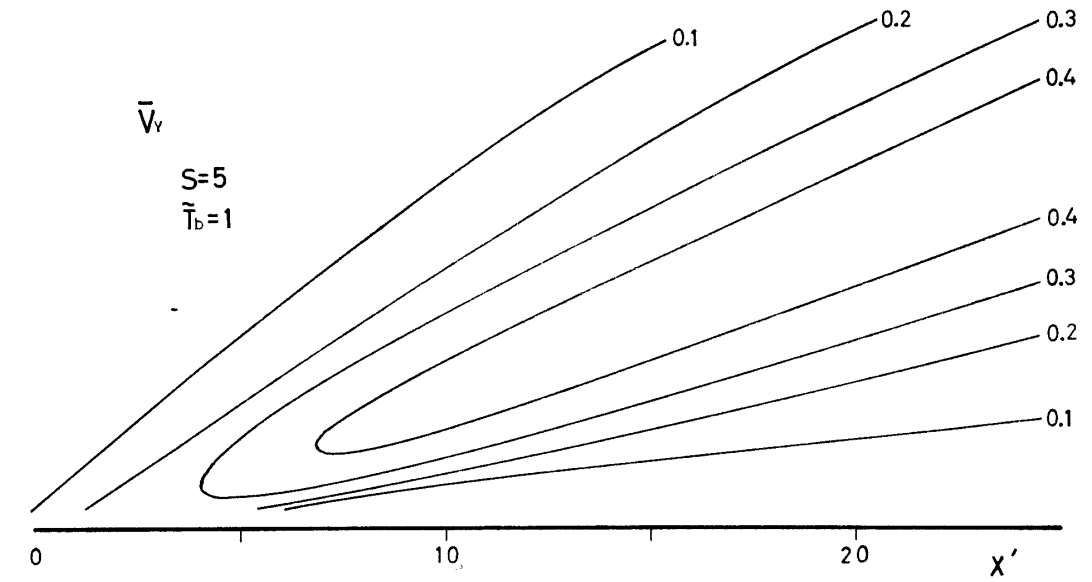


FIG. 9. (c) Equi-Normal-Velocity-Component Lines

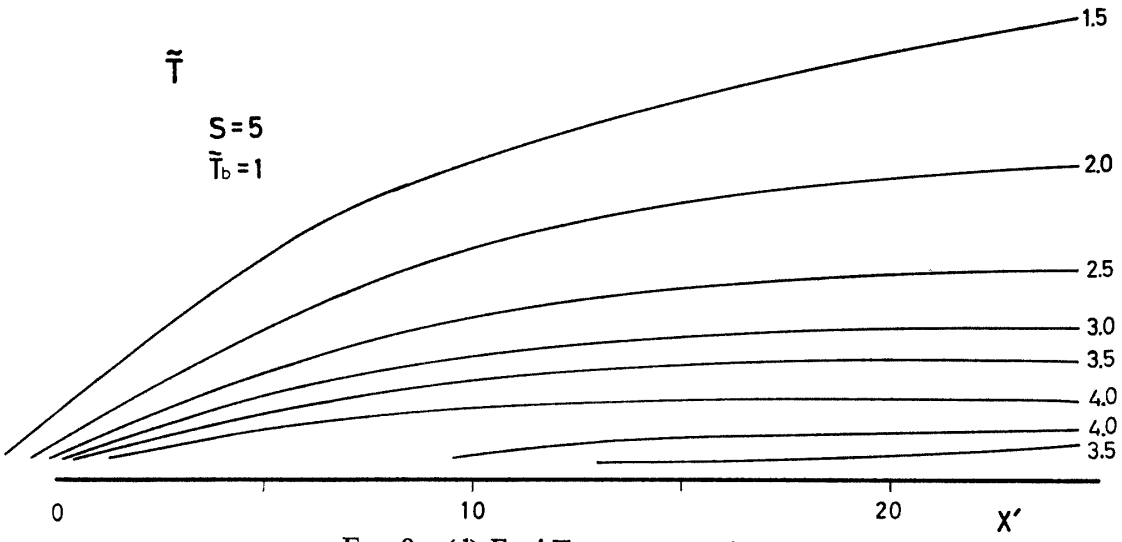


FIG. 9. (d) Equi-Temperature Lines

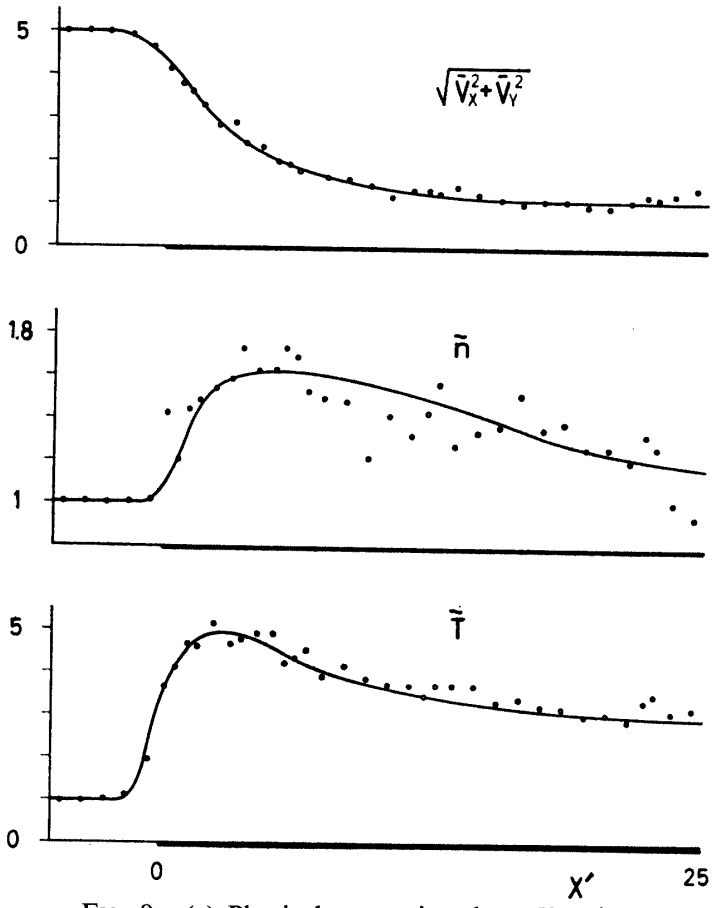


FIG. 9. (e) Physical properties along $X$-Axis

the peak and a valley between the ridge and the body (Fig. 9b). It can be explained as follows. The peak is formed by the molecules decelerated and gathered, where the tangential velocity component $\overline{V}_X$ is large enough to neglect the effect of the normal component $\overline{V}_Y$. As the flow is decelerated to some extent, the molecules are pulled apart from the body by the normal velocity component, whose profile is shown in Fig. 9c. It justifies the above inference that the position of the ridge in Fig. 9b almost coincides with that in Fig. 9c. It is apparent that the flow field is divided into two types. One of them ($X<5$) does not include the valley and another ($X>5$) does. The former is considered to be the kinetic region, and the latter is the continuum region which includes the shock layer and the boundary layer. The ridge may be steepened to a Rankine-Hugoniot shock in the downstream region. The heights of the peak and the ridge may be low and the location of the latter may be farther from the body as compared with the present case when the body temperature is higher than unity. Similar patterns of the density profile are also reported in the results obtained by the electron beam densitometry by Joss et al. [27] and Lillicrap et al. [29].

The temperature profile is shown in Fig. 9d, and indicates the presence of a peak and a ridge. The temperature peak is at almost the same place as the density peak. However, the temperature ridge is nearer to the body than the density ridge. This can be inferred from the following discussion. The high kinetic energy possessed by the molecules in the uniform flow is converted to the heat energy as they are decelerated and the temperature increases monotonically from the uniform flow value to its peak and the number of the molecules that have collided with the body, whose kinetic energy is low as compared with that of the molecules in the uniform flow, increases and the temperature decreases in the region very near to the body on the downstream side of the peak. On the other hand, the temperature may increase monotonically as $Y$ decreases at any fixed value of $X$ in the case where the body temperature is higher than the adiabatic wall temperature. The difference in the locations of the ridge in the density and temperature profiles is caused by the fact that the former is determined by the normal velocity components of the molecules and the latter by the speeds of the molecules.

Fig. 9e shows the macroscopic speed, density and temperature in the cells just adjacent to the X-axis ($Y_c=0$). The distribution of the macroscopic speed can be considered to be equal to that of the tangential velocity component $\overline{V}_X$, since the normal velocity component $\overline{V}_Y$ is very small as shown in Fig. 9c. A few points on the downstream side show a little different tendency as compared with others, since the downstream boundary exists and the molecules entering the flow field through it are neglected. If the body temperature is higher than unity, the disturbance of the body extends further upstream and the curves may be shifted to the left, and the density may be lower and the temperature higher as a whole, respectively.

The results shown in Fig. 9 agree at least qualitatively with those by Huang et al. with the discrete ordinate method [14] and by Vogenitz et al. with the Monte Carlo method [96].

*Flow Field over a Flat Plate, $M=10$ and $\tilde{T}_b=1$*

The equi-speed lines show that the region subject to the disturbance by the body is narrow as compared with the preceding case (see Figs. 10a and 9a), since it is determined by the ratio of the uniform flow velocity to the mean thermal speed of the molecules with the Maxwell-Boltzmann distribution at the body temperature, whcih is proportional to $S/\sqrt{\tilde{T}_b}$.

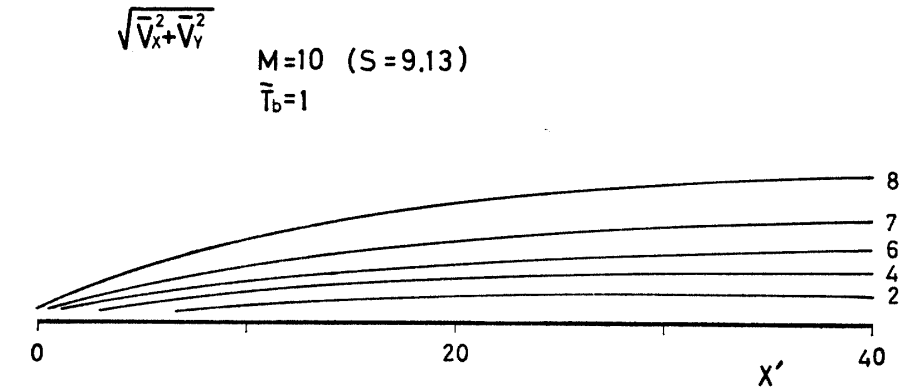


FIG. 10. Flow Field over a Flat Plate
(a) Equi-Speed Lines

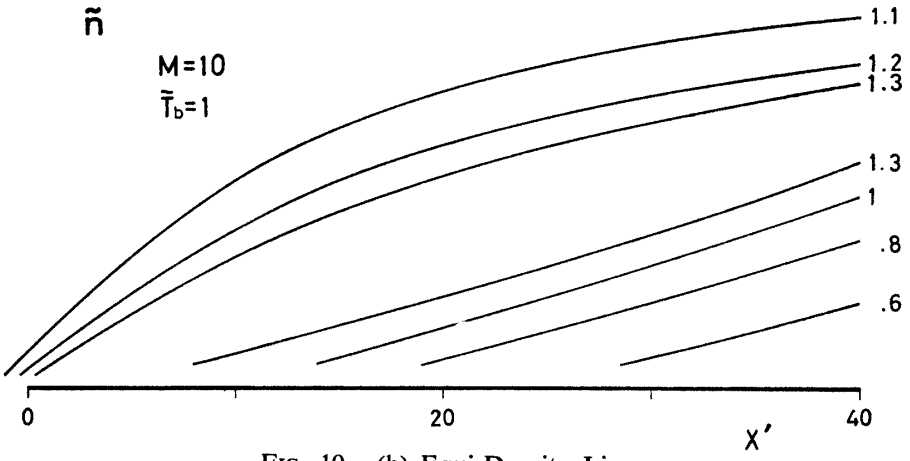


FIG. 10. (b) Equi-Density Lines

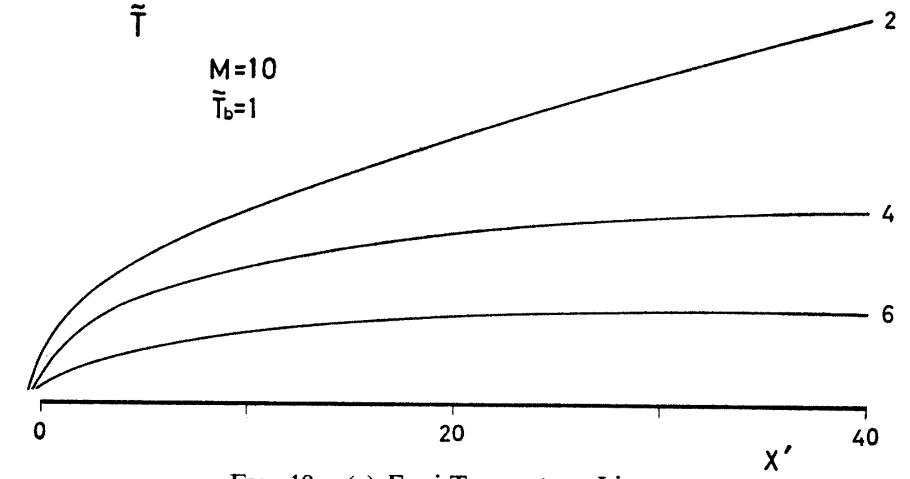


FIG. 10. (c) Equi-Temprature Lines

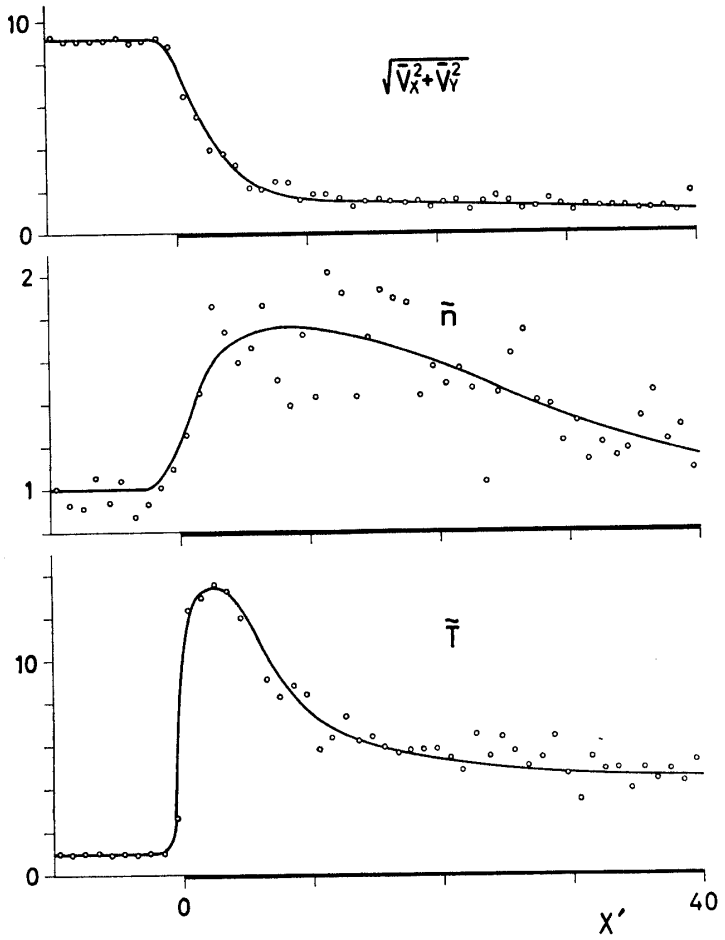


(d) Physical Properties along $X$-Axis

The density profile is shown in Fig. 10b and also consists of a peak, a ridge and a valley, of which the last is not seen in the figure and is very near to the body. The heights of the peak and the ridge are greater than in the preceding case, because of the higher value of $S/\sqrt{\tilde{T}_b}$.

The temperature profile shown in Fig. 10c indicate the higher temperature, sicne the stagnation temperature in this case is higher than in the preceding case. Of course it decrease as $Y$ decreases in the very near region of the body (it is not seen in the figure) in the region downstream of the peak.

The physical properties, that is, the macroscopic speed, the density and the temperature along the body are shown in Fig. 10d.

The results given by Fig. 10 agree well with those by Huang et al. [*15*] with the discrete ordinate method for the same flow condition.

*Surface Pressure*

The surface pressure distributions on the flat plate are shown in Figs. 11 and 12. The open and solid symbols correspond to the cases where $S=5$ and $T_b=0.091T_0$, and $M=10$ and $T_b=0.029T_0$, respectively. The rarefaction parameter $\bar{V}_{\infty,x}$ is defined by the following expression.

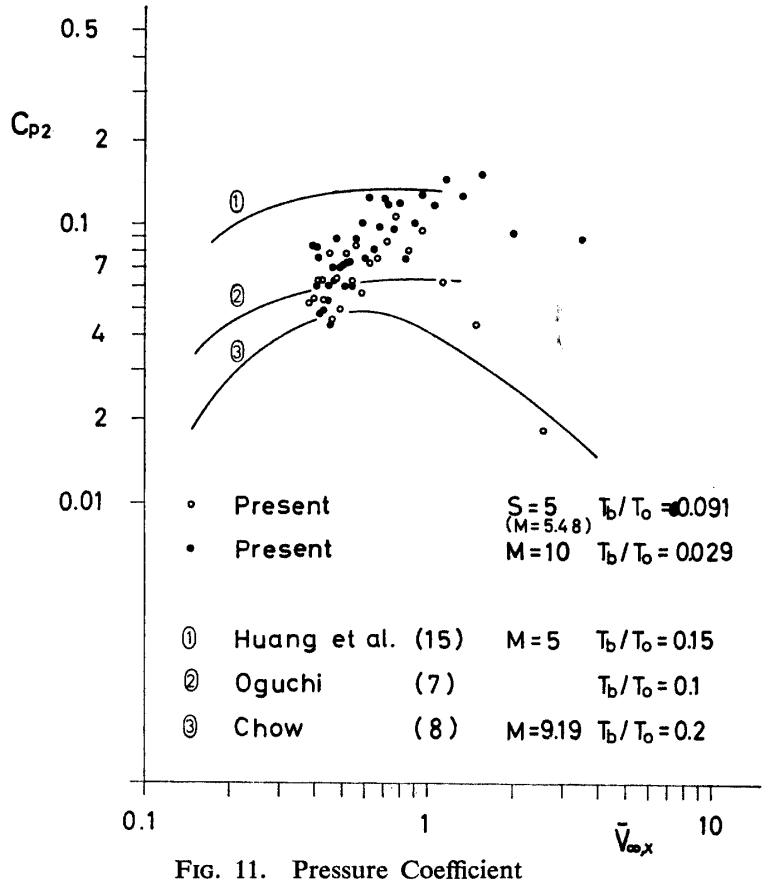


FIG. 11. Pressure Coefficient

$$\bar{V}_{\infty,x}=M\frac{\sqrt{C}}{\sqrt{\mathrm{Re}_1}}, \tag{4–1}$$

where $C$ is the so-called Chapman-Rubesin coefficient and is equal to unity in the present cases, and $Re_1$ is the Reynolds number defined by (4–2).

$$\mathrm{Re}_1=\frac{\rho_\infty u_\infty x'}{\mu_\infty}, \tag{4–2}$$

where $x'$ means the distance from the leading edge of the flat plate to the center point of the surface element $\Delta s$.

The pressure coefficient $C_{p2}$ is given as a function of the rarefaction parameter in Fig. 11. It is seen that the pressure coefficient has a maximum value in the neighborhood of $\bar{V}_{\infty,x}=1$, and it is scarcely affected by the Mach number and the temperature ratio in the region for smaller values of $\bar{V}_{\infty,x}$ (downstream side). On the other hand, it is affected by them in the region for larger values of $\bar{V}_{\infty,x}$ (upstream side). The present results agree qualitatively well with those by other theoretical studies as shown in the figure.

The surface pressure distributions are so re-arranged as to be easily compared with the strong interaction theory in Fig. 12. The values by the strong interaction theory [*3*] and the free molecule flow theory [*12*] are given by (4–3) and (4–4), respectively.

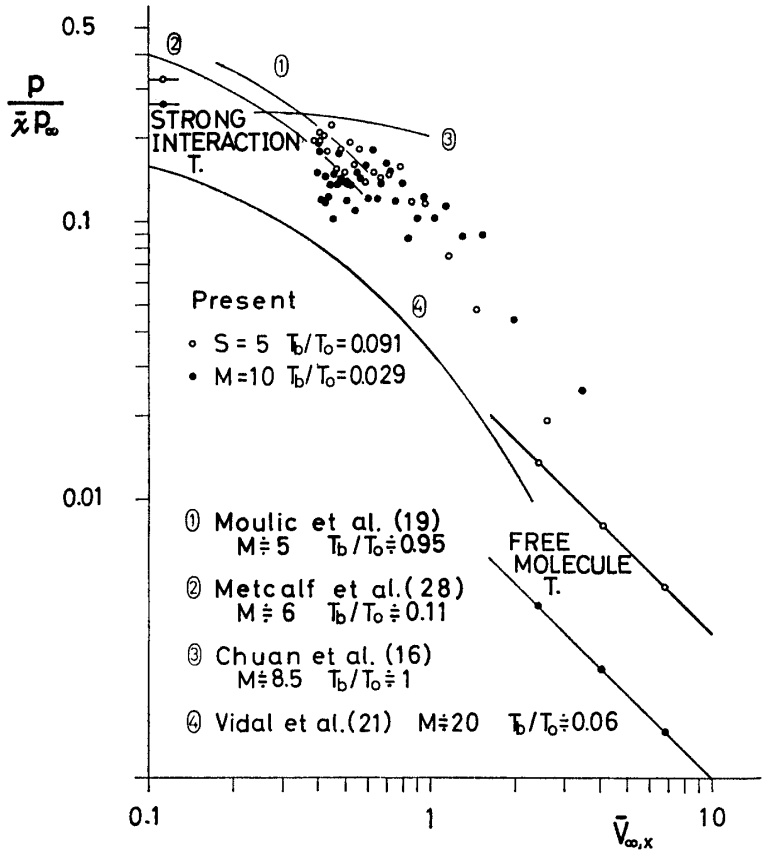


FIG. 12. Surface Pressure

$$\frac{1}{\bar{\chi}}\frac{p}{p_\infty}=\frac{\sqrt{3}}{2}\gamma\varepsilon\left(0.664+1.73\frac{T_0}{T_b}\right) \tag{4–3}$$

$$\frac{p}{p_\infty}=\frac{1}{2}(\sqrt{\tilde{T}_b}+1), \tag{4–4}$$

where $\bar{\chi}$ is the hypersonic interaction parameter and is defined by (4–5), and $\varepsilon$ the density ratio across the Rankine-Hugoniot shock defined by (4–6).

$$\bar{\chi}=M^3\frac{\sqrt{C}}{\sqrt{\mathrm{Re}_1}} \tag{4–5}$$

$$\varepsilon=\frac{(\gamma-1)M^2+2}{(\gamma+1)M^2} \tag{4–6}$$

It is seen that the pressure varies from the value given by the strong interaction theory to that by the free molecule flow theory as the rarefaction parameter incrases as expected. It is interesting that the pressure in the case of $S=5$ comes nearer to its free molecule value than that in the case of $M=10$. It may be because the changes of the physical properties in the flow near the body is larger in the latter case than in the former, that is, the deviation from the free molecule condition may be large when the value of $S/\sqrt{\tilde{T}_b}$ is large.

The present results agree at least qualitatively with other experimental results. They appear to agree quantitatively with those by Moulic et al. [*19*] and by Metcalf et al. [*28*]. However, they do not agree quantitatively if account is taken of the effect of the body temperature, since the pressure is strongly affected by the body temperature so far as the fully diffuse reflection is assumed. (The pressure may be high when the body temperature is high, since it determines the speed of the molecule reflected from the body.)

*Skin Friction*

The skin friction is shown in Fig. 13. The values by the strong intercation theory and by the free molecule flow theory are given by (4–7) and (4–8), respectively.

$$\frac{M^3 C_f}{\bar{\chi}^{3/2}} = 0.110\sqrt{\gamma\varepsilon\left(0.664+1.73\frac{T_b}{T_0}\right)} \tag{4–7}$$

$$C_f = \frac{1}{\sqrt{\pi}S} \tag{4–8}$$

The data indicate a tendency similar to that in the case of the pressure (Fig. 12), and are qualitatively good as compared with other theoretical and experimental

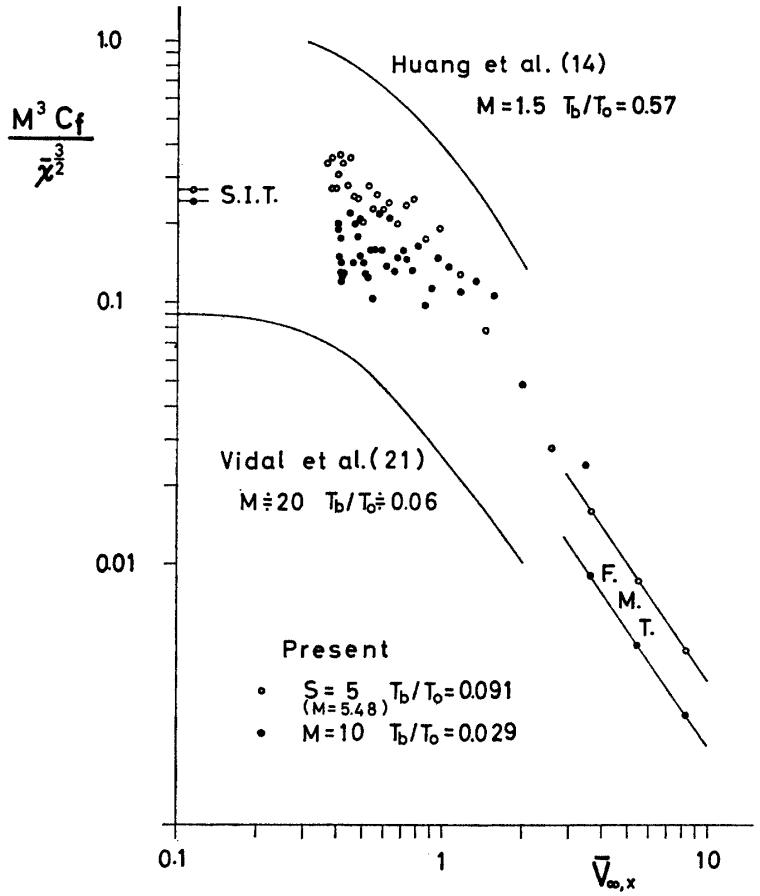


FIG. 13. Skin Friction

results. The skin friction may be scarcely affected by the body temperature, since it is determined by the tangential velocity components of the molecule before and after the collision with the body and the mean value of the latter vanishes so far as the fully diffuse reflection is assumed and is therefore independent of the body temperature.

*Heat Transfer*

Fig. 14 shows the heat transfer distributions. The results by the strong interaction theory with the Reynolds analogy and the free molecule flow theory are given by (4–9) and (4–10), respectively.

$$\frac{M^3C_h}{\bar{\chi}^{3/2}}=0.219\sqrt{\gamma\varepsilon\left(0.664+1.73\frac{T_b}{T_0}\right)} \tag{4–9}$$

$$C_h=\frac{\gamma-1}{2\gamma\sqrt{\pi}S(\tilde{T}_0-\tilde{T}_b)}\left\{S^2+\frac{1}{2}\frac{\gamma+1}{\gamma-1}(1-\tilde{T}_b)\right\} \tag{4–10}$$

The data again indicate a tendency similar to that in the case of the pressure, and are qualitatively good as compared with other theoretical and experimental results. The heat transfer is, of course, strongly affected by the body temperature and may change its sign at the adiabatic wall temperature.

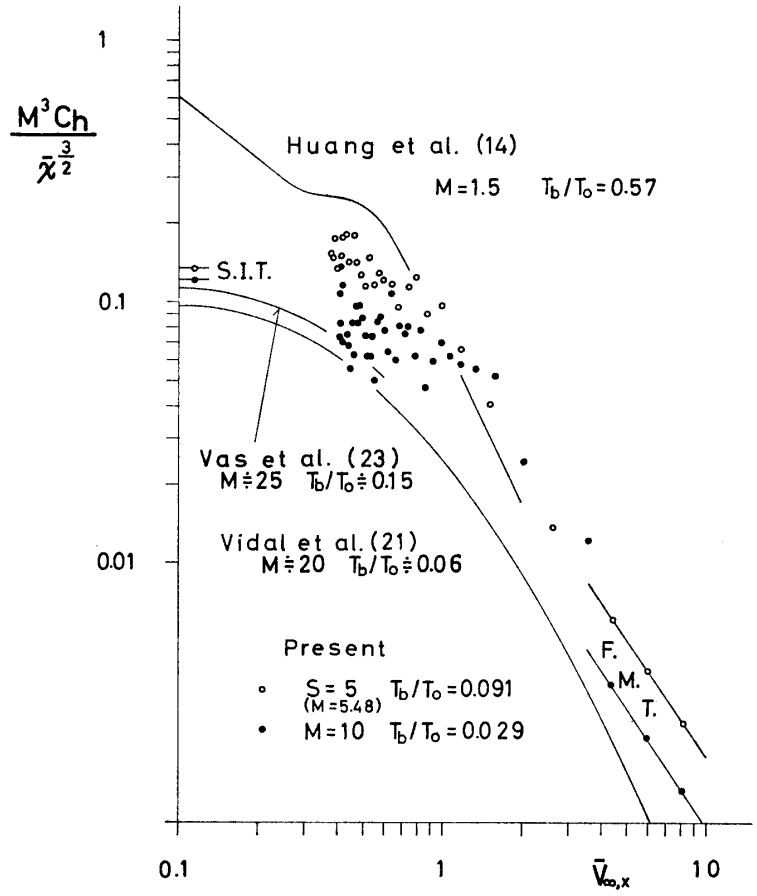


FIG. 14. Heat Transfer

*Slip Velocity*

The slip velocity at the wall is given in Fig. 15, which also includes other theoretical and experimental results. The present results show the effect of the Mach number of the uniform flow, that is, the value in the case of $S=5$ is higher than that of $M=10$ for the same rarefaction parameter, because of the difference in the values of $S/\sqrt{\tilde{T}_b}$ between the two cases. A few points on the left side are omitted from the figure, since they are affected by the downstream boundary. The slip velocity may be scarcely affected by the body temperature, because the mean value of the tangential velocity components of the molecules that have collided with the body vanishes regardless of the body temperature as far as the fully diffuse reflection is assumed.

It is again to be noted that the slip velocity evaluated by this method may be overestimated, since the molecules apart from the body by the order of magnitude of the mean free path in the uniform flow are included.

## § 2. *Blunt Body*

The flow fields around a circular cylinder and a sphere when $S=5$, $Kn=1$ and 0.1, and $\tilde{T}_b=1$ and 11 are investigated by the Method A. The Method B is applied to the case of a circular cylinder when $S=5$, $Kn=0.05$ and $\tilde{T}_b=1$. The

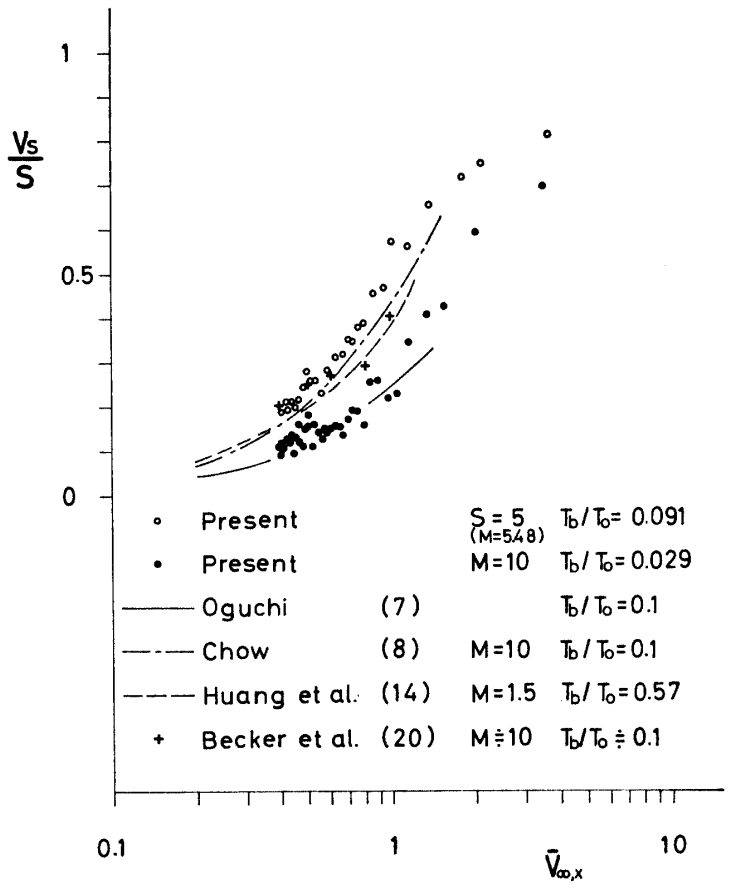


FIG. 15. Slip Velocity

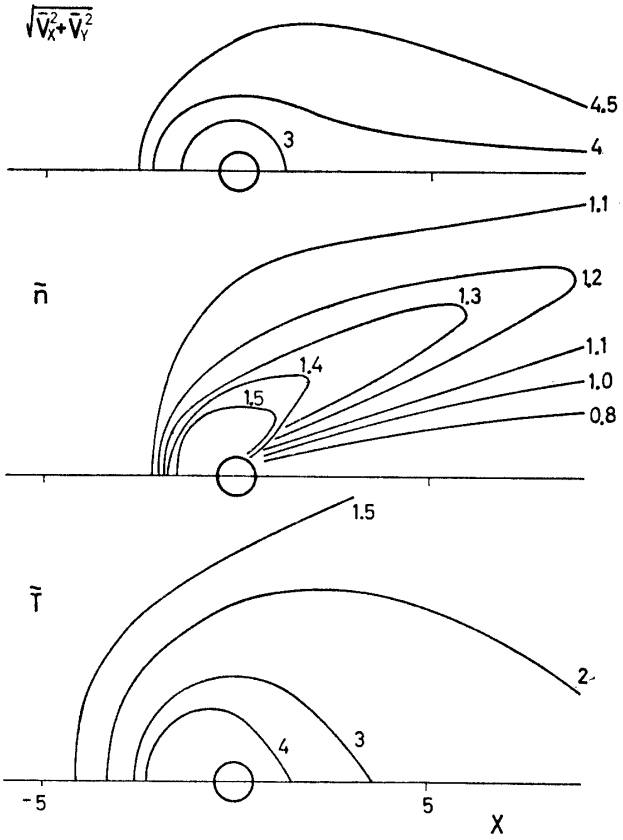


FIG. 16. (a) Flow Field around a Circular Cylinder $S=5$, $Kn=1$, $\tilde{T}_b=1$ ($M=5.48$)

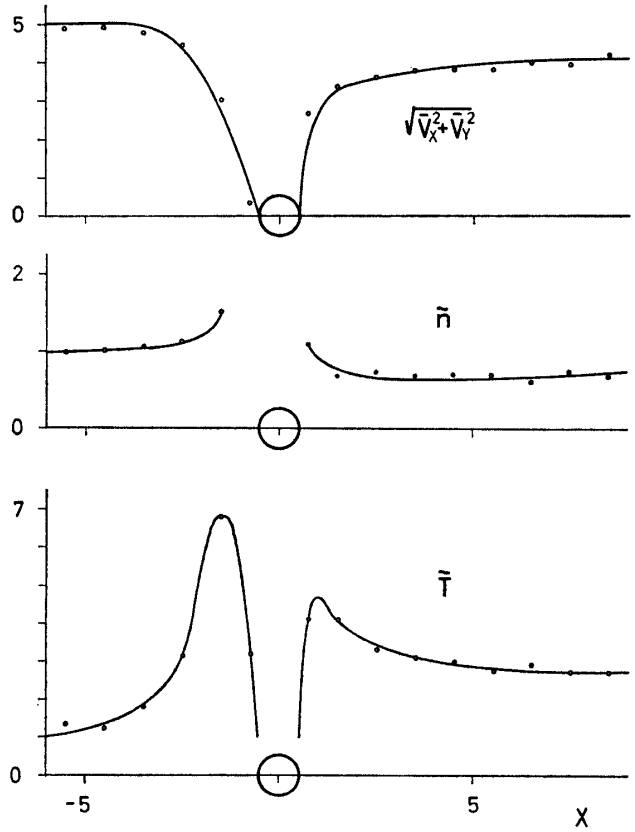


EIG. 16. (b) Physical properties along $X$-Axis

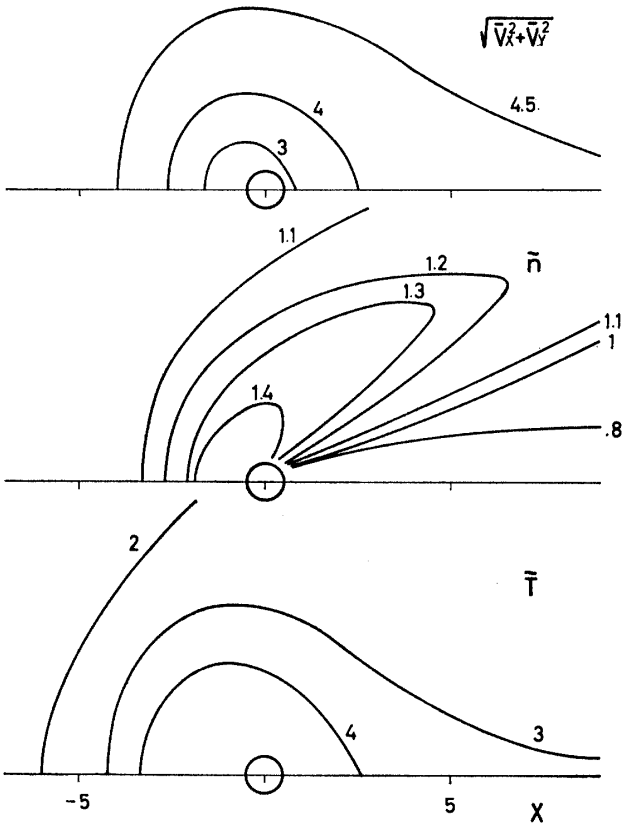


FIG. 17. (a) Flow Field around a Circular Cylinder
$S=5$, $Kn=1$, $\tilde{T}_b=11$ ($M=5.48$)

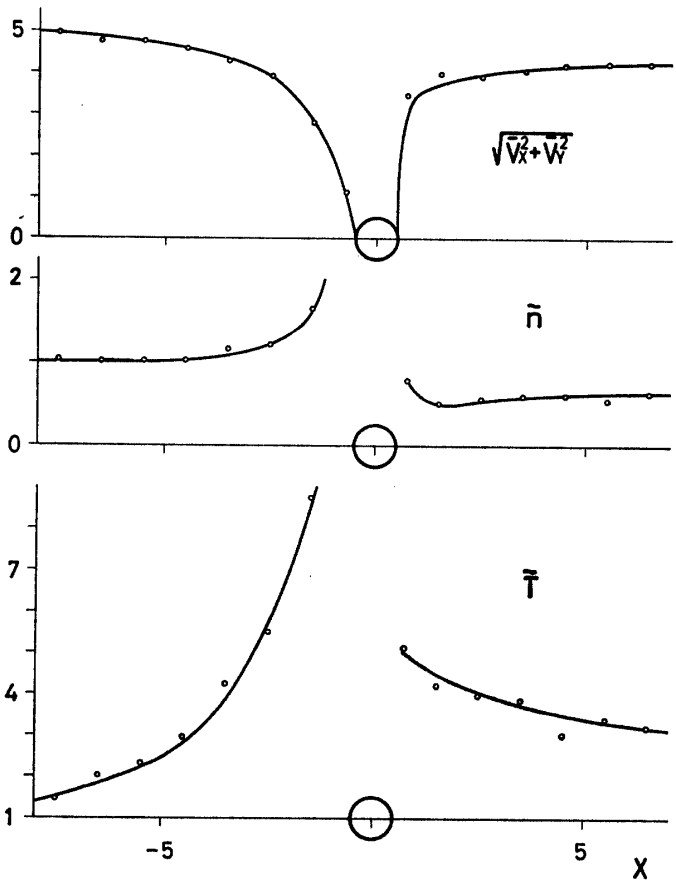


FIG. 17. (b) Physical Properties along $X$-Axis

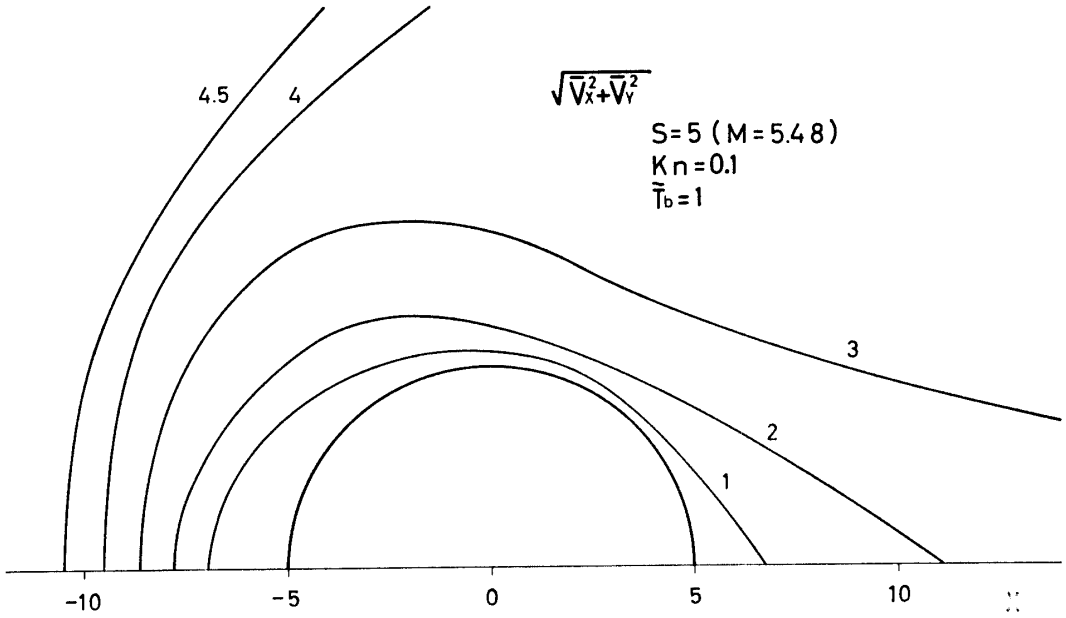


FIG. 18. Flow Field around a Circular Cylinder
(a) Equi-Speed Lines

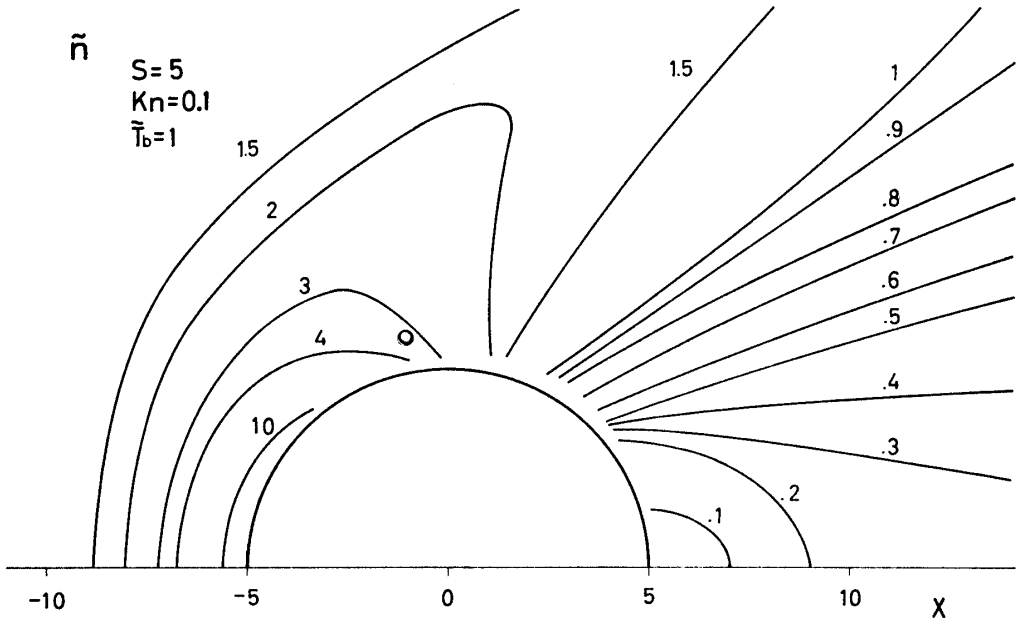


(b) Equi-Density Lines

discussion of the flow fields is mainly concentrated to the case $Kn=0.1$ for simplicity.

*Flow Field around a Circular Cylinder when $S=5$, $Kn=0.1$ and $\tilde{T}_b=1$ (Highly Cooled Case)*

The flow field around a circular cylinder with the temperature equal to that in the uniform flow when $S=5$ and $Kn=0.1$ is shown Fig. 18. It is easily seen that the existence of the body affects the flow in the directions upstream ($X<0$) and normal to it ($Y>0$) more than in the case of the flat plate.

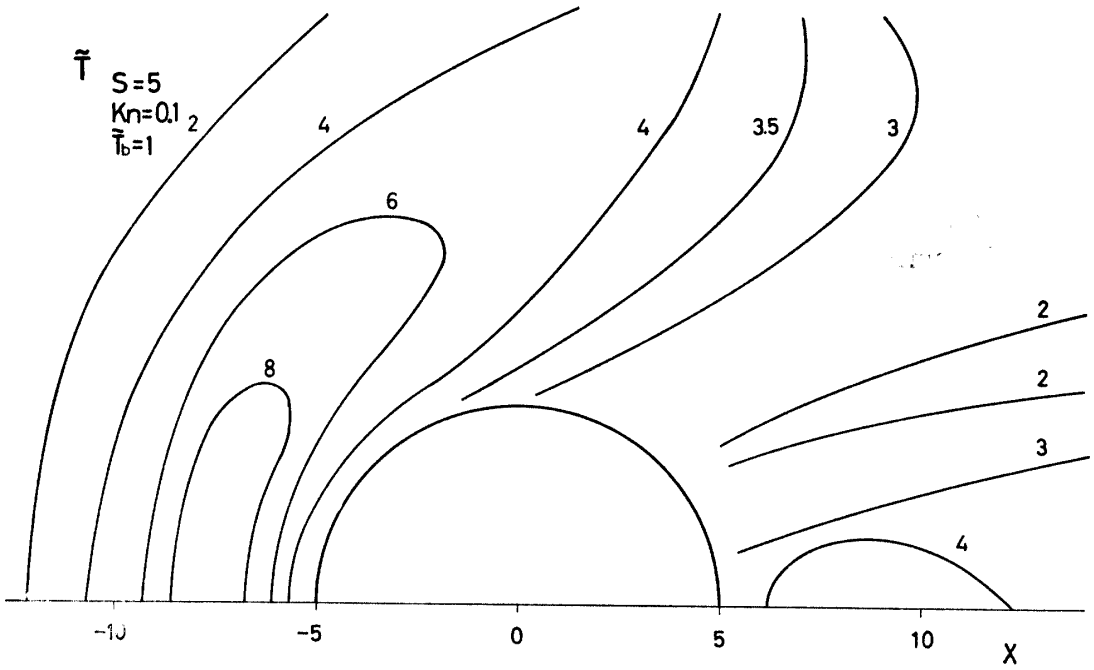


(c) Equi-Temperature Lines

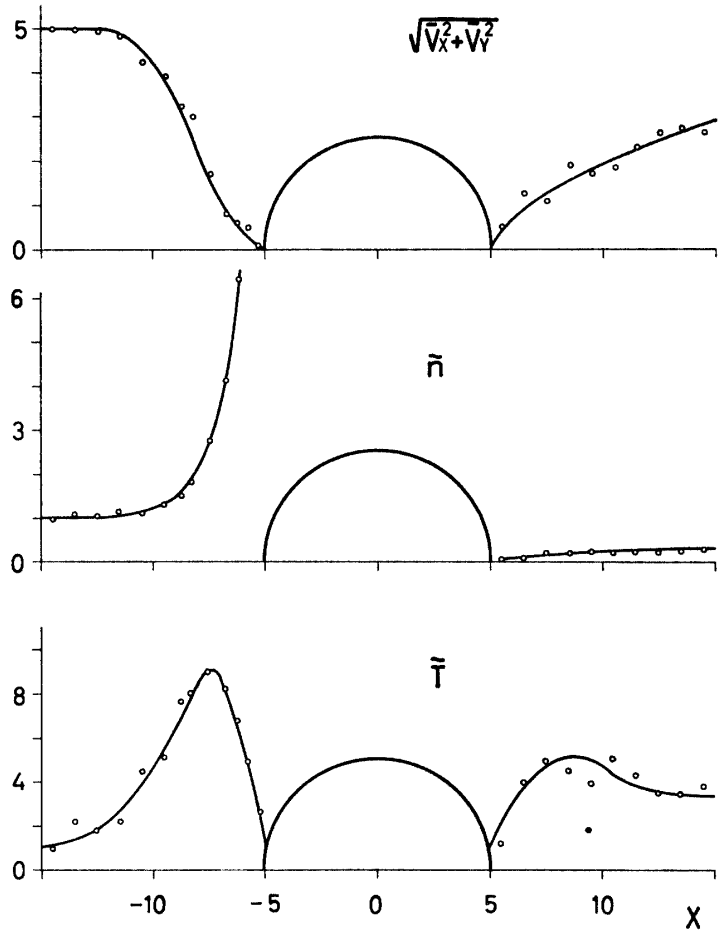


(d) Physical Properties along $X$-Axis

The equi-speed lines given by Fig. 18a show how the flow is decelerated and accelerated. Especially along the body surface the flow is accelerated from the forward stagnation point to some point, which may be the separation point, and subsequently decelerated. The reverse flow region near the rear stagnation point of the body, where the flow is directed to the body surface, does not exist.

The density profile in Fig. 18b shows that the density in the forward stagnation region becomes higher than ten (it reaches sixty at the very stagnation point) and

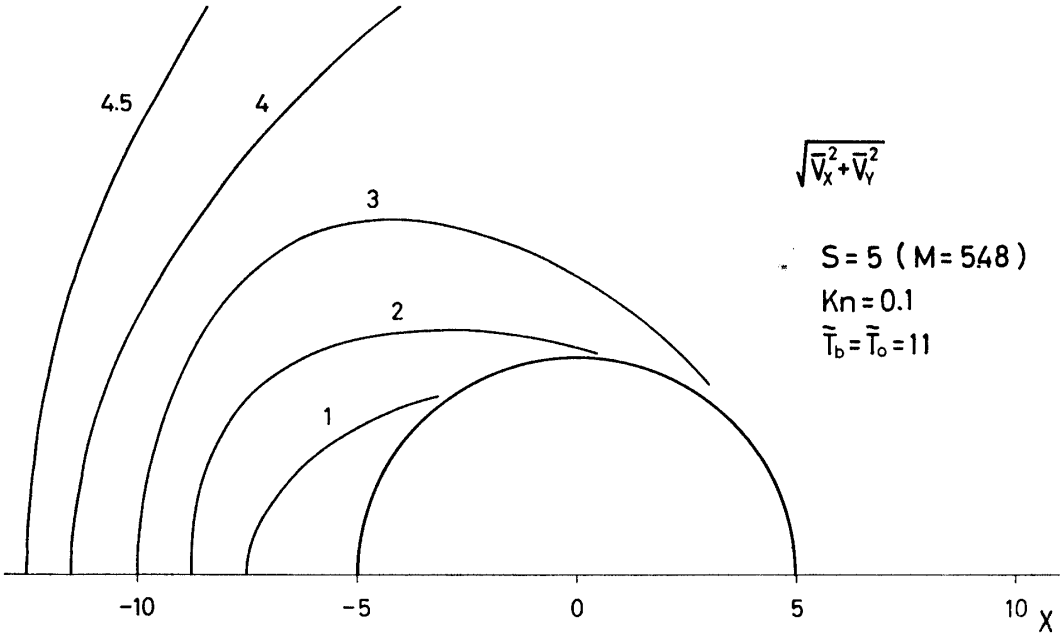


FIG. 19. Flow Field around a Circular Cylinder
(a) Equi-Speed Lines

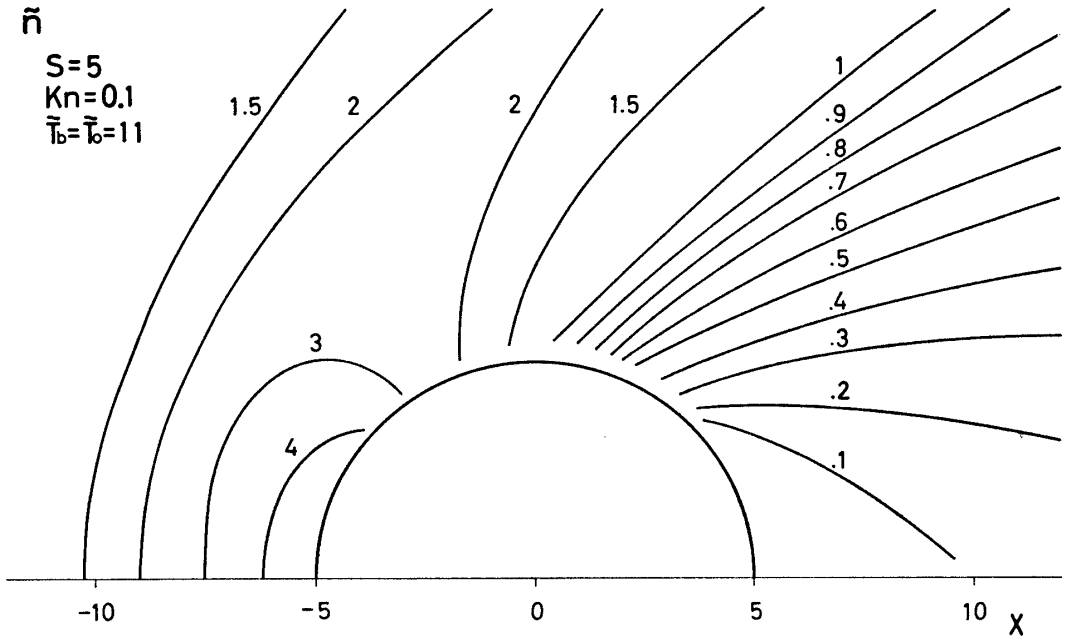


(b) Equi-Density lines

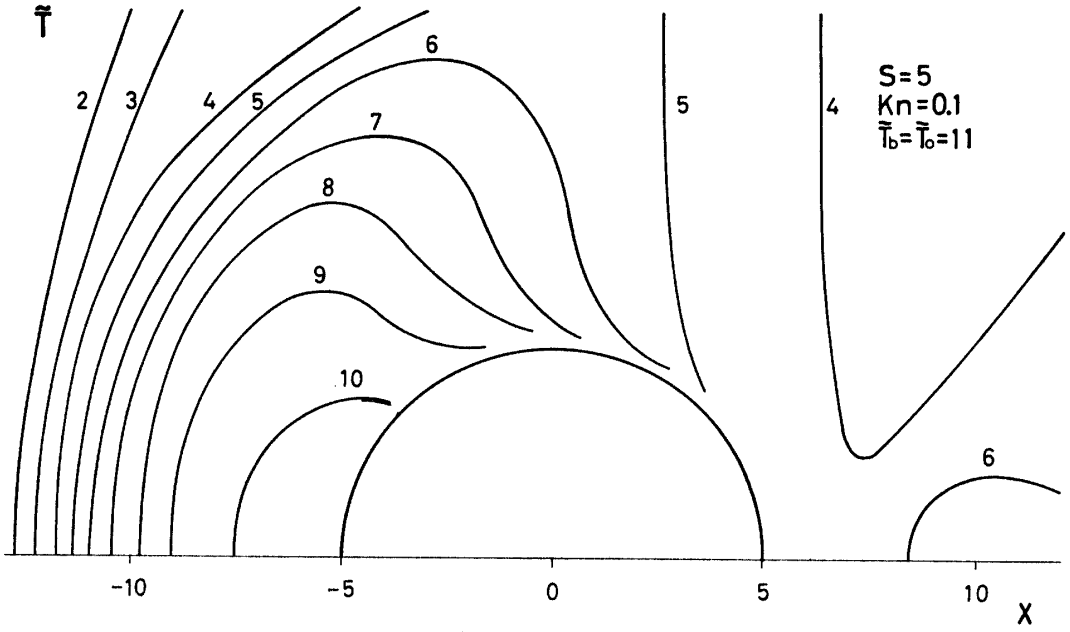


(c) Equi-Temperature Lines

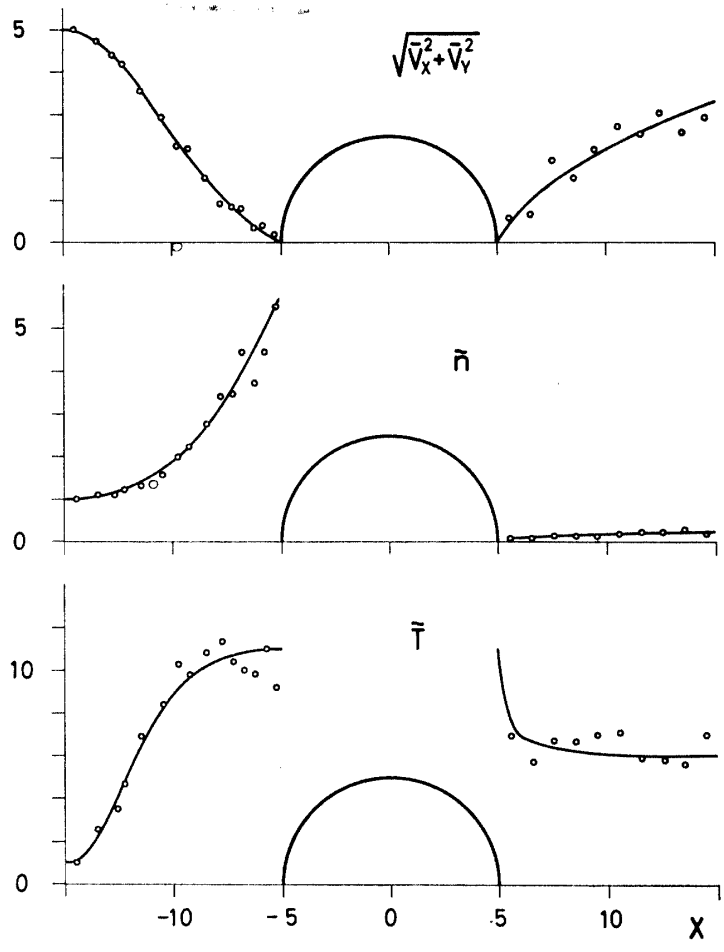


(d) Physical Properties along $X$-Axis

it monotonically decreases along the body surface to the rear stagnation point of the body, and that the region with the density less than unity is very wide in the downstream.

The temperature profile (Fig. 18c) shows that the temperature has a peak in the region somewhat upstream of the forward stagnation point and it decreases toward the body surface, since the body is highly cooled, and that it is considerably high in the wake.

Fig. 18d shows the variations of the macroscopic speed, density and temperature along the stagnation stream line, the left half of which (forward stagnation region) will be compared with other theoretical and experimental results afterwards. It is seen from the right half of the figure that the macroscopic speed recovers to its uniform flow value more rapidly than the density in the wake.

In a more rarefied case of $Kn=1$ the disturbance caused by the body affects a wider flow field as compared with the body diameter (see Fig. 16). The flow field in the case of $S=5$, $Kn=0.05$ and $\tilde{T}_b=1$, which is not shown in figures, has same tendencies as the case of $Kn=0.1$.

*Flow Field around a Circular Cylinder when $S=5$, $Kn=0.1$ and $\tilde{T}_b=1$ (Near Adiabatic Case)*

The flow field around a circular cylinder with the temperature equal to the

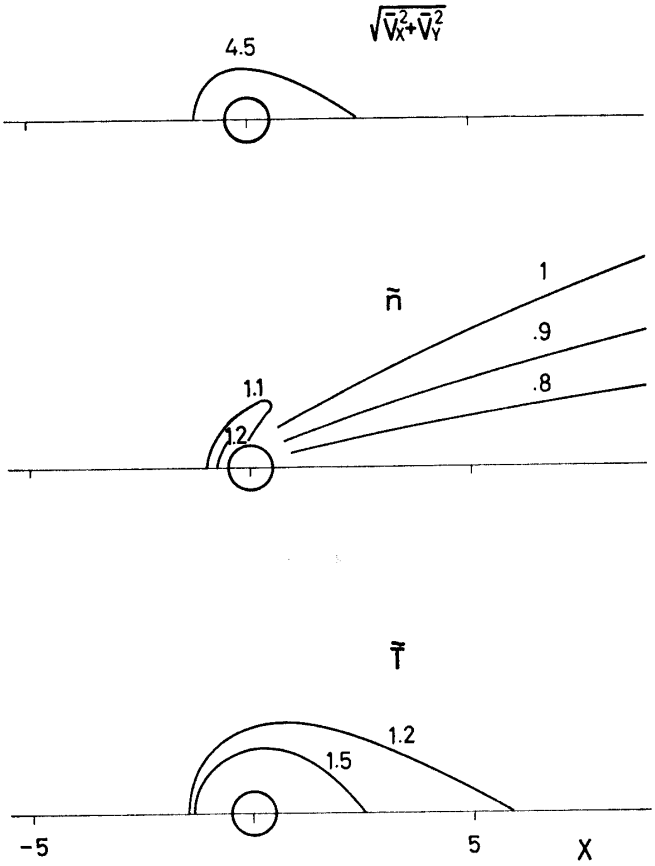


FIG. 20. (a) Flow Field around a Sphere
S=5, $Kn=1$ $\tilde{T}_b=1$ ($M=5.48$)

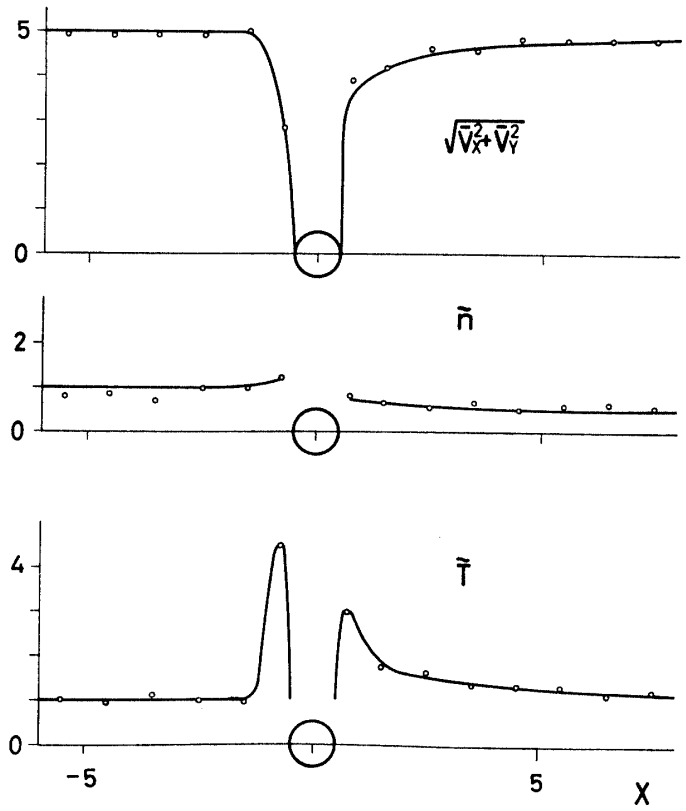


(b) Phisical Properties along $X$-Axis

stagnation temperature of the uniform flow when $S=5$ and $Kn=0.1$ is shown in Fig. 19. All of the differences between Figs. 18 and 19 can be explained by the different values of the body temperature, that is, the molecule that have collided with the body has a larger speed and it can travel farther from the body than in the highly cooled case.

It is seen from the comparison of Figs. 18a and 19a that the deceleration of the flow occurs in the region further upstream and the acceleration occurs more rapidly in the downstream in this case than in the preceding case. (Compare, for example, the lines with the values of 4.5 and 3 in the two figures.)

The disturbed region is widened also in the density profile shown in Fig. 19b (compare the lines with the values of 1.5 and 2 with those in Fig. 18b). The value of the density in the forward stagnation region, however, is about four and does not exceed six even at the forward stagnation point, since the molecules that have collided with the body have large speeds and are not gathered there. A similar tendency is seen in the wake, and the region with the density less than 0.5 is wider than in the preceding case.

The temperature profile (Fig. 19c) is quite different from that in the preceding case (Fig. 18c) as expected, that is, the temperature monotonically increases toward the body surface.

The variations of the macroscopic speed, density and temperature along the stagnation stream line are shown in Fig. 19d in this case. It is again found that

the macroscopic speed recovers to its uniform flow value more rapidly than the density in the wake. The temperature in the wake is higher than in the highly cooled case, because the body temperature is high in this case.

*Flow Field around a Sphere when $S=5$, $Kn=0.1$ and $\tilde{T}_b=1$ (Highly Cooled Case)*

It is seen at a glance that the flow field around the sphere (Fig. 21) indicates the smaller effect of the body on the flow than in the case of the circular cylinder with the same flow condition (Fig. 18), except that the region with the density less than unity is almost same. It is a remarkable difference between the two-dimensional and axisymmetric flows around the body, because the region which experiences the disturbance is always wider than the region which generates the disturbance. (Recall the difference between Figs. 2a and 2b.)

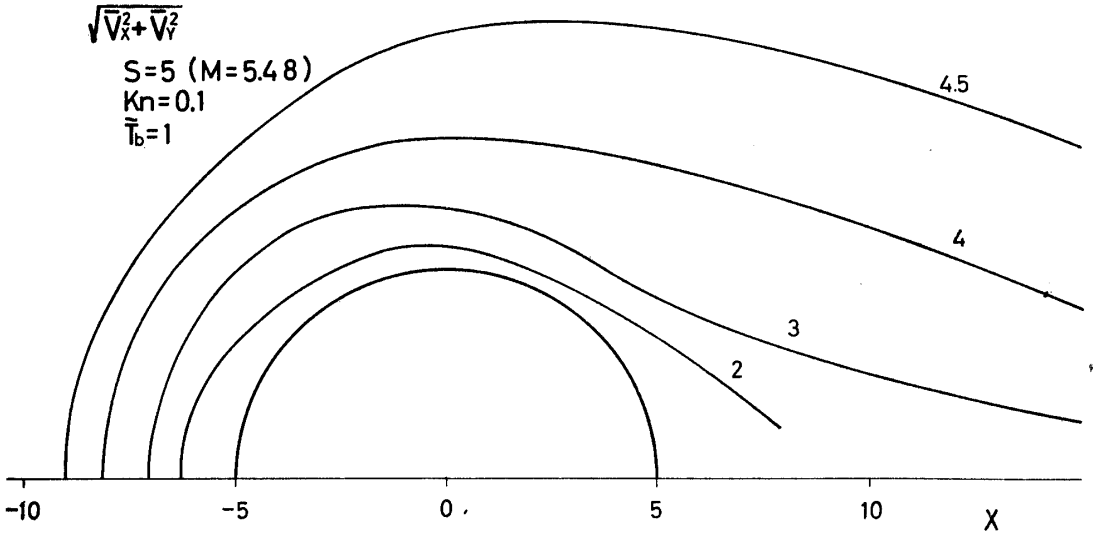


FIG. 21. Flow Field around a Sphere
(a) Equi-Speed Lines

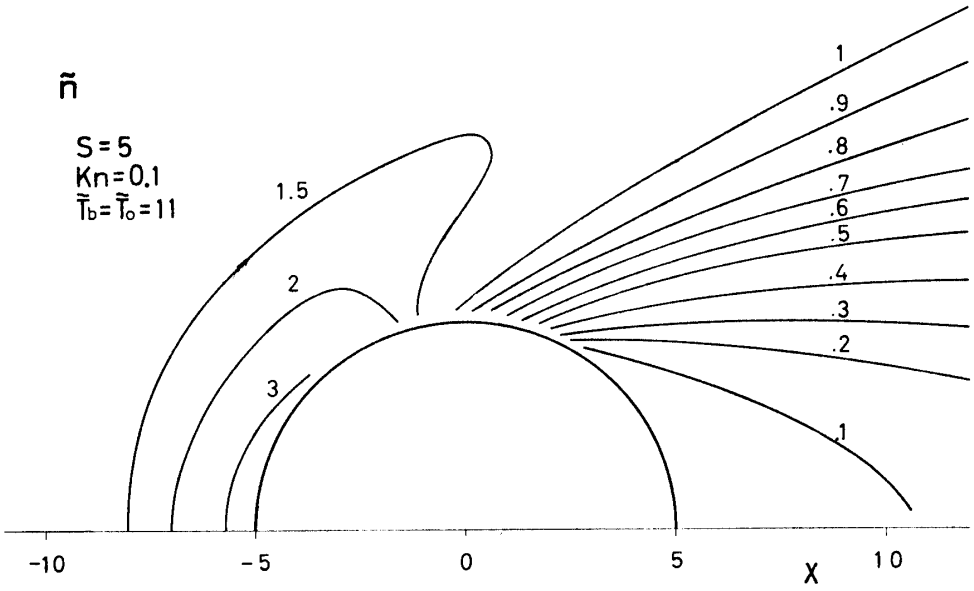


(b) Equi-Density Lines

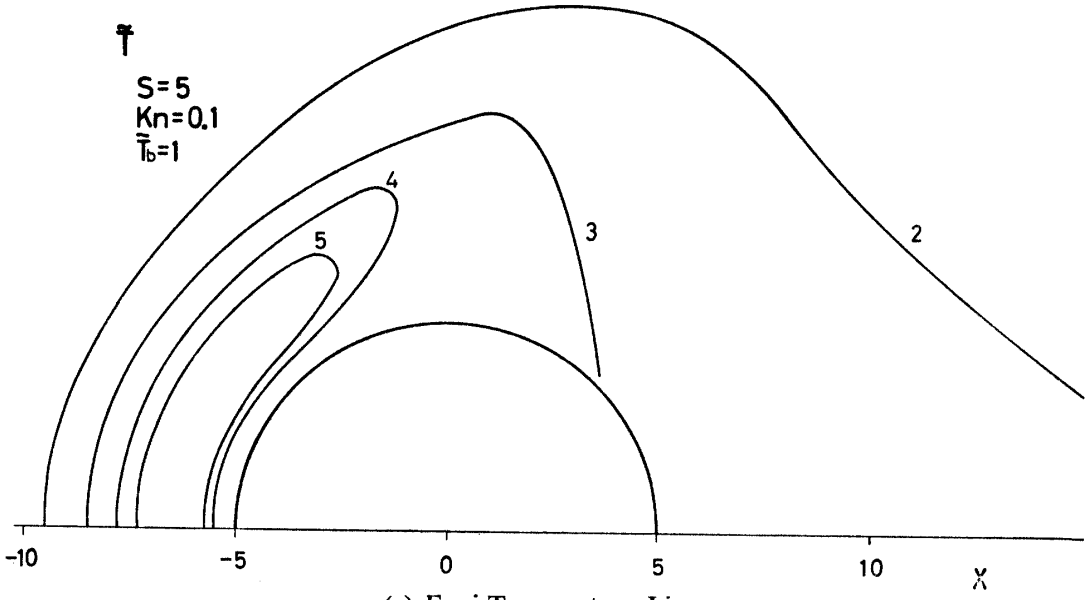


(c) Equi-Temperature Lines

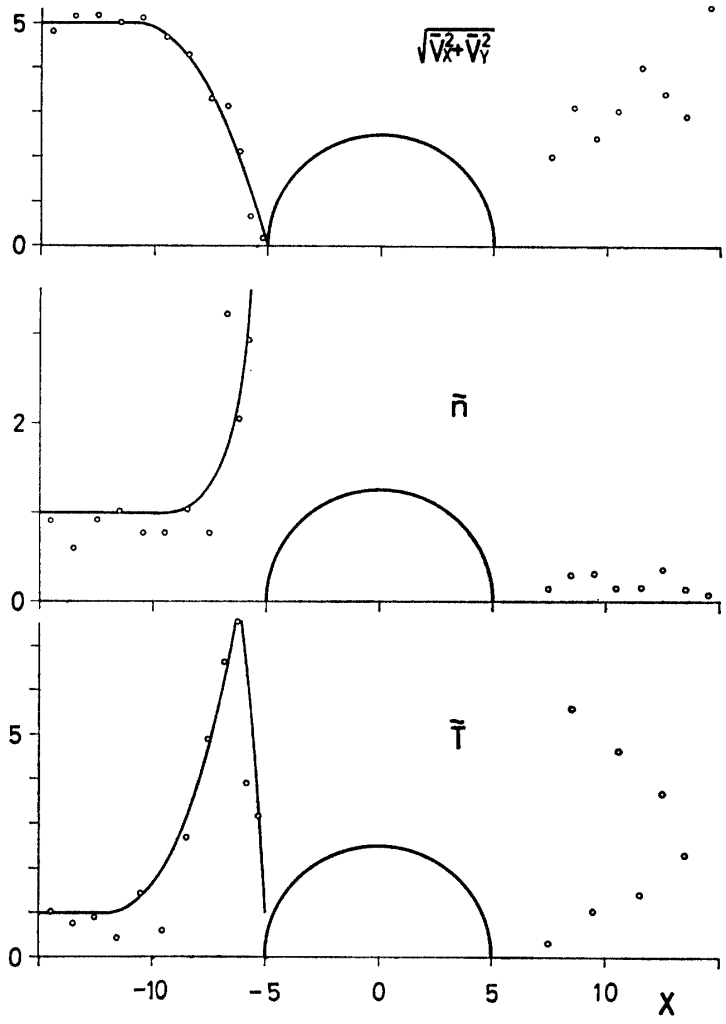


(d) Physical Properties along $X$-Axis

Another difference between the two-dimensional and axisymmetric flows is that the sample size at any moment varies with the $Y$-coordinate of the cell ($Y_c$) in the latter, on the other hand it is almost independent of the value of $Y_c$ in the former. It is a disadvantage in the axisymmetric flow that the sample sizes in the cells near to the symmetry (or center) line, which are most important and interesting to investigate, are always smaller than in the cells far from that line.

Similar arguments are applicable to the differences between Figs. 16 and 20, and Figs. 19 and 22, respectively.

*Flow Field around a Sphere when $S=5$, $Kn=0.1$ and $\tilde{T}_b=11$ (Near Adiabatic Case)*

The flow field around a sphere with the temperature equal to the stagnation temperature of the uniform flow when $S=5$ and $Kn=0.1$ is shown in Fig. 22. The

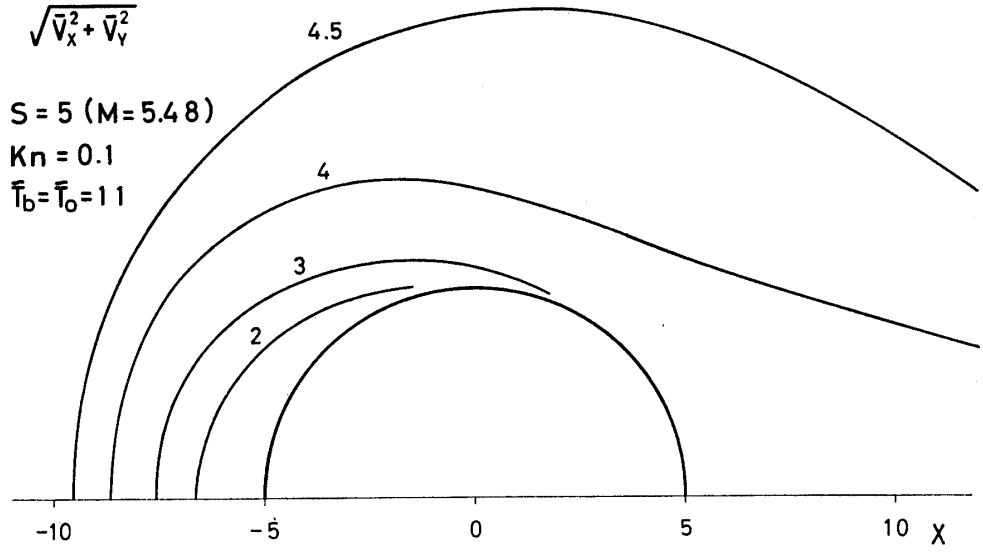


FIG. 22. Flow Field around a Sphere
(a) Equi-Speed Lines

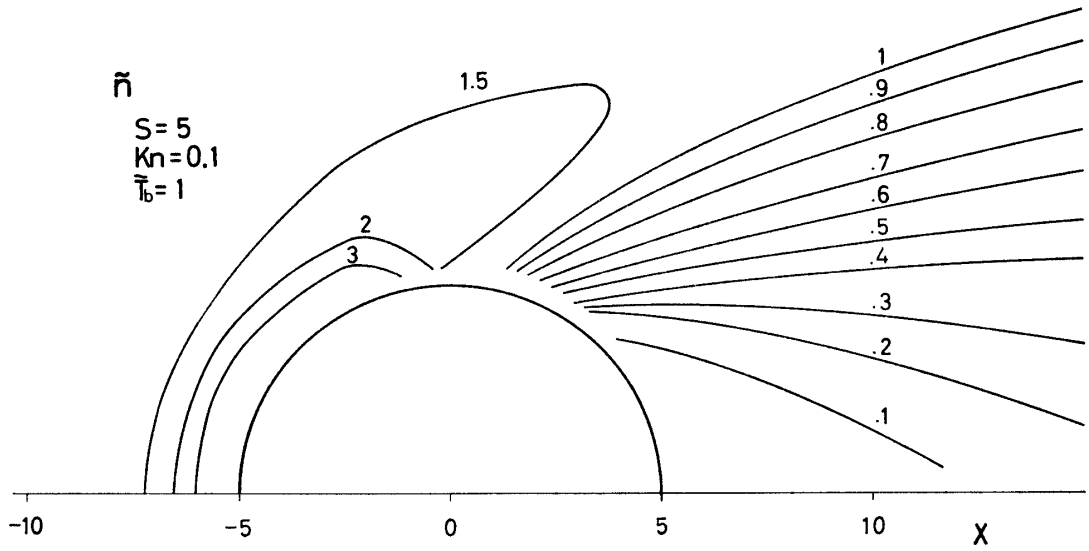


(b) Equi-Density Lines

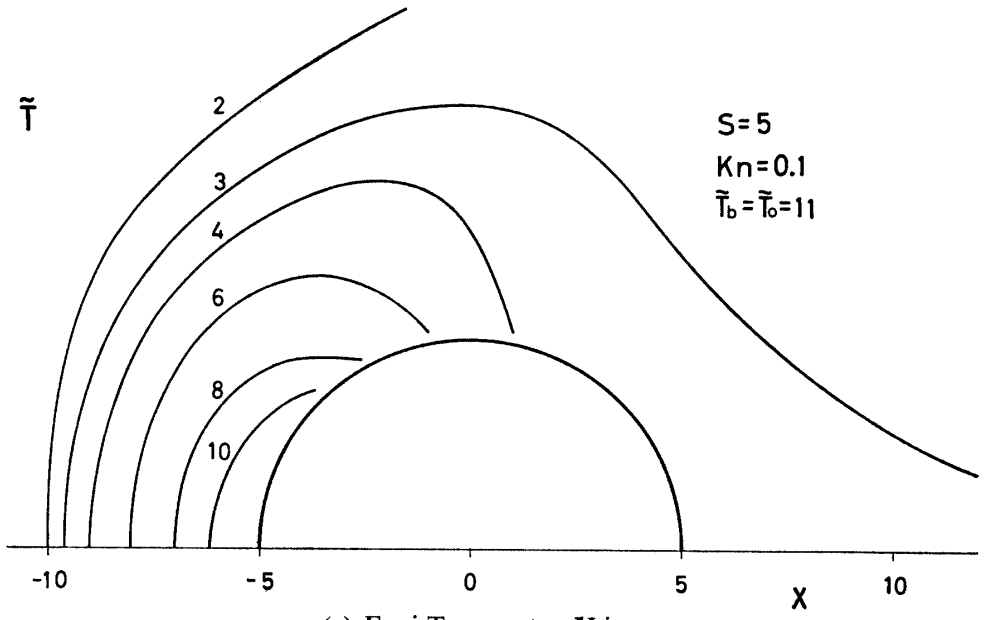


(c) Equi-Temperature Lines

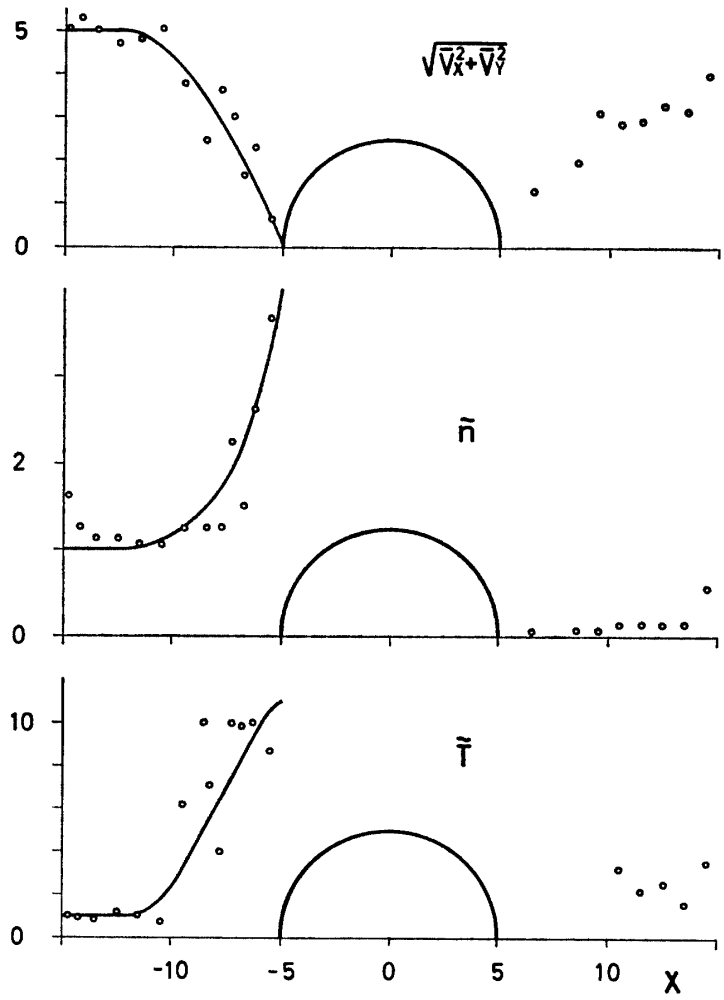


(d) Physical Properties along $X$-Axis

differences between Figs. 22 and 21 can be explained by the difference of the body temperature which determines the speed of the molecule that have collided with the body.

*Stagnation Line Velocity Profile*

The variations in the velocity component in the direction of the uniform flow along the stagnation stream line are shown in Fig. 23 for the cases of the circular cylinder and the sphere with highly cooled and near adiabatic conditions, which also includes other results.

It is seen from Fig. 23a that the deceleration of the flow in the case of the sphere occurs in the region closer to the body than in the case of the circular cylinder,

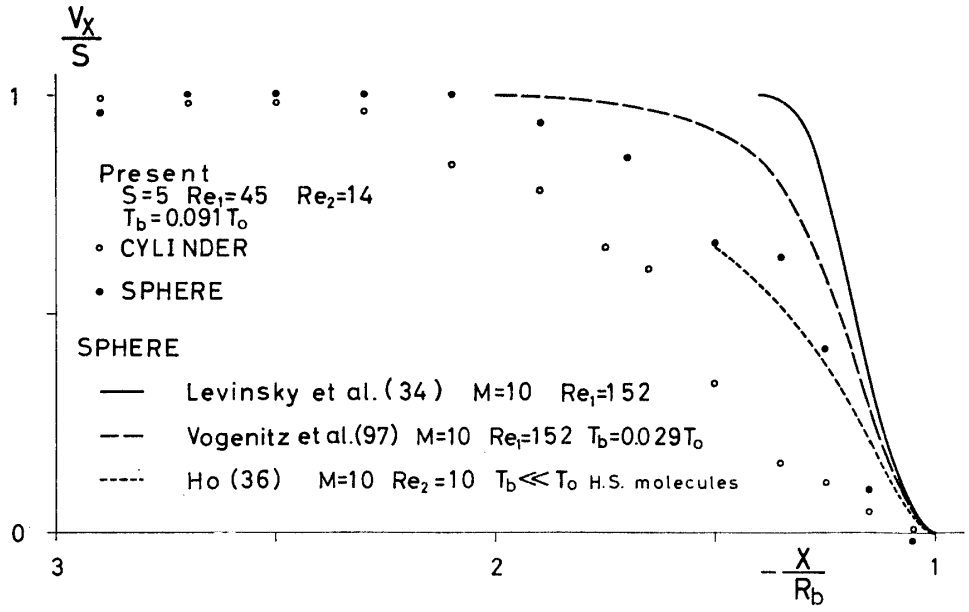


FIG. 23. Stagnation Line Velocity Profiles
(a) $T_b \ll T_0$

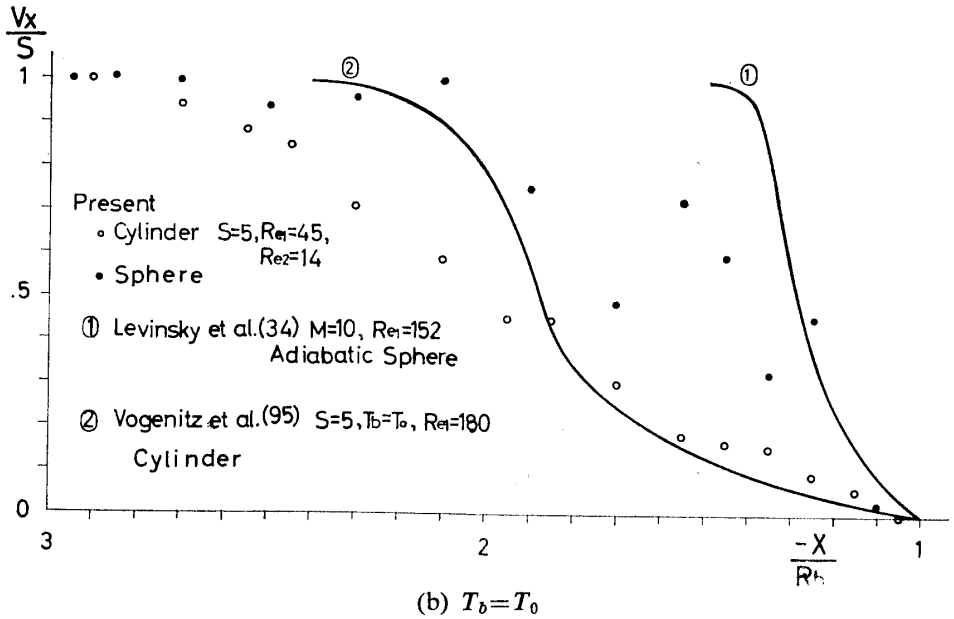


(b) $T_b = T_0$

because of the difference between the two-dimensional and axisymmetric flows as discussed above, and that it agrees well with the results by Ho [*36*], who used the kinetic theory with Kao's solution [*35*] as the zeroth approximation. This agreement means that the kinetic theory is to be applied to the analysis of the flow with a low Reynolds number. It is guaranteed by the difference between the results by Levinsky et al. [*34*] and by Vogenitz et al.[*97*], the former of which is based on the continuum theory and the latter on the Monte Carlo method. Reynolds numbers used here are defined by the following expressions.

$$\mathrm{Re}_1=\frac{\rho_\infty u_\infty r_b}{\mu_\infty} \tag{4-11}$$

$$\mathrm{Re}_2=\frac{\rho_\infty u_\infty r_b}{\mu_s}, \tag{4-12}$$

where $r_b$ is the body radius.

*Stagnation Line Density Profile*

The variations of the density along the stagnation stream line are shown in Fig. 24, which also includes the results by Russell [*39*] with the electron beam densitometry and by Vogenitz et al. [*95*] with the Monte Carlo method. The present results in the case of the highly cooled sphere agree well with the former, and the results in the case of the circular cylinder slightly exceed those in the case of the sphere, because of the reason discussed above (Fig. 24a). The results in the case of the near adiabatic sphere also agree well with those by Russel. The results in the case of the near adiabatic cylinder show a similar tendency as that obtained by Vogenitz et al. The agreement is not so good if the difference of the Reynolds numbers between the two cases is taken into account (Fig. 24b).

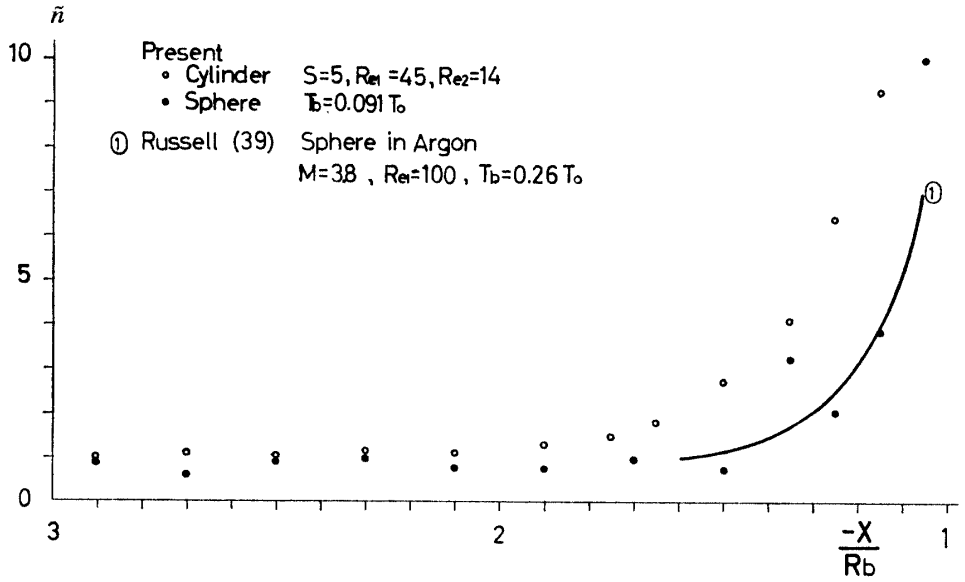


FIG. 24. Stagnation Line Density Profiles
(a) $T_b \ll T_0$

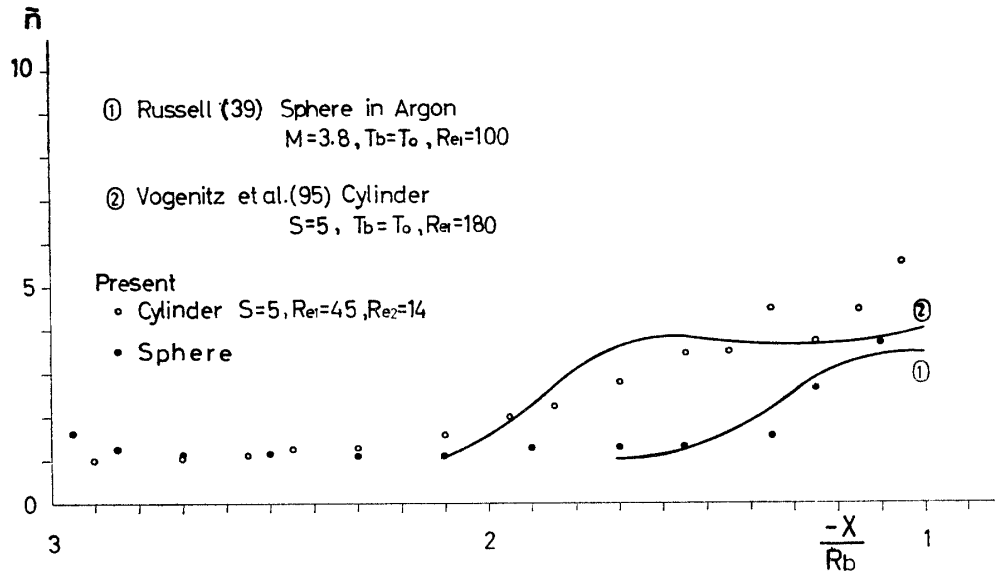


(b) $T_b = T_0$

*Stagnation Line Temperature Profile*

The temperature profiles along the stagnation stream line are shown in Fig. 25 with other results. The present results in the case of the highly cooled sphere are shifted further upstream and its maximum value is lower than in the case of the result by Vogenitz et al. [97] whose Mach and Reynolds numbers are higher than in the present case. It is reasonable because the former and latter differences can be explained by the differences of the Mach and Reynolds numbers between the two cases, respectively. The results in the case of the highly cooled cylinder have higher values than in the case of the sphere, because of the difference between the

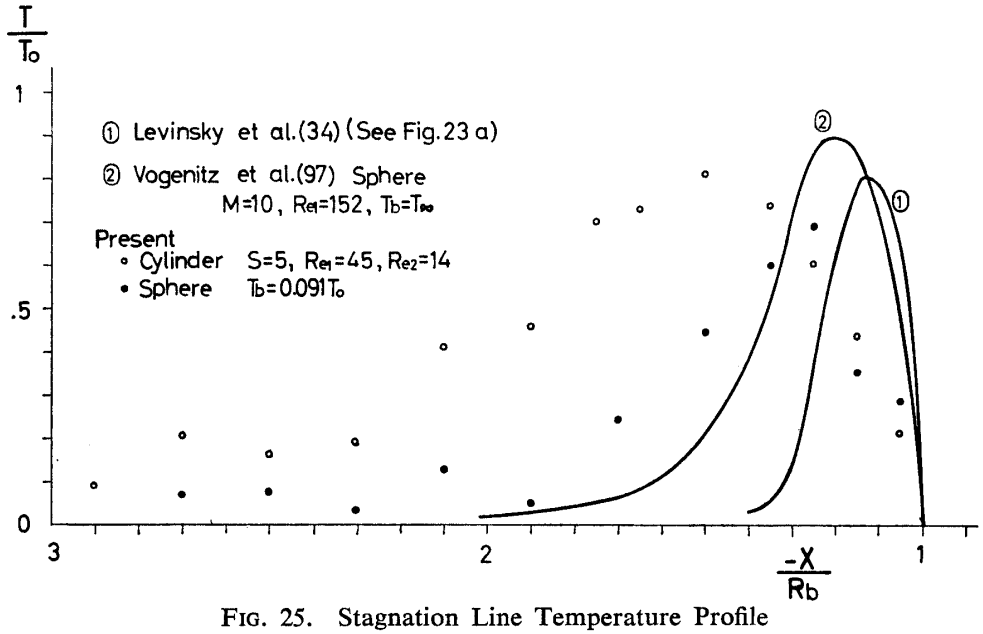


FIG. 25. Stagnation Line Temperature Profile

(a) $T_b \ll T_0$

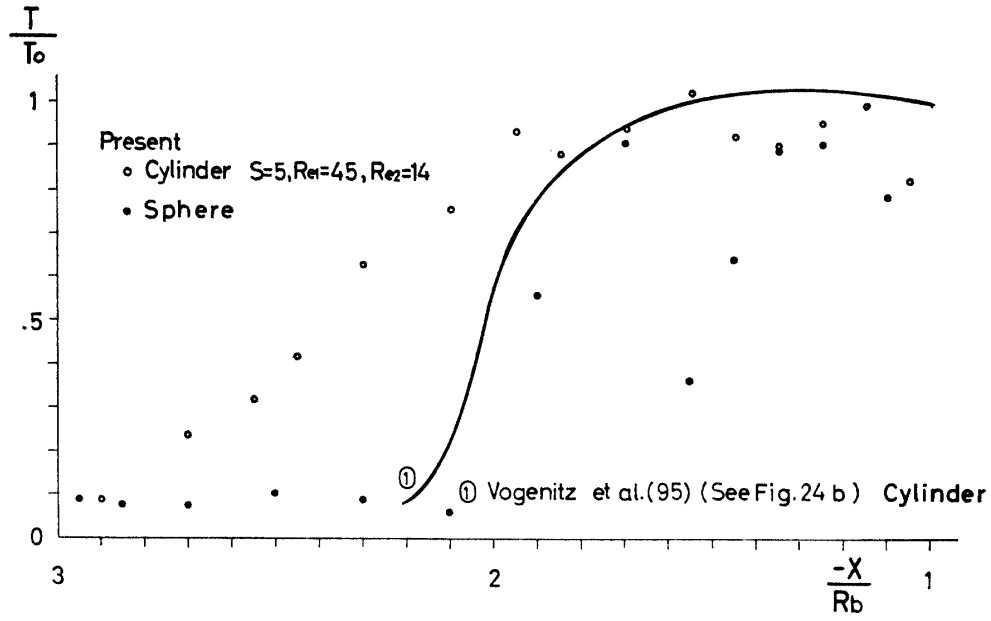


(b) $T_b=T_0$

two-dimensional and axisymmetric flows. Similar tendencies are seen in the near adiabatic case shown in Fig. 25b, which also includes the result for the circular cylinder by Vogenitz et al. [*95*] with the Monte Carlo method.

*Stagnation Point Pressure*

The pressures at the forward stagnation point are shown in Fig. 26 which also includes the experimental results by Potter et al. [*42*] and by Chang et al. [*44*] in the case of the sphere. $C_{p1}(0)_i$ appearing in the ordinate is given by the Rankine-Hugoniot relation as follows.

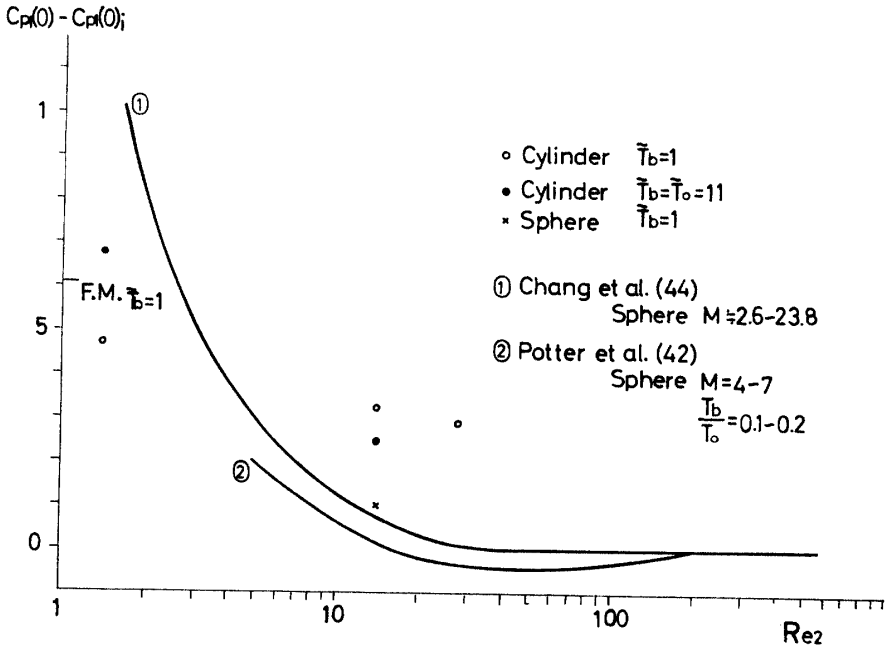


FIG. 26. Stagnation Point Pressure

$$C_{p_1}(0)_i=\frac{2}{\gamma M^2}\left[\frac{(\gamma+1)M^2}{2}\right]^{\gamma/\gamma-1}\left[\frac{\gamma+1}{2\gamma M^2-(\gamma-1)}\right]^{1/\gamma-1} \tag{4-13}$$

The free molecule value is calculated by the equation (4–17) with the value of theta equal to zero. It is to be noted that the Reynolds number in the abscissa $Re_2$ is the half of the ordinary definition of $Re_2$ in the stagnation point pressure study. The present results seem to be reasonable, although the data points are scarce and no other result about the circular cylinder is present.

*Stagnation Point Heat Transfer*

The heat transfers at the forward stagnation point in the highly cooled case are shown in Fig. 27 with other theoretical results. (Other experimental results agree with the theoretical curves.) Reynolds number used here is defined by the following expression.

$$\mathrm{Re}_3=\frac{\rho_s u_\infty r_b}{\mu_s}. \tag{4-14}$$

The result obtained by Lees [46] using the modified Newtonian and boundary layer theories for a highly cooled blunt body is expressed as follows.

$$\begin{aligned} C_h(0)&=\frac{\gamma-1}{\tilde{T}_0-\tilde{T}_b}\frac{2^{k/2}}{4}Pr^{-2/3}G\sqrt{H}\frac{M^2}{\sqrt{\mathrm{Re}_1}}\\ G&=\left[\frac{\gamma-1}{\gamma}\left(1+\frac{2}{\gamma-1}\frac{1}{M^2}\right)\left(1-\frac{1}{\gamma M^2}\right)\right]^{1/4}\\ H&=\frac{(\gamma+1)M^2}{(\gamma-1)M^2+2}\left[\frac{(\gamma+1)^2M^2}{2(2\gamma M^2-\gamma+1)}\right]^{1/\gamma-1}\sqrt{\tilde{T}_0}, \end{aligned} \tag{4-15}$$

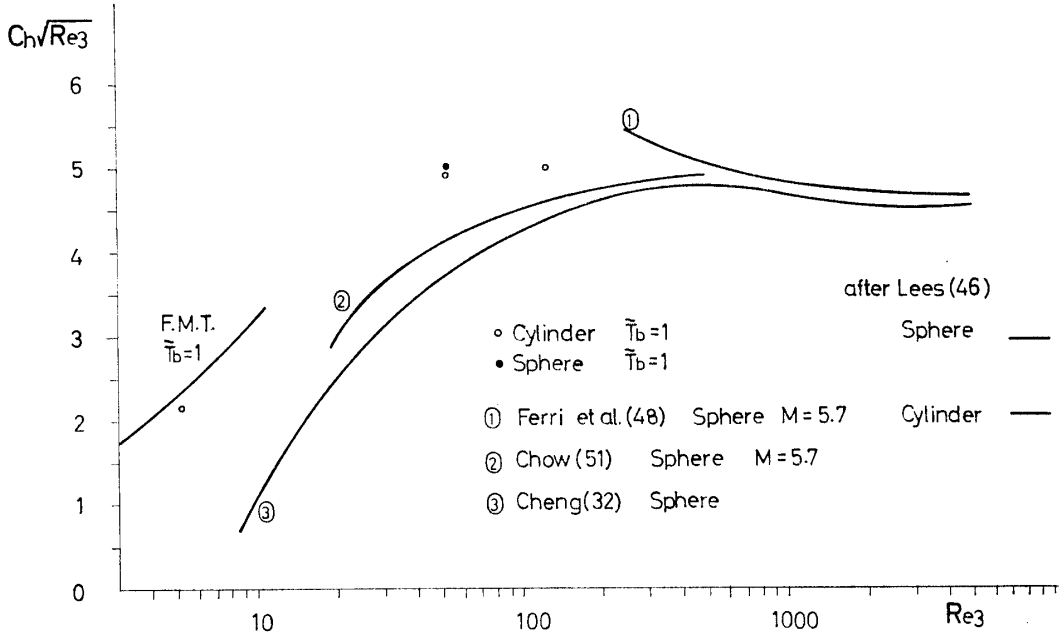


FIG. 27. Stagnation Point Heat Transfer ($T_b \ll T_0$)

where $k=0$ and 1 respectively correspond to the two-dimensional and axisymmetric bodies. The free molecule value is calculated by the equation (4–19) with the value of theta equal to zero. The present results agree reasonably well with the theoretical curves by Cheng [*32*] and by Chow [*51*].

*Surface Pressure Distribution*

The surface pressure distributions are shown in Fig. 28 including other theoretical results. It is expressed as follows by the modified Newtonian theory and by the free molecule flow theory, respectively.

$$C_{p1}(\theta)=C_{p1}(0)\cos^2\theta+\frac{2}{\gamma M^2}\sin^2\theta \tag{4–16}$$

$$C_{p1}(\theta)=\frac{1}{S^2}\left[\left(\frac{1}{\sqrt{\pi}}S\cos\theta+\frac{1}{2}\sqrt{\tilde{T}_b}\right)\exp\left(-S^2\cos^2\theta\right)+\left(S^2\cos^2\theta+\frac{1}{2}+\frac{1}{2}\sqrt{\pi\tilde{T}_b}S\cos\theta\right)\{1+erf(S\cos\theta)\}\right], \tag{4–17}$$

where *erf* is the so-called error function defined below.

$$erf(x)=\frac{2}{\sqrt{\pi}}\int_0^x \exp\left(-y^2\right)dy$$

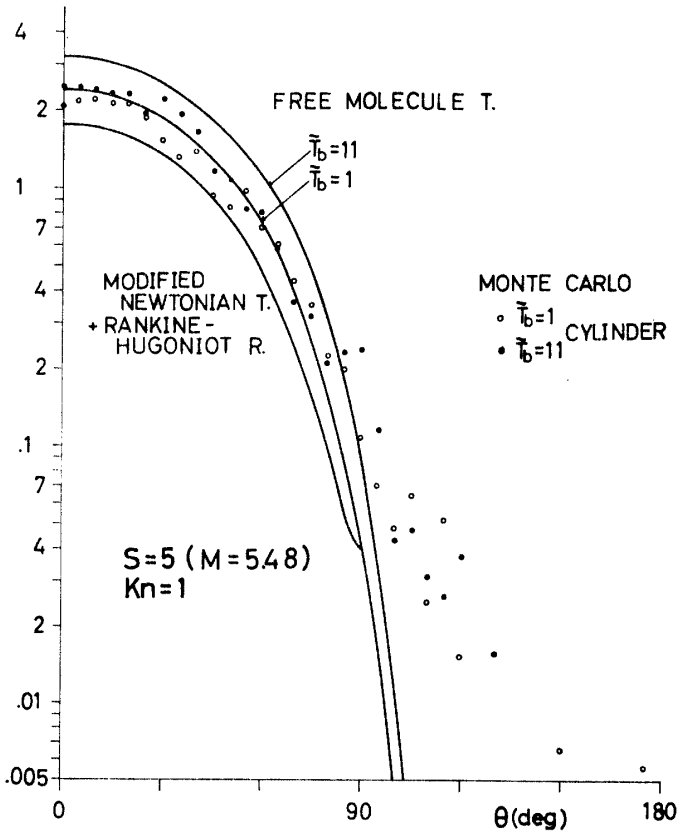


FIG. 28. Surface Pressure Distribution
(a) $Kn=1$

Fig. 28a shows that the pressure distribution of the circular cylinder at $\tilde{T}_b=11$ is a little higher than that at $\tilde{T}_b=1$ in the front part of the body and their difference can not be distinguishable in the rear part and that the Monte Carlo results are located between the values calculated by the modified Newtonian theory with the Rankine-Hugoniot relation (combination of (4–13) and (4–16)) and by the free molecule flow theory in the front part and then they become higher than the theoretical values in the rear part. Conversely, the reasonable agreement of the present results with the theoretical curves in Fig. 28a bears witness to the uniformity of the coordinates of the molecules in a cell, since the body radius is equal to the half of the side length of a unit cell in this case. The difference between the circular cylinder and the sphere is seen in Fig. 28b, that is, the results in the case of the sphere agree well with the modified Newtonian theory with the Rankine-Hugoniot relation in the front part, even when the Reynolds number is low ($Re_1=45$). The effect of the body temperature is found to be small also in this case. The results for the highly cooled cylinder in the case of $Kn=0.05$ show a similar tendency as in the case of $Kn=0.1$ (Fig. 28c).

Fig. 28d shows the present results both by the Monte Carlo method and by the experiment. The pressure coefficient $C_{p_1}$ divided by the value after a Rankine-

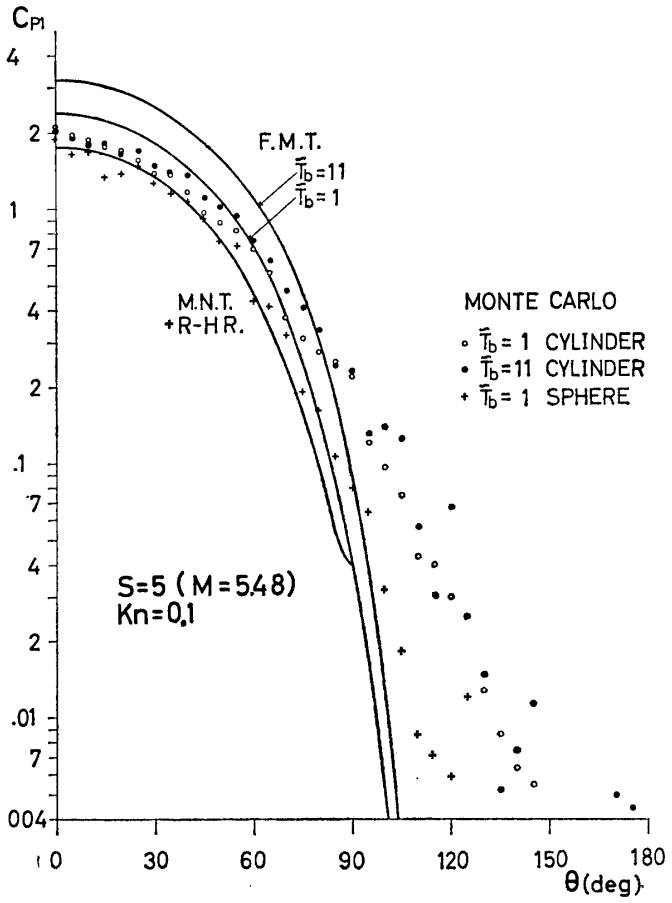


(b) $Kn=0.1$

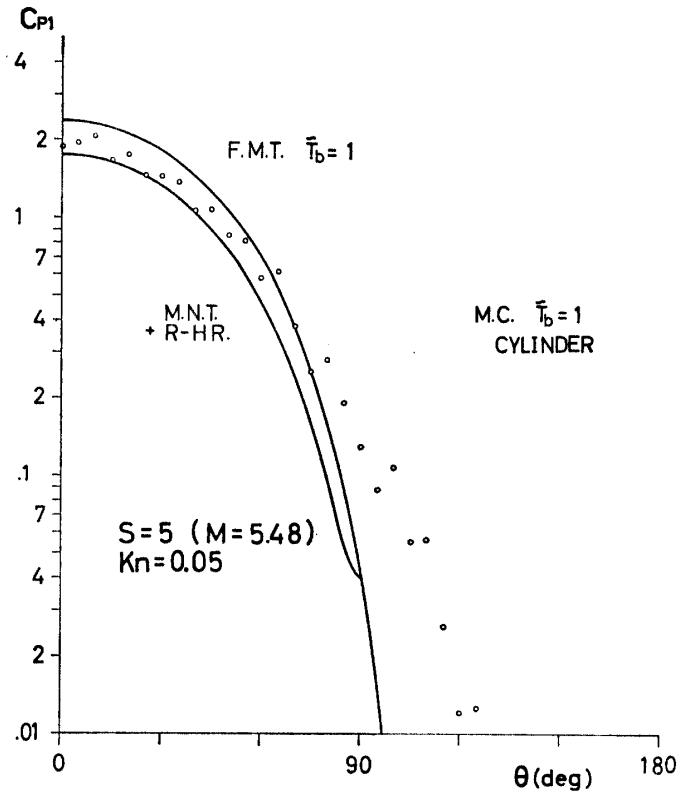


(c) $Kn=0.05$

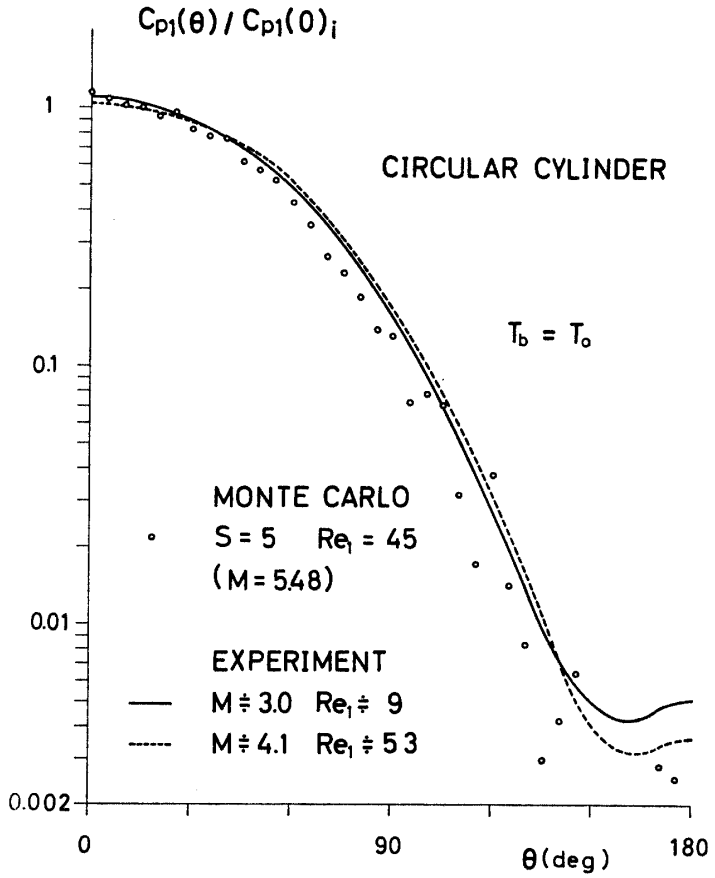


(d) Comparison of Experimental and Monte Carlo Results (Circular Cylinder)

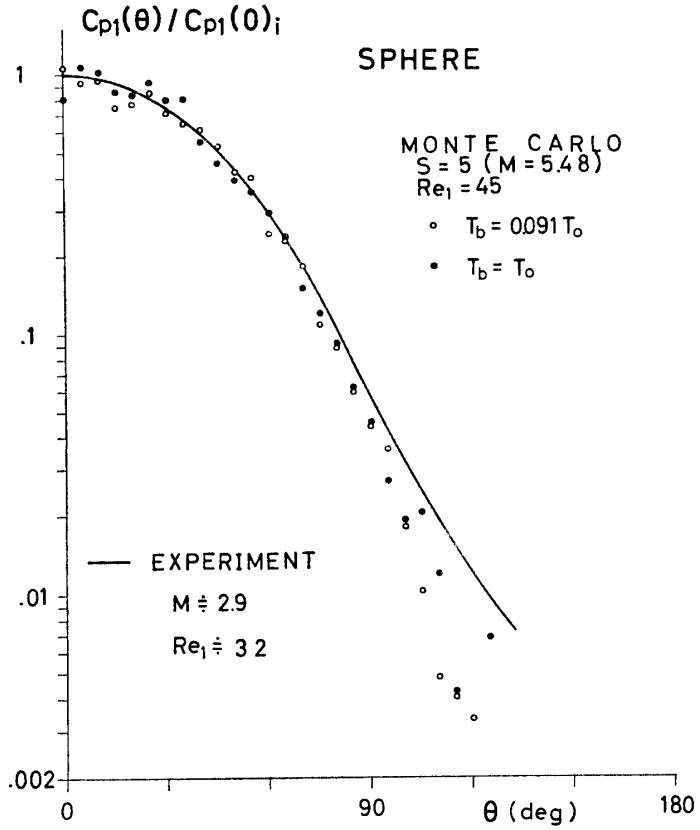


(e) Comparison of Experimental and Monte Carlo Results (Sphere)

Hugoniot shock is made use of, since the uniform flow Mach numbers are different between the cases of the Monte Carlo method and the experiment. The experimental curves respectively represent the mean values of several runs, and they show that the surface pressure is scarcely affected by the Mach and Reynolds numbers at least in the ranges of the present experiment. The agreement of the Monte Carlo and experimental results is quite well.

The comparison of all the results in Fig. 28 shows that the surface pressure is near to that obtained by the free molecule flow theory when the Knudsen number is large and it approaches that calculated by the modified Newtonian theory with the Rankine-Hugoniot relation as the Knudsen number decreases in the front part of the body.

*Heat Transfer Distribution*

The heat transfers to the body surface are shown in Fig. 29 including other theoretical curves. One of them is given by Lees [*46*] for a highly cooled sphere.

$$\frac{C_h(\theta)}{C_h(0)} = \frac{\theta \sin\theta\left[\cos^2\theta + \frac{1}{\gamma M^2}\sin^2\theta\right]}{2\left\{\int_0^\theta \theta \sin^2\theta\left[\cos^2\theta + \frac{1}{\gamma M^2}\sin^2\theta\right]d\theta\right\}^{1/2}} \tag{4–18}$$

Another is by the free molecule flow theory as follows.

$$C_h(\theta)=\frac{\gamma-1}{2\gamma\sqrt{\pi}S(\tilde{T}_0-\tilde{T}_b)}\left[\left(S^2+\frac{\gamma}{\gamma-1}-\frac{1}{2}\frac{\gamma+1}{\gamma-1}\tilde{T}_b\right)\right.$$
$$\times[\exp(-S^2\cos^2\theta)+\sqrt{\pi}S\cos\theta\{1+erf(S\cos\theta)\}] \qquad (4\text{–}19)$$
$$\left.-\frac{1}{2}\exp(-S^2\cos^2\theta)\right]$$

The results in the case with the larger Knudsen number are seen to come nearer to the free molecule value as expected in the front part of the body (Fig. 29a). Lees's results (combination of eqs. (4–15) and (4–18)) are qualitatively good and equation (4–18) only is quantitatively good if the value of the stagnation point is known. It is because his result (4–15) is to be valid for a faily large Reynolds number. The results in the rear part of the body are dispersed and a quantitative discussion can not be made, partly because the sample sizes are very small there. They, however, agree reasonably well with the experimental results, which are not shown in the figure for simplicity.

The results in the case of the near adiabatic cylinder are shown in Fig. 29b, and they are strongly dispersed and a quantitative discussion can not be made, although the sample sizes are almost same as in the preceding case. It may only be said that the region $C_h'<0$, that is, where the heat is transferred from the body

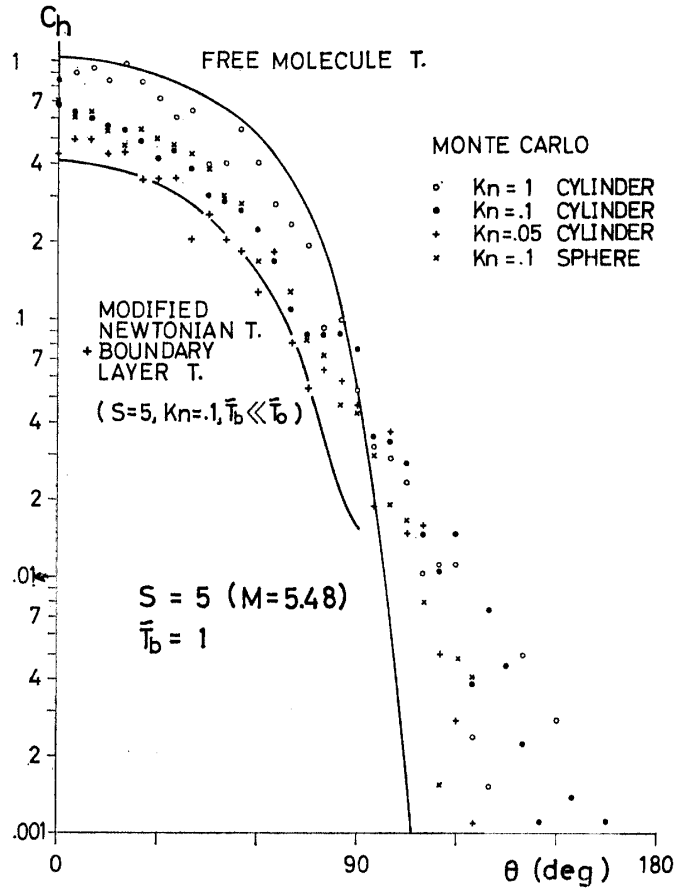


FIG. 29. Heat Transfer Distribution
(a) $\tilde{T}_b=1$

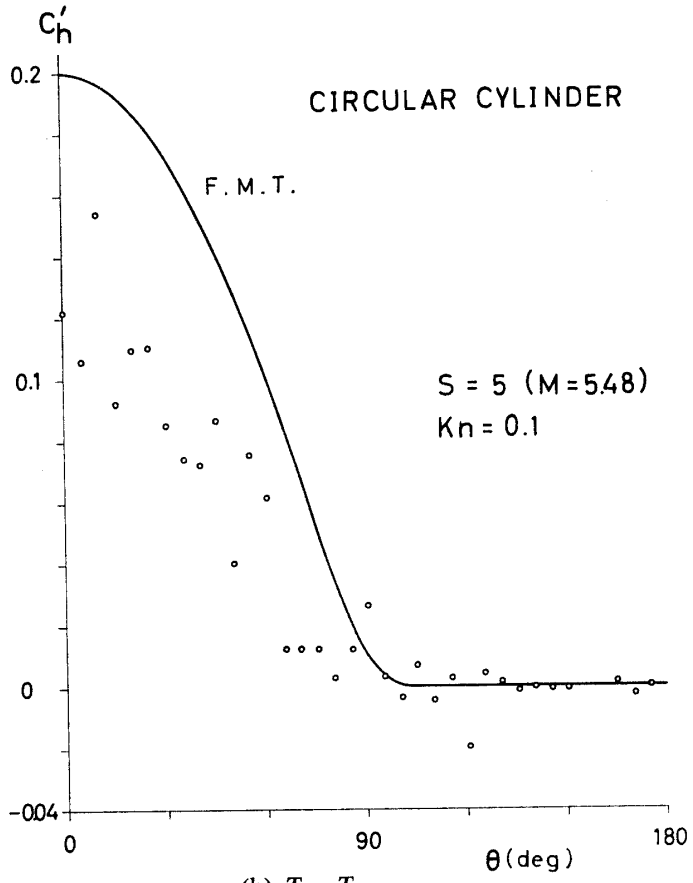


(b) $T_b=T_0$

to the flow can appear in the rear part of the body.

This difference between the dispersions of the results for the highly cooled and near adiabatic cases seems to clarify a weak point of the Monte Carlo method, that is, it can hardly treat a very small quantity. This difficulty has been pointed out by Kogan [*110*] and can also be seen in the density profile of the flat plate. (See Figs. 8e, 9e and 10d.) The quantity treated by the Monte Carlo method, of course, can be made small, if the sample size is increased, because the former is considered to be inversely proportional to the latter. However, it is not practical, since a very long computing time is required for such a calculation. Thus, it is seen that the Monte Carlo method can easily deal with the problem where all quantities deviate remarkably from the uniform flow values.

*Wake*

No useful information about the wake is obtained in the present study, because the sample sizes are very small there. Of course, it can be investigated if the cells are made small and the sample sizes are large, though very large computing time is required. However, the valley in the temperature profile in the downstream region may indicate the position of the separation shock (see, for example, the lines with the value of two in Fig. 18c). Thus, it is seen that the treatment of the wake by the Monte Carlo method requires a special arrangement of the cells and the body.

*Drag*

The drags exerted on the circular cylinder and the sphere obtained by the Monte Carlo method and by the experiment are shown in Fig. 30, also including other theoretical and experimental results. Davis et al. [*56*] calculated the flow fields around the sphere in the case of $M=10$ and $T_b=0.2T_0$ for several values of the Reynolds number making use of the first- and second-order boundary layer theories, and obtained the following expression for the drag.

$$C_D=0.89+\frac{2.8}{\sqrt{2\,\mathrm{Re}_2}} \tag{4–20}$$

It is to be noted that $2Re_2$ above corresponds to $Re_2$ in an oridnary definition in the drag study. Whitfield [*69*] calculated the drag as follows on the basis of the kinetic theory, introducing the concept of the collision surface.

$$\frac{C_D}{C_{D\mathrm{fm}}}=\frac{1}{1+\left[1+\dfrac{2\sqrt{2\,Kn}}{\sqrt{\left[\dfrac{4S}{3\sqrt{\pi\tilde{T}_b}}\right]^2+2\dfrac{4S}{3\sqrt{\pi\tilde{T}_b}}\cos\theta+1}}\right]^{-k}} \tag{4–21}$$

where $k=1$ and 2 respectively represent the cases of the circular cylinder and the sphere, the value of $\theta$ is determined by the location of the collision surface, and $C_{D\mathrm{fm}}$ is given by the free molecule flow theory in the cases of the circular cylinder and the sphere, respectively, as follows.

$$C_{D\mathrm{fm}}=\frac{\sqrt{\pi}}{S}\exp\left(-\frac{S^2}{2}\right)\left[\left(S^2+\frac{3}{2}\right)I_0\left(\frac{S^2}{2}\right)+\left(S^2+\frac{1}{2}\right)I_1\left(\frac{S^2}{2}\right)\right]+\frac{\pi}{4S}\sqrt{\pi\tilde{T}_b} \tag{4–22}$$

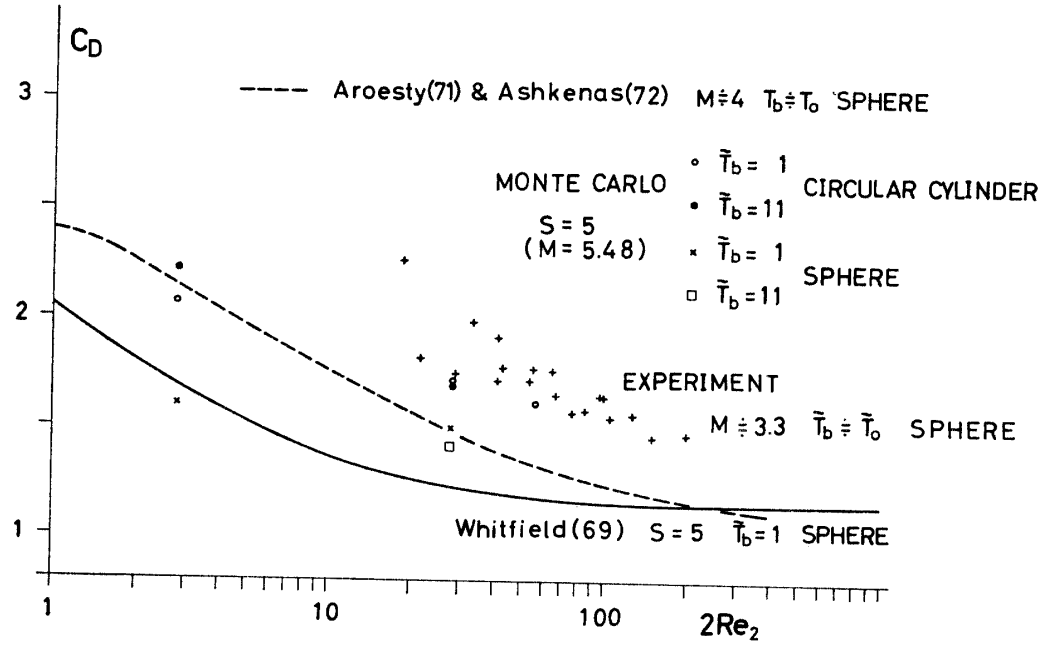


FIG. 30. Drag

$$C_{Dfm}=\frac{\exp(-S^2)}{\sqrt{\pi}\,S^3}(2S^2+1)+\frac{erf(S)}{2S^4}(4S^4+4S^2-1)+\frac{2}{3S}\sqrt{\pi\tilde{T}_b} \qquad (4\text{–}23)$$

$I_i$ appearing in (4–22) is the $i$th-order Bessel function of the first kind with imaginary argument. Experimental results in the case of the sphere by other authors are scarcely affected by the Mach number so far as the Mach number is higher than four when the body temperature is nearly equal to the stagnation temperature of the uniform flow and they are represented by those obtained by Aroesty [71] and by Ashkenas [72] in the figure. The lower the body temperature becomes, the lower the drag becomes. It is considerably higher in the case of the circular cylinder than in the case of the sphere.

It is seen that the present experimental results are located higher as a whole than the other experimental curves, partly because the surface of the present model is relatively rough. On the other hand, the Monte Carlo results shows the lower values and the effect of the body temperature can not be clearly seen. The results for the highly cooled sphere, however, agree well with the theory by Whitfield.

## V. Conclusion

It is concluded that the Monte Carlo method without the sampling in the velocity space is of use for calculating the hypersonic rarefied gas flow past a two-dimensional or axisymmetric body in consequence of the present study.

It is also concluded that this method enables us to easily obtain the important quantities with respect to the body, that is, the pressure, the skin friction, the drag force and the heat transfer.

It is shown that the Monte Carlo results agree well with the values measured by the present author in a low density wind tunnel in respect of the pressure distributions of the circular cylinder and the sphere. The present results of calculations concerning the density fields are also shown to agree well with the existing experimental results obtained by the electron beam densitometry.

## Acknowledgments

The author wishes to express his sincere thanks to Professor Fumio Tamaki for his advice and encouragement during the course of the work.

He also wishes to express his appreciation to Dr. M. Hinada and Mr. M. Terada for their invaluable advice and permission to reproduce their experimental results.

He is indebted to Miss A. Togawa and Miss Y. Tamaki for their fruitful suggestions to improve the details of the computer program.

To the members in the Data Process Center at the Institute of Space and Aeronautical Science, University of Tokyo, goes his special thanks for use of their HITAC 5020F computer. Special thanks are also due to Mr. M. Kurosaki, Mr. S. Nakao and Miss H. Sakurai for doing the numerous drawings and typing the manuscript.

*Department of Space Technology*
*Institute of Space and Aeronautical Science*
*University of Tokyo*
*October 5, 1971*

## REFERENCES

Note: Abbreviated expressions listed below are used here.

RGD, 1960 Rarefied Gas Dynamics, Devienne, F. M. ed., Pergamon Press, 1960
RGD, 1961 Rarefied Gas Dynamics, Talbot, L. ed., Academic Press, 1961
RGD, 1963 Rarefied Gas Dynamics, Laurmann, J. A. ed., Vol. II, Academic Press, 1963
RGD, 1965 Rarefied Gas Dynamics, de Leeuw, J. H. ed., Vol. I, Academic Press, 1965
RGD, 1966 Rarefied Gas Dynamics, de Leeuw, J. H. ed., Vol. II, Academic Press, 1966
RGD, 1967 Rarefied Gas Dynamics, Brundin, C. L. ed., Academic Press, 1967
RGD, 1969 Rarefied Gas Dynamics, Trilling, L. and Wachman, H. Y. ed., Academic Press, 1969
RGD, 1970 Paper presented at the Seventh International Symposium on Rarefied Gas Dynamics, Pisa, Italy, 1970

[ *1* ] Potter, J. L.: "The Transitional Rarefied-Flow Regime," RGD, 1967, pp. 881–937.
[ *2* ] Hayes, W. D. and Probstein, R. F.: "Hypersonic Flow Theory," Academic Press, New York and London, 1959.
[ *3* ] Cheng, H. K., Hall, J. G., Golian, T. C. and Hertzberg, A.: "Boundary-Layer Displacement and Leading-Edge Bluntness Effects in High-Temperature Hypersonic Flow," JAS, **28**, 1961, pp. 353–381.
[ *4* ] Oguchi, H.: "The Sharp Leading Edge Problem in Hypersonic Flow," RGD, 1961, RGD, 1961, pp. 501–524.
[ *5* ] Oguchi, H.: "Leading Edge Slip Effects in Rarefied Hypersonic Flow, "RGD, 1963, pp. 181–193.
[ *6* ] Morito, J. II and Street, R. E.: "The Incipient Continuum Flow Near the Leading Edge of a Flat Plate," RGD, 1965, pp. 416–432.
[ *7* ] Oguchi, H.: "Shock Wave and Viscous Layer Structure in a Rarefied Hypersonic Flow Near the Leading Edge of a Sharp Flat Plate," ISAS, University of Tokyo, Report 418, 1967.
[ *8* ] Chow, W. L.: "Hypersonic Rarefied Flow Past the Sharp Leading Edge of a Flat Plate," AIAA Journal, **5**, 1967, pp. 1549–1557.
[ *9* ] Shorenstein, M. L. and Probstein, R. F.: "The Hypersonic Leading-Edge Problem," AIAA J., **6**, 1968, pp. 1898–1906.
[ *10* ] Charwat, A. F.: "Molecular Flow Study of the Hypersonic Sharp Leading Edge Interaction," RGD, 1961, pp. 553–578.
[ *11* ] Ziering, S., Chi, L. K. and Fante, R.: "Kinetic Theory of the Leading Edge," RGD, 1965, pp. 394–415.
[ *12* ] Shidrovskiy, V. P.: "Introduction to Dynamics of Rarefied Gases," American Elsevier Pub. Co., Inc., 1967. (translated from Russian)
[ *13* ] Kogan, M. N.: "Rarefied Gas Dynamics," Plenum Press, New York, 1969. (translated from Russian)
[ *14* ] Huang, A. B. and Hartley, D. L.: "Kinetic Theory of the Sharp Leading Edge Problem in Supersonic Flow," Phys. Fluids, **12**, 1969, pp. 96–108.
[ *15* ] Huang, A. B. and Hwang, P. F.: "Kinetic Theory of the Sharp Leading Edge Problem II. Hypersonic Flow," IAF Paper RE63, 1968.
[ *16* ] Chuan, R. L. and Waiter, S. A.: "Experimental Study of Hypersonic Rarefied Flow near the Leading Edge of a Thin Flat Plate," RGD, 1963, pp. 328–342.
[ *17* ] Vidal, R. J. and Witliff, C. E.: "Hypersonic Low Density Studies of Blunt and Slender Bodies," RGD, 1963, pp. 343–378.

[18] McCroskey, W. J., Bogdonoff, S. M. and McDougall, J. G.: "An Experimental Model for the Sharp Flat Plate in Rarefied Hypersonic Flow," AIAA J., 4, 1966, pp. 1580–1587.
[19] Moulic, E. S. and Maslach, G. J.: "Induced Pressure Measurements on a Sharp-Edged Insulated Flat Plate in Low Density Hypersonic Flow," RGD, 1967, pp. 971–992.
[20] Becker, M. and Boylan, D. E.: "Experimental Flow Field Investigations near the Sharp Leading Edge of a Cooled Flat Plate in a Hypervelocity, Low-Density Flow," RGD, 1967, pp. 993–1014.
[21] Vidal, R. J. and Bartz, J. A.: "Surface Measurements on Sharp Flat Plates and Wedges in Low-Density Hypersonic Flow," AIAA J. 6, 1969, pp. 1099–1109.
[22] Kobayashi, Y.: "Experimental Study of the Hypersonic Rarefied Gas Flow past a Flat Plate and Around a Cylinder," ISAS, University of Tokyo, Report 439, 1969.
[23] Vas, I. E., Iacavazzi, C., Carlomagno, G. and Bogdonoff, S. M.: "Effect of Body Inclination on the Merging of a Hypersonic Low Density Flow over Sharp Two-Dimensional Linear Bodies," RGD, 1969, pp. 501–507.
[24] Wada, I.: "Experimental Study of Low Pressure Hypersonic Flow by Using an Electron Beam Densitometer," RGD, 1965, pp. 535–547.
[25] Harbour, P. J. and Lewis, J. H.: "Preliminary Measurements of the Hypersonic Rarefied Flow Field on a Sharp Flat Plate Using an Electron Beam Probe," RGD, 1967, pp. 1031–1046.
[26] Wada, I.: "Experimental Study of Low Density Hypersonic Flow by Using the Electron-Beam Densitometry," NAL (Japan) TR-157, 1968.
[27] Joss, W. W. and Bogdonoff, S. M.: "A Detailed Study of the Flow Around the Leading Edge of a Flat Plate in Hypersonic Low Density Flow," RGD, 1969, pp. 483–492.
[28] Metcalf, S. C., Lillicrap, D. C. and Berry, C. J.: "A Study of the Effect of Surface Temperature on the Shock-Layer Development over Sharp-Edged Shapes in Low-Reynolds-Number High-Speed Flow," RGD, 1969, pp. 619–634.
[29] Lillicrap, D. C. and Berry, C. J.: "Experimental Model for High-Speed Rarefied Flow over a Sharp Flat Plate," Phys. Fluids, 13, 1970, pp. 1146–1152.
[30] Probstein, R. F.: "Aerodynamics of Rarefied Gases" and "Continuum Theory and Rarefied Hypersonic Aerodynamics," RGD, 1960, pp. 258–275 and pp. 416–431.
[31] Ho, H. T. and Probstein, R. F.: "The Compressible Viscous Layer in Rarefied Hypersonic Flow," RGD, 1961, pp. 525–552.
[32] Cheng, H. K.: "Viscous Hypersonic Blunt-Body Problems and the Newtonian Theory," Fundamental Phenomena in Hypersonic Flow, Hall, J. G. ed., Cornell University Press, Ithaca, New York, 1966, pp. 90–132.
[33] Oguchi, H. and Nishikawa, N.: "The Rarefied Hypersonic Blunt Body Problem," J. of Japan Society for Aero. and Space Sciences, 17, 1969, pp. 391–396.
[34] Levinsky, E. S. and Yoshihara, H.: "Rarefied Hypersonic Flow over a Sphere," Hypersonic Flow Research, Riddell, F. R. ed., Academic Press, New York, 1962, pp. 81–106.
[35] Kao, H. C.: "Hypersonic Viscous Flow Near the Stagnation Streamline of a Blunt Body," AIAA J. 2, 1964, pp. 1892–1906.
[36] Ho, N. C.: "An Analysis of Shock-Layer Structure Around a Blunt Body in a Rarefied Hypersonic Flow," Doctoral Thesis, University of Tokyo, 1969.
[37] Sugimura, T. and Liu, C. Y.: "High-Speed Rarefied Gas Flow near a Stagnation Point with Application to Sphere Drag," RGD, 1969, pp. 797–804.
[38] Zavarzina, I. F. and Skokov, I. V.: "Flow of a Rarefied Gas past a Sphere," Soviet Phys.-Doklady, 12, 1967, pp. 1–3.
[39] Russell, D. A.: "Density Disturbance Ahead of a Sphere in Rarefied Supersonic Flow," Phys. Fluids, 11, 1968, pp. 1679–1685.
[40] Liu, V. C.: "Contributions to the Theory of Almost-Free-Molecule Flows," RGD, 1960, pp. 239–245.
[41] Enkenhus, K. R.: "Pressure Probes at Very Low Density," UTIA Report 43, 1957.
[42] Potter, J. L. and Bailey, A. B.: "Pressures in the Stagnation Regions of Blunt Bodies

in Rarefied Flow," AIAA J., **2**, 1964, pp. 743–745.

[*43*] Daum, F. L., Shang, J. S. and Elliott, G. A.: "Impact Pressure Behavior in Rarefied Hypersonic Flow," AIAA J., **3**, 1965, pp. 1546–1548.

[*44*] Chang, J. H. and Fenn, J. B.: "Viscous Effects on Impact Pressure Measurements in Low Density Flows at High Mach Numbers," RGD, 1969, pp. 835–838.

[*45*] Reshotko, L. and Cohen, C. B.: "Heat Transfer at the Forward Stagnation Point of Blunt Bodies," NACA TN 3513, 1955.

[*46*] Lees, L.: "Laminar Heat Transfer over Blunt-Nosed Bodies at Hypersonic Flight Speed," Jet Propulsion, **26**, 1956, pp. 259–269 and p. 274.

[*47*] Ferri, A., Zakkay, V. and Ting, Lu: "Blunt-Body Heat Transfer at Hypersonic Speed at Low Reynolds Numbers," JAS, **28**, 1961, pp. 962–971 and p. 991.

[*48*] Ferri, A., Zakkay, V. and Ting, Lu: "Measurements of Stagnation Point Heat Transfer at Low Reynolds Numbers" and "On Blunt-Body Heat Transfer at Hypersonic Speed and Low Reynolds Numbers," JAS, **29**, 1962, pp. 847–850 and pp. 882–883.

[*49*] Van Dyke, M.: "Second-Order Compressible Boundary Layer Theory with Application to Blunt Bodies in Hypersonic Flow," Hypersonic Flow Research, Riddell, F. R. ed., Academic Press, New York, 1962, pp. 37–76.

[*50*] Van Dyke, M.: "A Review and Extension of Second-Order Hypersonic Boundary-Layer Theory," RGD, 1963, pp. 212–227.

[*51*] Chow, R.: "Stagnation Point Heat Transfer of a Blunt-Nosed Body in Low-Density Flow," AIAA J., **1**, 1963, pp. 1220–1222.

[*52*] Wittliff, C. E. and Wilson, M. R.: "Low Density Research in the Hypersonic Shock Tunnel," RGD, 1961, pp. 579–591.

[*53*] Talbot, L., Schaaf, S. A. and Hurlbut, F. C.: "Pressure Distributions on Blunt-Nosed Cones in Low Density Hypersonic Flow," Jet Propulsion, 28, 1958, pp. 832–834.

[*54*] Zapata, R. N., Haas, J. and Mruk, G. K.: "Low Reynolds Number Effects on Hypersonic Flow over a Two-Dimensional Cylinder," RGD, 1967, pp. 1161–1176.

[*55*] Takagi, M.: "Experimental Studies on Rarefied Supersonic Flows past a Sphere and a Circular Cylinder," Master Thesis, University of Tokyo, 1968.

[*56*] Davis, R. T. and Flugge-Lotz, I.: "Second-Order Boundary-Layer Effects in Hypersonic Flow past Axisymmetric Blunt Bodies," J. Fluid Mech., **20**, 1964, pp. 593–623.

[*57*] Tewfik, O. K. and Giedt, W. H.: "Heat Transfer, Recovery Factor, and Pressure Distributions Around a Circular Cylinder Normal to a Supersonic Rarefied-Air Stream," JAS, **27**, 1960, pp. 721–729.

[*58*] Koppenwallner, G.: "Heat Transfer to Circular Cylinders in Hypersonic Rarefied Flow," RGD, 1970.

[*59*] Grange, J. M., Klineberg, J. M. and Lees, L.: "Laminar Boundary-Layer Separation and Near-Wake Flow for a Smooth Blunt Body at Supersonic and Hypersonic Speeds," AIAA J., **5**, 1967, pp. 1089–1096.

[*60*] McCarthy, J. F. Jr. and Kubota, T.: "A Study of Wakes Behind a Circular Cylinder at M=5.7," AIAA J., **2**, 1964, pp. 629–636.

[*61*] Wada, I.: "Experimental Study of Hypersonic Low Density Flow by Using the Electron Beam Fluorescence Method," RGD, 1967, pp. 1193–1204.

[*62*] Coudeville, H., Viviand, H., Raffin, M. and Brun, E. A.: "An Experimental Study of Wakes of Cylinders at Mach 20 in Rarefied Gas Flows," RGD, 1969, pp. 881–895.

[*63*] Chuan R. L. and Yang, H. T.: "Hypersonic Low Density Wakes," Phys. Fluids, **8**, 1965, pp. 44–55.

[*64*] Trepaud, P. and Brun, E. A.: "A Study of Wakes Behind Cylinders in Free-Molecule Flow," RGD, 1967, pp. 1177–1192.

[*65*] Sentman, L. H. and Karamcheti, K.: "Rarefied Flow past a Sphere," AIAA J., **7**, 1969, pp. 161–163.

[*66*] Baker, R. M. L. and Charwat, A. F.: "Transitional Correction to the Drag of a Sphere in Free Molecule Flow," Phys. Fluids, **1**, pp. 73–81.

[*67*] Rose, M. H.: "Drag on an Object in Nearly-Free Molecular Flow," Phys. Fluids, **7**, 1964, pp. 1262–1269 and "The Transitional Drag on a Cylinder at Hypersonic Mach Numbers," RGD, 1965, pp. 312–325.

[68] Pan, Y. S.: "Drag on a Cylinder in Hypersonic Nearly-Free Molecular Flow," RGD, 1969, pp. 779–787.
[69] Whitfield, D. L.: "Analysis of Sphere and Cylinder Drag in Rarefied Flow," RGD, 1970.
[70] Wegener, P. P. and Ashkenas, H.: "A Simple Method of Sphere Drag Measurement in Rarefied Supersonic Gas Flows," RGD, 1961, pp. 663–667 and "Wind Tunnel Measurements of Sphere Drag at Supersonic Speeds and Low Reynolds Numbers," J. Fluid Mech., **10**, 1961, pp. 550–560.
[71] Aroesty, J.: "Sphere Drag in a Low-Density Supersonic Flow," RGD, 1963, pp. 261–277.
[72] Ashkenas, H.: "Low-Density Sphere Drag with Equilibrium and Non-equilibrium Wall Temperature," RGD, 1963, pp. 278–290.
[73] Schaaf, S. A. and Maslach, G. J.: "A Comparison of Some Recent Aerodynamic Experiments and Theory at the Borders of the Transition Flow Regime," RGD, 1963, pp. 317–327.
[74] Bailey, A. B.: "High-Speed Sphere Drag in the Transition-Flow Regime in an Aeroballistic Range," RGD, 1967, pp. 1127–1143.
[75] Phillips, W. M. and Kuhlthau, A. R.: "Drag Measurements on Magnetically Supported Spheres in Low Density High Speed Flow," RGD, 1969, pp. 711–721.
[76] Legge, H. and Koppenwallner, G.: "Sphere Drag Measurements in a Free Jet and a Hypersonic Low Density Tunnel," RGD, 1970.
[77] 雛田元紀, 寺田守男: "吊下げ法による高速希薄気流中の物体の抵抗測定", 東京大学宇宙航空研究所報告, **7**, pp. 414–423.
[78] Bird, G. A.: "Approach to Translational Equilibrium in a Rigid Sphere Gas," Phys. Fluids, **6**, 1963, pp. 1518–1519.
[79] Nordsieck, A. and Hicks, B. L.: "Monte Carlo Evaluation of the Boltzmann Collision Integral," RGD, 1967, pp. 695–710.
[80] Koura, K. and Kondo, J.: "Solutions of Unsteady Nonlinear Molecular Flow Problems by the Monte Carlo Method," RGD, 1969, pp. 181–184.
[81] Koura, K.: "Relaxation of Binary and Ternary Gas Mixtures," RGD, 1970.
[82] Bird, G. A.: "Shock-Wave Structure in a Rigid Sphere Gas," RGD, 1965, pp. 216–222.
[83] Bird, G. A.: "The Velocity Distribution Function Within a Shock Wave," J. Fluid Mech., **30**, 1967, pp. 479–487.
[84] Perlmutter, M.: "Model Sampling Applied to the Normal Shock Problem," RGD, 1969, pp. 327–330.
[85] Bird, G. A.: "The Structure of Normal Shock Waves in a Binary Gas Mixture," J. Fluid Mech., **31**, 1968, pp. 657–668.
[86] Sinclair, M. and deLeeuw, J. H.: "A Monte Carlo Solution to a Modelled Diffusion Shock Problem," RGD, 1969, pp. 319–326.
[87] Bird, G. A.: "The Formation and Reflection of Shock Waves," RGD, 1969, pp. 301–311.
[88] Perlmutter, M.: "Analysis of Couette Flow and Heat Transfer Between Parallel Plates Enclosing Rarefied Gas by Monte Carlo," RGD, 1967, pp. 455–488.
[89] Koura, K.: Transient Coutte Flow of Rarefied Binary Gas Mixtures," Phys. Fluids, **13**, 1970, pp. 1457–1466.
[90] Yen, S. M. and Schmidt, H. J.: "Monte Carlo Solutions of the Boltzmann Equation for Heat Transfer Problems," RGD, 1969, pp. 205–213.
[91] Yoshizawa, Y.: "A Monte Carlo Calculation of Unsteady Rarefied Gas Flow Between Parallel Plates," RGD, 1969, pp. 177–180.
[92] Ballance, J. O.: "A Monte Carlo Approach to Transition and Free Molecular Flow Problems," RGD, 1967, pp. 575–588.
[93] Fan, C. and Robertson, S. J.: "Monte Carlo Solutions of Mass, Momentum and Energy Transfer for Free Molecule and Near-Free Molecule Flow Through Circular Tubes," RGD, 1969, pp. 655–666.
[94] Bird, G. A.: "Aerodynamic Properties of Some Simple Bodies in the Hypersonic Transition Regime," AIAA J., **4**, 1966, pp. 55–60.

[*95*] Vogenitz, F. W., Bird, G. A., Broadwell, J. E. and Rungaldier, H.: "Theoretical and Experimental Study of Low Density Supersonic Flows about Several Simple Shapes," AIAA paper 68-6, 1968 and AIAAJ., **6**, 1968, pp. 2388–2394.

[*96*] Vogenitz, F. W., Broadwell, J. E. and Bird, G. A.: "Leading Edge Flow by the Monte Carlo Direct Simulation Technique," AIAA J., 8, 1970, pp. 504–510.

[*97*] Vogenitz, F. W. and Takata, G. Y.: "Monte Carlo Study of Blunt Body Hypersonic Viscous Shock Layer," RGD, 1970.

[*98*] Yoshizawa, Y.: "The Sharp Leading Edge Problem by a Monte Carlo Technique," RGD, 1970.

[*99*] Yoshizawa, Y.: "A Monte Carlo Calculation of a Chemically Reacting Gas," RGD, 1967, pp. 641–660.

[*100*] Perlmutter, M.: "Monte Carlo Solution for the Characteristics of a Highly Rarefied Ionized Gas Flowing Through a Channel with a Transverse Magnetic Field," RGD, 1966, pp. 1–21.

[*101*] Chapman, S. and Cowling, T. G.: "The Mathematical Theory of Nonuniform Gases," Cambridge University Press, 1964.

[*102*] Patterson, G. N.: "Molecular Flow of Gases," John Wiley and Sons, Inc., New York, 1956.

[*103*] Shreider, Yu. A. ed.: "The Monte Carlo Method," Pergamon Press, 1966. (translated from Russian)

[*104*] Hammersley, J. M. and Handscomb, D. C.: "Monte Carlo Methods," Methuen and Co., Ltd., London, 1965.

[*105*] Kendall, M. G. and Babington Smith, B.: "Tables of Random Sampling Numbers," Tracts for Computers, **24**, Cambridge University Press, 1939.

[*106*] RAND Corporation: "A Million Random Digits with 100,000 Normal Deviates," Glencoe, Illinois, Free Press, 1955.

[*107*] Guttman, I. and Wilks, S. S.: "Introductory Engineering Statistics," John Wiley and Sons, Inc., 1965.

[*108*] von Mises, R. and Geiringer, H.: "Mathematical Theory of Probability and Statistics, Academic Press, 1964.

[*109*] Good, I. J.: "The Serial Test for Sampling Numbers and Other Tests for Randomness," Proc. Camb. Phil. Soc., **49**, 1953, pp. 276–284.

[*100*] Kogan, M. N.: "Recent Developments in the Kinetic Theory of Gases," RGD, 1969, pp. 1–39.

[*111*] Гориславский, В. С. и Толстых, А. И., "Численный Расчет Течения в Области Сферическго Затупления при Малых Числах Рейнольдса," Механика Жидкости и Газа, Известия Академий Наук СССР, 1967, No. 5, стр. 93–98.

[*112*] Скоков, И. В., "Обтекание Цилиндра Потоком Разреженного Газа," МЖГ, Изв. АН СССР, 1967, No. 1, стр. 140–142.

[*113*] Иванов, А. В., "Структура Ударной Волны в Воздухе при Числах Маха от 2.6 до 6," МЖГ, Изв. АН СССР, 1967, No. 2, стр. 152–155,

[*114*] Иванов, А. В., "Экспериментальное Исследование Влияния Чисел Маха и Рейнольдса на Структуру Сверхзвукового Потока Разреженного Газа в Окрестности Передней Критической Точки Затупленного Тела," МЖГ, Изв. АН СССР, 1967, No. 3, стр. 108–115.

[*115*] Заварзина, И. Ф., "Экспериментальные Исследования Локальных Потоков на Сфере и Сферическом Притуплений Осесиметричного Тела," МЖГ, Изв. АН СССР, 1970, No. 4, стр. 157–161.

[*116*] Воронин, Ф. С., "Экспериментальное Исследование Обтекания Сферы Гиперзвуковым Потоком Разреженного Газа," МЖГ, Изв. АН СССР, 1967, No. 2, стр. 148–151.

[*117*] Горелов, С. Л., и Коган, М. Н., "Решение Линейных Задач Динамики Разреженного Газа Методом Монте-Карло," МЖГ, Изв. АН СССР, 1968, No. 6, стр. 136–139.

[*118*] Власов, В. И., Горелов, С. Л. и Коган, М. Н., "Математический Эксперимент для Вычисления Коэффицентов Переноса," Доклады Академий Наук СССР, **179**, 1968, стр. 1293–1296.

[*119*] Ясинский, Ф. Н., "О Применений Метода Монте-Карло к Нелинейным Аэродинамическим Задачам," МЖГ, Изв. АН СССР, 1968, No. 6, стр. 69–73.

[*120*] Bird, G. A.: "Direct Simulation and the Boltzmann Equation," Phys. Fluids, **13**, 1971, pp. 2676–2681.